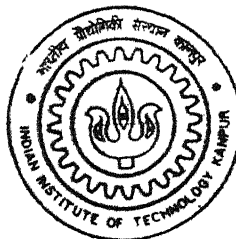


DYNAMIC INTERLAMINAR TOUGHNESS OF UNIDIRECTIONAL GFRP LAMINATES UNDER IMPACT LOADING

by

MANISH PANDEY

TH
ME/2000/N
P192d



DEPARTMENT OF MECHANICAL ENGINEERING
INDIAN INSTITUTE OF TECHNOLOGY KANPUR
February, 2000

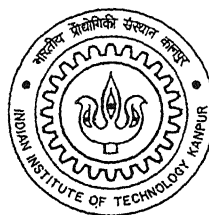
DYNAMIC INTERLAMINAR TOUGHNESS OF UNIDIRECTIONAL GFRP LAMINATES UNDER IMPACT LOADING

Thesis
*A Thesis Submitted
in Partial Fulfillment of the Requirements
for the Degree of*

MASTER OF TECHNOLOGY

By

MANISH PANDEY



to the

**Department of Mechanical Engineering
Indian Institute of Technology Kanpur**

February, 2000

6 OCT 2000 / 117

LIBRARY
I.I.T., KANPUR

A132016

RECEIVED
FILED

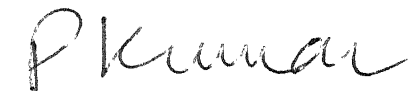


A132016

CERTIFICATE

It is certified that the work contained in the thesis entitled "Dynamic Interlaminar Toughness of Unidirectional GFRP Laminates under Impact Loading", by Manish Pandey, has been carried out under my supervision and this work has not been submitted elsewhere for a degree.

February, 2000



(Dr. Prashant Kumar)
(Professor and Head)

Dept. of Mechanical Engineering
Indian Institute of Technology
Kanpur

Contents

Acknowledgements	v
Abstract	vi
List of Tables	viii
List of Figures	ix
1 Introduction	
1.1 Introduction.....	1
1.2 Literature Survey.....	3
1.3 Present work.....	6
2 Experimental Technique	
2.1 Introduction.....	7
2.2 Specimen Description	7
2.2.1 Dimensions of the specimen.....	7
2.2.2 Basic raw materials.....	8
2.2.3 Laminate Preparation and curing.....	8
2.3 Overall Experimental Setup.....	9
2.3.1 Rigid Block.....	10
2.3.2 Load bar and striker bar.....	10
2.3.3 Description of Bridge Circuit.....	13
2.3.4 Monitoring Response of the Load Bar Strain Gauges.....	15
2.3.5 Monitoring Response of the Velocity Strain Gauges	16
2.3.6 Digital Storage Oscilloscope	16
2.4 Bonding the Velocity Strain Gauges.....	17
2.4.1 Crack Velocity	18
2.4.2 Initiation Time.....	19
2.5 Experimentation.....	20
2.6 Closure.....	20
3 Numerical and Finite Element Analysis for Dynamic Crack Propagation	
3.1 Introduction.....	34
3.2 Finite Element Formulation.....	35
3.2.1 Formulation.....	35
3.2.2 Time Integration Method.....	36

3.3 J-integral.....	36
3.4 The FE Code.....	37
3.4.1 Flow Chart.....	37
3.4.2 Mesh Size.....	37
3.4.3 Simulation of Crack Propagation.....	38
3.4.4 Stiffness Matrix for Composite Laminates.....	39
3.4.5 Input Parameters.....	40
3.4.6 Initiation and Propagation Toughness.....	41
3.4.7 Effect of Time Step.....	41
3.5 Closure	
4 Results and Discussions	
4.1 Introduction.....	50
4.2 Dynamic Interlaminar Initiation Fracture Toughness.....	51
4.2.1 Initiation Toughness for Thin Specimen.....	51
4.2.2 Initiation Toughness for Thick Specimen.....	55
4.3 Dynamic Interlaminar Propagation Fracture Toughness.....	56
4.3.1 Propagation Toughness for Thin Specimen.....	57
4.3.1 Propagation Toughness for Thick Specimen.....	59
4.4 Comparison of Dynamic Interlaminar Fracture Toughness with Quasistatic Interlaminar Fracture Toughness.....	60
4.4 Discussion.....	61
4.5.1 Comparison with Ramakrishna's work.....	62
4.5.1 Comparison with Babu and Mallikharjuna's work.....	63
4.5 Closure.....	64
5 Conclusion and scope for further work	
5.1 Conclusions	77
5.2 Scope for future work.....	78
Appendix – 1	
REFERENCES.....	

ACKNOWLEDGEMENTS

I wish to express my profound gratitude towards Prof. Prashant Kumar for his able guidance at every stage of my thesis work. Without his constructive suggestions and detailed instruction I could not have completed my work successfully.

I am thankful to Prof. N.N. Kishore for his invaluable suggestions during the computational part.

I want to deliver a special word of appreciation to Mr. Anurag Goel for in his kind cooperation in the specimen preparation and experimentation. I am also obliged to Mr. Tewari and Pandey for their help in preparing the specimens. Mr. Pankaj deserves special thanks for his constant help throughout the present work. A word of appreciation is also due to Mr. Divakar for his invaluable help.

It gives me immense pleasure to recall my association with Dhiraj, S.P., Jagdish, Shobhit, Chaudhary, Vimal, Bhatt, Ruchin, Padmaja, Praveen, Sharad, Anupam and Arjun who made my stay at IIT, Kanpur a pleasant memory. It is noteworthy that the above list is neither complete nor I repudiate any help offered by my other friends.

Last, but not least I am grateful to Aeronautical Research and Development Board (Structure Panel) for providing financial assistance.

ABSTRACT

In order to determine the interlaminar dynamic fracture toughness of unidirectional glass fibres reinforced polymer (GFRP) laminates, a combined experimental and numerical technique is developed. For the present study, the specimen is prepared by stacking a number of GFRP laminae over each other. The laminate has a precrack on the midplane of the laminate.

For the experimentation, a special fixture is designed to mount the specimen and to apply an impact load on one end of the specimen which is in a cantilever form. A load bar is screwed to the cantilever end. The load bar is impacted by a striker bar activated by an air gun. The incident and reflected pulses in the load bar due to this impact are monitored by two strain gauges bonded on the load bar. These strain gauges are connected to a bridge circuit which is in turn connected to a digital storage oscilloscope. Using one dimensional elastic wave propagation theory in the load bar, the displacement history of the load bar is obtained. The high speed crack propagation in the specimen is monitored by two strain gauges bonded ahead of the crack tip. These strain gauges are also connected to the same oscilloscope as mentioned above through another bridge circuit. The peak response of the strain gauges gives the crack propagation history. Thus, the experimentation provides (i) deflection history of the cantilever-end, (ii) crack initiation time, and (iii) crack propagation history.

The data obtained through experimentation is used as input to a FE code, along with the material properties of the specimen. The code determines the toughness of the specimen in terms of the \hat{J} -integral given by Kishimoto, Aoki and Sakata (1980). A modified gradual release technique is used to model the propagation of the interlaminar crack. For experiments, the initiation fracture toughness and the propagation fracture toughness are evaluated. At the same time, the variation of the above two toughness with the crack

velocity and the thickness of the specimen is also studied.

Two types of specimens are used in the present study; one about 4 mm thick and the other about 7 mm thick. The initiation toughness (J_{ini}) and propagation toughness (J_{prop}) for the 4mm thick specimen come out to be in the the range of 22-119 J/m^2 and 5-8 J/m^2 respectively for the crack velocity ranging between 900-1750 m/s . The initiation toughness (J_{ini}) and propagation toughness (J_{prop}) for the 7mm thick specimen come out to be in the range of 96-590 J/m^2 and 6-30 J/m^2 respectively for the crack velocity ranging between 430-1700 m/s .

List of Tables

2.1 Description of strain gauge used.....	17
4.1 Experimental Measurement for A1 to A5.....	52
4.2 Precrack length, time of peak strain at different strain gauges, initiation time & initiation toughness for Expt. A1 to A5	54
4.3 Experimental Measurements for Expt. B1 to B9.....	55
4.4 Precrack length, time of peak strain at different strain gauges, initiation time & initiation toughness for Expt. B1 to B9.....	56
4.5 Crack velocity, initiation toughness (J_{ini}) and propagation toughness (J_{prop}) for Expt. A1 to A5.....	59
4.6 Crack velocity, initiation toughness (J_{ini}) and propagation toughness (J_{prop}) for Expt. B1 to B5.....	60
4.7 Quasistatic Interlaminar toughness (G_{Ic}) for thin specimen.....	61
4.8 Quasistatic Interlaminar toughness (G_{Ic}) for thick specimen.....	61

List of figures

2.1 Specimen Geometry.....	22
2.2 Photograph of the Specimen.....	23
2.3 Schematic diagram of the impact loading setup.....	24
2.4 Photograph of the experimental setup.....	25
2.5 Specimen fastened to the block.....	26
2.6 A typical responses of stress pulse in the load bar.....	27
2.7 Time distance ($t - x$) diagram.....	28
2.8 Configuration of bridge circuit.....	29
2.9 Photograph of the bridge circuit.....	30
2.10 (a) Schematic diagram of Strain Gauge.....	31
2.10 (b) Schematic diagram of Strain Gauge after trinning.....	31
2.11 Placement of the Strain Gauges.....	32
2.12 Details of extrapolation to find initiation time.....	33
2.13 Crack tip speed history (Ref: Rosakis et al 1996).....	33
3.1 Isometric view of the specimen.....	43
3.2 Contour for J-integral.....	44
3.3 Flow chart of FE code.....	45
3.4 Mesh Generation.....	46
3.5 Crack opening scheme.....	47
3.6 Principal Directions of the specimen.....	48
3.7 A typical variation of J-integral for stationary crack.....	49
3.8 A typical variation of J-integral for propagating crack.....	49
4.1(a) Oscilloscope record , and	65
(b) Zoomed view of oscilloscope record for Expt.A1.....	65
4.2 Velocity record of the load bar end for Expt.A1.....	66
4.3 Displacement record of cantilever end for Expt A1.....	66
4.4 Blown up view of peaks of velocity strain gauges for Expt A1.....	67
4.5 Extrapolation of initiation time for Expt A1.....	67
4.6 J-integral record for stationary crack for Expt.A1.....	68
4.7 J-integral record for propagating crack for Expt.A1.....	68

4.7 J-integral record for propagating crack for Expt.A1	68
4.8 Zoomed view of J-propagation for Expt. A1.....	69
4.9 Zoomed views of J-propagation for Expt A1 to A5.....	70
4.10 (a) Zoomed views of J-propagation for Expt. B1 to B5.....	71
4.10 (b) Zoomed views of J-propagation for Expt.B6 to B9.....	72
4.11 (a) Variation of J-initiation with crack velocity for thin specimen.....	73
4.11 (b) Variation of J-initiation with crack velocity for thick specimen.....	73
4.12 (a) Variation of J-propagation with crack velocity for thin specimen.....	74
4.12 (b) Variation of J-propagation with crack velocity for thick specimen.....	74
4.13 Comparison of J_{ini} for present work and Ramakrihana's work.....	75
4.14 Comparison of J_{prop} for present work and Ramakrihana's work.....	75
4.15 Comparison of J_{ini} for present work and Babu & Mallikharjuna's work.....	76
4.16 Comparison of J_{prop} for present work and Babu & Mallikharjuna's work ...	76

Chapter 1

INTRODUCTION

1.1 Introduction

Laminated fibre composites are now becoming one of the most emerging class of structural materials. They are being used as structural members of aircrafts, rockets and space ships, automobiles, boats, sports materials, etc. The reason for the laminated fibre composite becoming more popular day by day is that they possess certain desirable properties such as high specific strength and stiffness, high fatigue strength, high corrosion, etc. Despite having the above mentioned attractive properties, there is a draw back attached to the laminated fibre composites.

A laminate is generally made by stacking many laminae over each other before curing them at high temperature and pressure. Therefore, the neighbouring laminae are mutually bonded with the help of matrix material which is considered to be having comparatively low strength. The result is that the fibres do not reinforce the laminate through the thickness direction.

The above mentioned drawback does not affect the usefulness of the laminated fibre composites when they are loaded in quasistatic conditions. The drawback comes into real picture when fibre composite laminate is impacted on by a foreign object at high velocity. When a sheet made up of a conventional metal is impacted on by a light mass with high

velocity, the material at the point of impact yields and a small dent is formed. It is generally not considered to be serious because it just workhardens the material locally. In contrast, when such an impact of a foreign object is made on the surface of a fibre composite laminate, it generates high stresses and stress waves causing interlaminar failure or delamination. As a result, the laminates are less tough and fracture spreads to large areas. It may be difficult to detect such interlaminar damage because they are not visible from outside, specially in opaque laminates like CFRP.

As explained above, a composite laminate is susceptible to severe delamination when it is impacted by a projectile under impact loading. The cracks can propagate at high velocities (Takeda et al., 1982). The comparative very high values of interlaminar toughness for fibre reinforce composite (FRP) laminate obtained under quasistatic loading condition fails to explain very high speeds of interlaminar crack propagation with impact energy as low as $4-10 \text{ J/m}^2$. Thus, it becomes imperative to monitor and characterize the interlaminar fracture toughness under dynamic crack propagation in FRP laminates to enhance its usefulness under impacts loads.

There can be two ways to study and to characterize the dynamic fracture phenomenon, experimental and numerical. In both the above mentioned cases, the monitoring of dynamic fracture is cumbersome. The reasons being following:

- (1) While performing experimental study, many related parameters are to be measured in very short time duration. This requires sophisticated instrumentation, very precise methodology and skilled personnel.
- (2) In the case of numerical analysis, the iterative procedure involves a huge amount of computation. This is due to the reason that the inertia effect and the changing boundary conditions are to be accounted for. Also, the numerical method is not able to characterize the material properties when used alone.

Hence to overcome the above mentioned shortcomings when either of the above two methods is used alone, it was felt that a combined technique should be developed which will require not too sophisticated instrumentation but will also take help of numerical modelling. Therefore, in the present work, a new hybrid technique is used which invokes both experimentation and finite element modelling to determine the interlaminar fracture toughness of glass fibre reinforced polymer (GFRP) laminates at high crack speeds ($> 400 \text{ m/s}$).

1.2 LITERATURE SURVEY

In the field of dynamic crack propagation, most of the work done has been confined to large plates with a through the thickness crack. The duration of the study is so controlled that the monitoring of the important parameters is completed before the stress waves, reflecting from free boundaries, start interfacing with the loading pulse. Thus, the experiments are controlled to isolate the effect of the specimen edges. Such control on experiments is not possible in case of thin and slender specimen with an embedded crack, in which the free surfaces are close to the crack tip. Thus, a new and modified approach has to be adopted in order to find dynamic fracture toughness of interlaminar cracks in slender specimens. The literature survey on the work done in the related fields is presented in this section.

Raman P.S. et.al (1996) explained experimental observations of various phenomena characteristic of dynamic intersonic decohesion of bimaterial interfaces. Two separate but complementary optical methods are used in conjunction with high speed photography to explore the nature of the large scale contact and shock wave formation at the vicinity of running cracks in two different bimaterial systems.

Lambros John and Rosakis A.J. (1997) investigated dynamic delamination of thick fiber

reinforced polymeric matrix composite laminates using optical techniques and high speed photography. They used 65% fiber volume fraction of Graphite/epoxy laminates consisting of 48 plies. $152mm \times 152mm$ square plates were impacted in an out-of-plane configuration using high speed gas gun. Real time imaging of the laminate out-of-plane displacement was performed using lateral shearing of interferometer of Coherent Gradient Sensing in conjunction with high speed photography, delamination crack velocities up to 1800 m/s were observed.

Truss R.W. et.al (1997) attempted to find interlaminar fracture toughness of uniaxial continuous and discontinuous carbon fiber/epoxy composites, using compact tension and double cantilever beam test geometries. The discontinuous carbon fiber/epoxy composites have been found to have a slightly misalignment of the fibers from the average fiber direction and this misalignment was found to increase both initiation fracture toughness and to greater extent the propagation fracture toughness. The increase in fracture toughness in discontinuous carbon fibers. epoxy samples was due to fibers bridging the crack and this has been modelled as if the the bridging fibers provide an increase in compressive stress across the crack analogues to a craze at the crack tip.

Sun and Grandy (1988) investigated dynamic delamination fracture toughness in a [90/0]5s T900/934 graphite/epoxy laminate using impact loading. Delamination cracks of different sizes were embedded at the midplane of the composite specimen. The threshold impact velocity that causes propagation of delamination crack was used in the dynamic analysis with the finite element method. From the finite element solution, the history of the strain energy release rate was calculated. The critical strain energy release rate was taken equal to that of maximum value of the response history.

Nishioka and Atluri (1983) studied the use of path independent J-integral for dynamic

crack propagation, which has physical meaning of energy release rate, by the finite element method. Other path integrals were also investigated along with J-integral. Numerical results showed that combined use of J-integral and the finite element method is a useful tool to obtain the fracture parameters such as stress intensity factors and energy release rates.

Kolednik (1991) presented his theoretical study for physical interpretation of the J-R curves for elastic-plastic fracture. He derived the difference between the exact initiation toughness and crack growth toughness using energy balance under quasi-static conditions. He considered three point flexure specimens each of which consists of two parts glued together along the ligament.

Potty (1992) investigated SIF in a DCB specimen with thin cantilevers through a combined scheme of measuring the strain near the crack tip and analyzing the experimental data using FEM. He developed a relationship between stress intensity factor and strain near the crack tip. The strain measured near crack tip with help of a very small strain gauge (gauge length 0.2 mm) was used in the FEM programme to obtain the SIF of the DCB specimen. Lövi [1993] improved Potty's method by using two strain gauges on each cantilever to neutralize the possibility of recording the bending strains in the cantilevers which might develop during the specimen preparation.

Verma (1995) developed an experimental technique to investigate the dynamic interlaminar toughness of slender steel DCB specimens. A load bar technique is used to apply dynamic load pulse to one of the cantilevers of the DCB specimen. Propagation gauges, which are bonded to the side face of DCB specimen, monitor the crack velocity. These experimental data was used as input to FE code, developed by Verma [1995], to obtain the dynamic interlaminar toughness parameters for slender laminates.

Ramakrishna (1996) and later Babu (1998) and Mallikharjuna (1998) investigated the interlaminar initiation and propagation fracture toughnesses of unidirectional GFRP laminates under impact loading. They all used the technique developed by Verma (1995) while making some modifications in it.

1.3 Present Work

To investigate the dynamic interlaminar toughness of unidirectional GFRP laminates under impact loading, a modified version of the technique developed by Verma (1995) has been adopted. The emphasis has been given on the variation of dynamic interlaminar toughness with the crack velocity.

Chapter 2 discusses the specimen preparation and the experimental setup. Chapter 3 outlines the details of the FE code used in the present study. The results and the discussion are presented in Chapter 4. The conclusions and the scope for future work are outlined in Chapter 5.

Chapter 2

EXPERIMENTAL TECHNIQUE

2.1 Introduction

In order to obtain the initiation toughness and propagation toughness, the experiments are conducted to determine the deflection of the cantilever end, crack propagation velocity and initiation time under impact load on the specimen. The impact loading technique was originally developed by Verma for isotropic steel plates in (1995). The technique of Verma has been modified in the present study to determine the initiation and propagation toughness of unidirectional glass fibre/epoxy (GFRP) laminates. Also some structural changes have been made in the experimental setup to suit the requirements. This chapter describes the specimen details and its preparation, setup for impact loading, crack velocity strain gauges and the experimentation.

2.2 Specimen Description

This section describes the material, geometry and preparation of specimen. The specimen used in this study is made up of unidirectional glass fibre/epoxy laminates.

2.2.1 Dimensions of the specimen

For the present work, a specimen of 25 mm width is prepared with thickness varying between 4 and 7 mm and length ranging from 170 mm to 200 mm. As shown in Fig.

2.1 a precrack is introduced during the fabrication of the specimen. The portion of the specimen, which is on the front side of the precrack is cut to an offset of 12 mm (Fig. 2.1) and a small hole of diameter 6.2 mm is drilled on the cantilever. The portion that is on the front side of the precrack remains straight during experimentation because it is bonded to the steel block. The rear portion of the specimen work as a cantilever plate. Figure 2.2 shows the photograph of the specimen.

2.2.2 Basic raw materials

The basic raw materials are glass fibres and epoxy resin mixture. The epoxy resin mixture has the following compositions.

Araldite	LY556	100 parts by weight
Hardener	HT976	35 parts by weight
Accelerator	XY73	1 part by weight
Coupling agent		0.5 parts by weight
$(\gamma$ -Amino propyl triethoxy silane)		

Unidirectional glass fibres (of diameter 5-20 μm) are used as reinforcing material. These fibres have been procured from Ceat Tyres, India.

2.2.3 Laminate Preparation and Curing

The laminate is made of unidirectional prepgs (preimpregnated fibres in semicured matrix). Prepgs are made of glass fibres with the above mentioned epoxy mixture through a 80 mm wide prepg making machine available in the laboratory. The prepg is cut to the length of 240 mm and the required number of laminae are stacked together to have the desired thickness of the specimen. For 7 mm thickness of specimen, 52 laminae are stacked and for other thickness of the specimen, number of laminae required is determined. Precrack is made by placing a thin teflon film (20 μm thick) at the middle

of the laminate at one end. The stacked laminate is then placed in between two platens of hydraulic press. Initially the laminate in hydraulic press is heated to $120^{\circ} C$ by increasing pressure gradually for about half an hour till the pressure becomes 0.7 MPa . It is cured at this pressure and temperature ($120^{\circ} C$) for about one and a half hours. For complete curing the temperature is increased upto $150^{\circ} C$ at the same pressure and is maintained for about one hour. It is then allowed to cool in between the pressed platens of the hydraulic press to room temperature. A diamond cutter is used to cut 25 mm wide strips as per the requirements shown in Fig. 2.1. The specimen cut faces are then well polished by an emery paper.

2.3 Overall Experimental Setup

The overall view of the impact loading setup is as shown in Fig.2.3. The main parts of the experimental setup are an air gun, a load bar, a striker, several bridge circuits, a digital storage oscilloscope, a rigid block and strain gauges. The front face of the specimen is bonded to the rigid block and the rigid block is fastened to the base plate of the setup with the help of two M12 bolts and specially designed washers. Two through holes of diameter 18 mm are drilled in the solid block. The cantilever end of the specimen is screwed to the load bar with a M6 screw. When the Load bar is impacted by a striker with air gun, almost elastic compressive and reflected tensile stress pulses are generated in it due to propagation of waves . These elastic stress pulses are monitored by two strain gauges, which are bonded on the load bar at symmetrically opposite locations in the longitudinal direction. These two strain gauges are connected to Oscilloscope through a half-bridge circuit. With the two stress pulses the cantilever-end-displacement can be evaluated. To measure the crack initiation time as well as crack velocity, two strain gauges are bonded ahead of the crack-tip on one side face of the cantilever. These strain gauges are henceforth addressed as velocity strain gauges. The velocity strain gauges are

also connected to the oscilloscope through quarter-bridge circuits (The photograph of the setup is shown in Fig. 2.4).

2.3.1 Rigid Block

For applying an impact load on the cantilever end of the specimen, the front face of the specimen needs to be bonded to a rigid support. A rigid solid block of mild steel ($70\text{ mm} \times 70\text{ mm} \times 150\text{ mm}$) with serrations on a face to which the specimen is bonded. The rigid block is bolted to the rigid base plate. Two matching holes of diameter 12 mm with internal threads are tapped in the base plate of the setup. Highly oversized holes in the rigid block are made to allow the adjustment of the solid block on the setup base plate. The rigid block is bolted to the rigid base plate in such a way that the specimen is normal to the axis of the load bar (Fig. 2.5). The specimen is bonded to the block by Araldite (supplied Ciba Specialty Chemicals, India Ltd.). To reinforce the bonding a carbon steel strip of dimensions $28\text{X}8\text{X}1\text{mm}$ is used with two specially designed pressing fingers. When the specimen is bonded to the block, the strip is inserted into the precrack up to a depth of 6 to 8 mm . Then upper end and lower ends of the strip which protrude beyond the width of the specimen are pressed with the help of pressing fingers. Pressing fingers are fastened to the block with the help of M6 screws. After completion of the experimentation firstly the pressing fingers and strip are removed and then the specimen is removed from the rigid block using a chisel. The rigid block is cleaned by burning the epoxy with an oxy-acetylene flame and then degreased by acetone to make it ready for fixing another specimen to it.

2.3.2 Load bar and striker bar

The load bar and striker bar are made of cold rolled mild steel rod of 19 mm diameter. The striker bar is of 300 mm length, approximately one fourth of the load bar length. The striker bar is used for generating a square shape compressive stress pulses in the load bar. The impact face of the load bar is flat whereas the striker bar face is convex with

a small curvature so that impact would always be at a center portion of the flat face of the load bar. Due to the impact a compressive stress pulse (incident pulse) propagates in the load bar towards the specimen end and after transmitting a certain amount of energy to specimen, it reflects back as reflected pulse. For monitoring these incident as well as reflected pulses two strain gauges of 120Ω resistance and 6 mm gauge length are bonded to the load bar along its axis. The strain gauges are bonded diagonally opposite to each other to cancel the effect of bending wave, if there is any. Care is taken to align the centre line of the load bar with the centre line of the striker.

A typical record of the incident pulse and reflected pulses recorded by the strain gauges is shown in the Fig.2.6. From this experimental record the displacement of the cantilever-end of the specimen can be obtained by using one dimensional wave propagation theory. Figure 2.7 shows the time-distance (t-x) diagram for the propagation of the stress pulses in the load bar. When the striker impacts the load bar, the compressive incident pulse propagates towards the specimen and is recorded at location S. The reflected tensile pulse is recorded at the same location but at a different time and is predicted by the t-x diagram.

By using the incident and reflected pulses the displacement of cantilever end is found out using one dimensional wave propagation theory for elastic wave propagation in the load bar and the striker bar. The duration T of the stress pulse is $2l_s/c$, where l_s is the length of the striker bar and c is the longitudinal wave velocity. In fact, when the striker bar impacts the load bar compressive stress is developed and wave fronts of the compressive stress start moving in both bars with longitudinal wave velocity c . As the wave front in the striker bar reaches the free end, it is reflected back with no stress and zero particle velocity for the symmetric impact of the bars of same material and cross sectional area. Therefore this wave front on reaching at the impact face, brings the striker bar to rest. Wave propagation in the load bar is analyzed through relations along characteristic. Line

1-2 is the characteristic along the positive direction and relation between the stress and particle velocity is given by

$$d\sigma - \rho c dv = 0$$

where σ is stress, v is particle velocity and ρ is density of the load bar material.

Relation along negative characteristic (line 2-3) is given by

$$d\sigma + \rho c dv = 0$$

Using the above equations the relation along characteristic 1-2 simplifies to

$$\sigma_2 - \rho c v_2 = \sigma_1 - \rho c v_1 \quad . \quad (2.1)$$

Along the characteristic 1-5 the relation is

$$\sigma_1 + \rho c v_1 = \sigma_5 + \rho c v_5 \quad . \quad (2.2)$$

But $\sigma_5=0$ and $v_5=0$, because the load bar is initially at rest and stress wave never reaches point 5. Then the above equation gives

$$\sigma_1 = -\rho c v_1 \quad . \quad (2.3)$$

Substituting Eq.2.3 in Eq.2.1, one obtains

$$\sigma_2 - \rho c v_2 = 2\sigma_1 \quad . \quad (2.4)$$

Relations along the characteristics 2-3 and 3-4 are

$$\sigma_2 + \rho c v_2 = \sigma_3 + \rho c v_3 \quad . \quad (2.5)$$

and

$$\sigma_3 - \rho c v_3 = \sigma_4 - \rho c v_4 \quad . \quad (2.6)$$

It is worth noting that $\sigma_4 = 0$ and $v_4 = 0$ at point 4, because the striker bar and the load bar, as mentioned earlier, are of the same material and same diameter and the striker comes to rest after time T (Fig. 2.7). The above two equations yield

$$\sigma_2 + \rho c v_2 = 2\sigma_3 . \quad (2.7)$$

Adding equation 2.4 and Eq.2.7, one obtains

$$\sigma_2 = \sigma_1 + \sigma_3 . \quad (2.8)$$

By substituting σ_2 from the above equation in Eq. 2.4, v_2 is determined as

$$v_2 = \frac{\sigma_3 - \sigma_1}{\rho c} . \quad (2.9)$$

Noteworthy is that σ_1 is compressive and σ_3 is tensile in nature and the particle velocity of cantilever end is found by summing the absolute value of incident and reflected pulses. Displacement u_2 , of the point 2 at any time t is found by integrating Eq. 2.9 and therefore is given by

$$u_2(t) = \int_0^t v_2 dt = \int_0^t \left(\frac{\sigma_3 - \sigma_1}{\rho C} \right) . \quad (2.10)$$

Note that time t at the cantilever-end is measured only after the head of the incident pulse reaches the strain gauge at point S on the load bar. Similarly time t , is measured for reflected pulse when the head of the reflected tensile pulse reaches at point S.

2.3.3 Description of Bridge Circuit

The change in resistance of the strain gauges bonded to the load bar due to stress pulses has to be converted into a potential difference. This is done with the help of the bridge circuit. This potential difference is monitored by a digital storage oscilloscope. Figure 2.8 shows the configuration of the bridge circuit used in this study. Figure 2.9 shows the photograph of the same. R_1 , R_2 , R_3 and R_4 are four strain gauges used in each bridge. For monitoring incident and reflected pulses in the load bar, the half bridge is used. R_1

and R_3 are active strain gauges bonded on the load bar diagonally opposite to each other along the axis of the load bar whereas R_2 and R_4 are dummy strain gauges. These dummy strain gauges are bonded on a bar of same material as of the load bar. This bar acts as heat sink to the heat generated in the strain gauges when current flows through it. Bridge circuit is balanced to zero voltage output by connecting 1Ω resistance in series to R_2 and variable resistors $1 M\Omega$ for coarse adjustment and $1 k\Omega$ in parallel to R_2 for fine adjustments as shown in the circuit. To calibrate the bridge circuit a calibration resistance R_c ($47 k\Omega$) connected in parallel to one of the active gauges through a switch (K).

For a balanced bridge circuit the output voltage Δe is given by

$$\frac{\Delta e}{E} = \frac{R_1 \cdot R_2}{(R_1 + R_2)^2} \left(\frac{\Delta R_1}{R_1} - \frac{\Delta R_2}{R_2} + \frac{\Delta R_3}{R_3} - \frac{\Delta R_4}{R_4} \right) \quad (2.11)$$

where E is the input voltage. It can be seen from the equation that similar (both positive or both negative) changes in resistance of opposite arms of the bridge circuit are added up and dissimilar (one positive and other negative) changes are cancelled out. Thus by having the active strain gauges at the opposite arms only compressive pulse is recorded and bending effect is nullified.

The relation between the strain in the strain gauge and corresponding change in its resistance is governed by the following equation

$$S_g = \frac{\Delta R/R}{\epsilon} \quad (2.12)$$

where S_g is the gauge factor, R is the strain gauge resistance, and ϵ is the strain recorded by the strain gauge. Rearranging the above equation, one obtains

$$\epsilon = \frac{\Delta R/R}{S_g} . \quad (2.13)$$

2.3.4 Monitoring Response of the Load Bar Strain Gauges

For Half Bridge, the change in resistance of the arm CD after connecting R_c is given by

$$\Delta R_3 = R_3 - \left(\frac{R_3 \cdot R_c}{R_3 + R_c} \right) \quad (2.14)$$

leading to

$$\Delta R_3/R_3 = \frac{R_c}{R_3 + R_c} . \quad (2.15)$$

Corresponding to this change in resistance a voltage difference (Calibration Voltage, V_c) develops between terminals A and C. Similar resistance change will also occur in R_1 and R_3 , when the load bar experiences the load pulses. From Eqs. 2.12 and 2.14 the calibration voltage corresponds to the strain

$$\epsilon_c = \frac{R_3}{2(R_3 + R_c)S_g} . \quad (2.16)$$

The strain value, ϵ_c , will thus correspond to the calibration voltage, V_c . A factor of half is introduced to take average of the strains recorded by the strain gauges R_1 and R_3 which are at the opposite arms of the bridge circuit. By the linear relationship between the voltage drop across AC and strain in the strain gauges bonded on the load bar, the strain in the load bar corresponding to a voltage V recorded on the oscilloscope can be given as

$$\epsilon = \frac{\epsilon_c}{V_c} \cdot V = \frac{R_3 V}{2 (R_3 + R_c) S_g V_c} . \quad (2.17)$$

Now, the magnitude of the incident compressive stress is obtained by

$$\sigma = E\epsilon$$

where E is the young's modulus of the load bar material. This will give a measure of incident load on the specimen.

2.3.5 Monitoring Response of the Velocity Strain Gauges

Similarly for monitoring crack velocity strain gauges response, crack velocity strain gauges are connected to digital storage oscilloscope through the quarter-bridge circuits. These circuits are same as the half-bridge circuit except R_3 is also dummy strain gauge here (i.e., R_1 is only one active strain gauge). Due to only one active strain gauge ϵ_c is

$$\epsilon_c = \frac{R_3}{(R_3 + R_c)S_g} \quad (2.18)$$

and strain at the crack velocity strain gauge is

$$\epsilon = \frac{\epsilon_c}{V_c} \cdot V = \frac{R_3 V}{(R_3 + R_c) S_g V_c} \quad (2.19)$$

The fast changing signals from the impact experiment are shielded through the use of coaxial cables at all places including on the wires used from strain gauges to the bridge circuits. The bridge circuits, the battery and the dummy strain gauges are enclosed within a shield box made of good conductor aluminium. The ground wire of all the coaxial wires are connected together as they are screwed to the aluminium shield box.

2.3.6 Digital Storage Oscilloscope

A 4-channel differential input digital storage oscilloscope (DSO 1624, Gould Inc., U.K.) is used to monitor strain gauge responses. There are 50 memories in the oscilloscope and

the digitally connected responses remain in the memory blocks for a period of 6 months irrespective of whether the power is switched on or off. It is noteworthy that for one experiment three memory blocks are used. One for storing the signals of load bar, and one each for the two velocity strain gauges ahead of the crack tip. It has 8 bit (ie., 256 points) resolution in vertical direction and 12 bit (ie., 4096 points on the screen) resolution in horizontal direction. The maximum sensitivity is 0.025 mV in vertical direction and 0.5 μ s in the horizontal direction for single mode when only one channel is active. For dual mode (using multiple channels) sensitivity in horizontal direction is 1 μ s. In fact, this limitation on the sensitivity in horizontal direction poses a problem on the accurate measurement of crack velocity; thus very high crack velocities could not be monitored accurately. The digital storage oscilloscope is integrated with personal computer (PC 386) with the GPIB soft ware, so that the stored data can be transferred to the PC for further processing.

2.4 Bonding the Velocity Strain Gauges

For the present experimentation strain gauges of very small gauge length and size are needed. The strain gauges used for these experiments have been supplied by Tokyo Sokki Kenkyujo Co. Ltd., Japan. Three types of strain gauges are used in the present work.

Table 2.1 Description of strain gauges used

Sl. No	Specification	Gauge Length	Comment
1	FLA-3-8	3 mm	General Purpose
2	BFLA-2-8	2 mm	For Polymer Composites
3	BFLA-5-8	5 mm	For Polymer Composites

The resistance of all these strain gauges is $120 \pm 0.3 \Omega$ with a gauge factor of 2.05. Before bonding, the unnecessary portion of the strain gauge is trimmed and thrown away. Figure 2.10 shows the views of the strain gauges prior to and after cutting. Initially the surface of the specimen is polished and degreased. Then the strain gauge are placed in their marked locations taking the help of a cello tape. Fevi-quick (Pedilite Industries) is used to bond the strain gauges. The strain gauges are placed very close to the crack plane and perpendicular to the crack plane.

It is noteworthy that Verma et. al (1995), Mallikharjuna and Babu (1998) used the strain gauge of type FLG-02-11 whose gauge length is very small, 0.2 mm. This strain gauge was found to be suitable for specimen made of isotropic and homogeneous steel. However, for heterogeneous GFRP laminates, strain gauges of longer length (≥ 2 mm) are required; also the strain gauges specially designed for composite materials are found to be more reliable. Therefore, in the present study strain gauges of BFLA series have been used.

2.4.1 Crack Velocity

Crack velocity is obtained by monitoring the responses of the strain gauges bonded ahead of the crack tip Verma (1995) developed a technique for isotropic steel DCB specimen. He used to bond three strain gauges at a certain angle. In present work, a modification of the above technique is used. Only two strain gauges are used and both the strain gauges are kept at an angle 90° to the crack plane. It is noteworthy that upper end of a strain gauge is kept at a distance of 0.5 - 0.8 mm from the midplane or crack plane of the specimen. Figure 2.11 shows that how close the strain gauges are bonded near the crack plane. Since the strain gauges are very close to the crack plane, the singular strain field associated with the crack tip gives a strain peak when the crack tip passes close to the

strain gauge. There are two such velocity strain gauges, the distance between the two strain gauges is measured accurately through travelling microscope; the velocity can be found (Fig. 2.12) using the formula

$$\text{Velocity} = \frac{a_2 - a_1}{T_2 - T_1}$$

where a_1 and a_2 are the location of the first and second strain gauges from the cantilever end and T_1 and T_2 the time of the strain peaks, monitored by the two strain gauges respectively.

2.5 Initiation Time

The initiation time could be found out by extrapolating the data procured by the crack velocity strain gauges. Figure 2.12 shows the details of crack tip location as a function of time.

Lambros and Rosakis (1997a) conducted an impact loading test on an edge-notched unidirectional graphite/epoxy specimen. For obtaining crack initiation and monitoring crack growth, an experimental technique with high speed photography was used. The measured crack velocity (Fig. 2.13) is in microsecond domain; the crack, acquires high velocity immediately after the initiation with rise time much less than $1 \mu\text{s}$. Based on this result, it is expected that rise time of experiments of this study on a similar kind of FRP specimen is quite small. Furthermore, the first velocity strain gauge is bonded very close to the crack tip ($\leq 1.5\text{mm}$) and the crack velocity is very high ($\geq 400\text{m/s}$). Thus, it takes very small time for the tip of the precrack to move to the first velocity strain gauge.

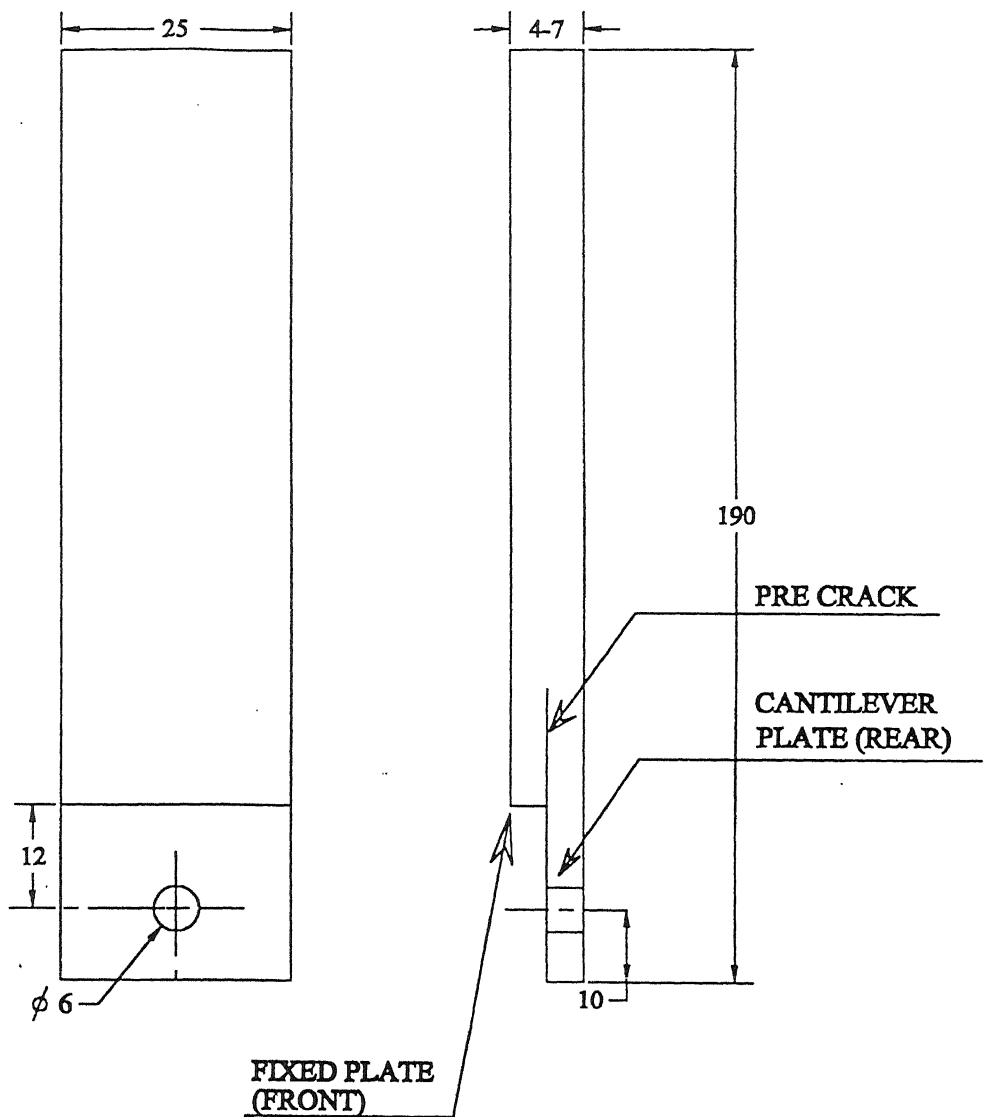
2.6 Experimentation

Specimen is prepared as explained in Section 2.2. The strain gauges are bonded on the specimen cantilever face for monitoring crack velocity. Then the specimen is screwed to the load bar and the front plate is bonded to the rigid block. Crack velocity strain gauge leads (coaxial) are soldered to bridge arms which are connected to the Digital Storage Oscilloscope. The input voltage to the bridge circuits are supplied by 9 V battery boxes. Once the bridge circuits are balanced further experimentation is carried as follows.

First of all the digital storage oscilloscope is set with three memory blocks made available to store the signals. The striker bar is inserted to its proper firing position. The airgun is then prepared to fire the striker bar. First of all the required pressures are set. Then the valves are operated to fire the striker bar. As the striker bar impacts the load bar, the compressive stress pulse propagates in the load bar towards the specimen. A part of its energy is transmitted through the specimen and rest is reflected back as the tensile stress pulse. These two pulses are monitored by the two strain gauges bonded on the load bar. The part of the stress pulse transmitted to the specimen causes deflection of the cantilever end and extends the crack. The oscilloscope records strain pulses in the load bar, which are analysed using one dimensional elastic wave analysis to obtain the deflection history of the cantilever-end. Responses of strain gauges on the cantilever face, recorded by the same oscilloscope, yields the initiation time of the crack growth and crack velocity.

2.7 Closure

Once the experiment is performed, the signals obtained from the strain gauges are stored in the oscilloscope. From these signals following are deduced :



All Dimensions in mm

Fig 2.1 : Specimen Geometry

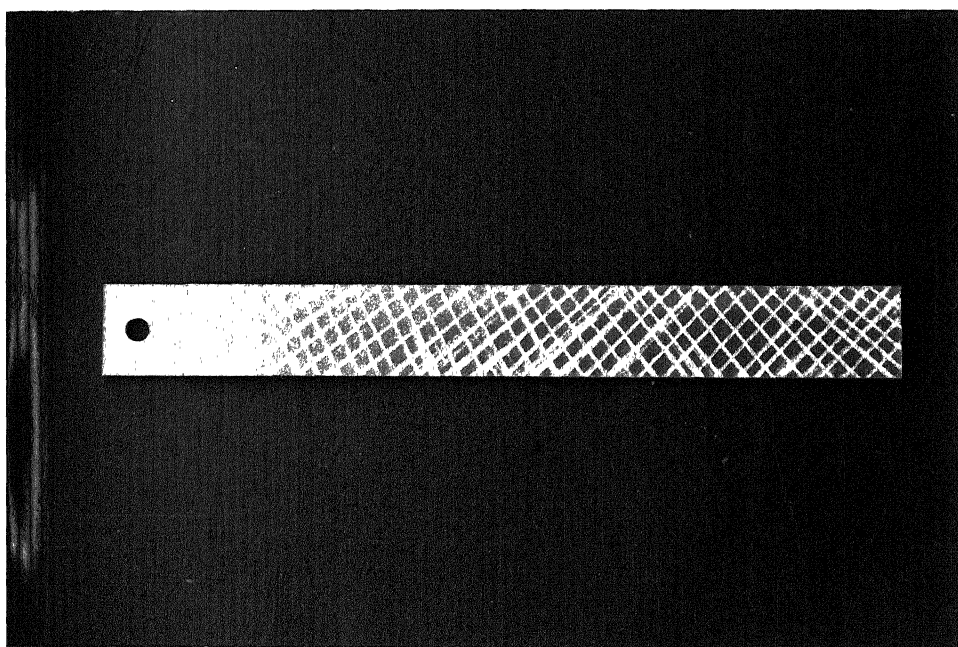


Figure 2.2 : Photograph of the specimen

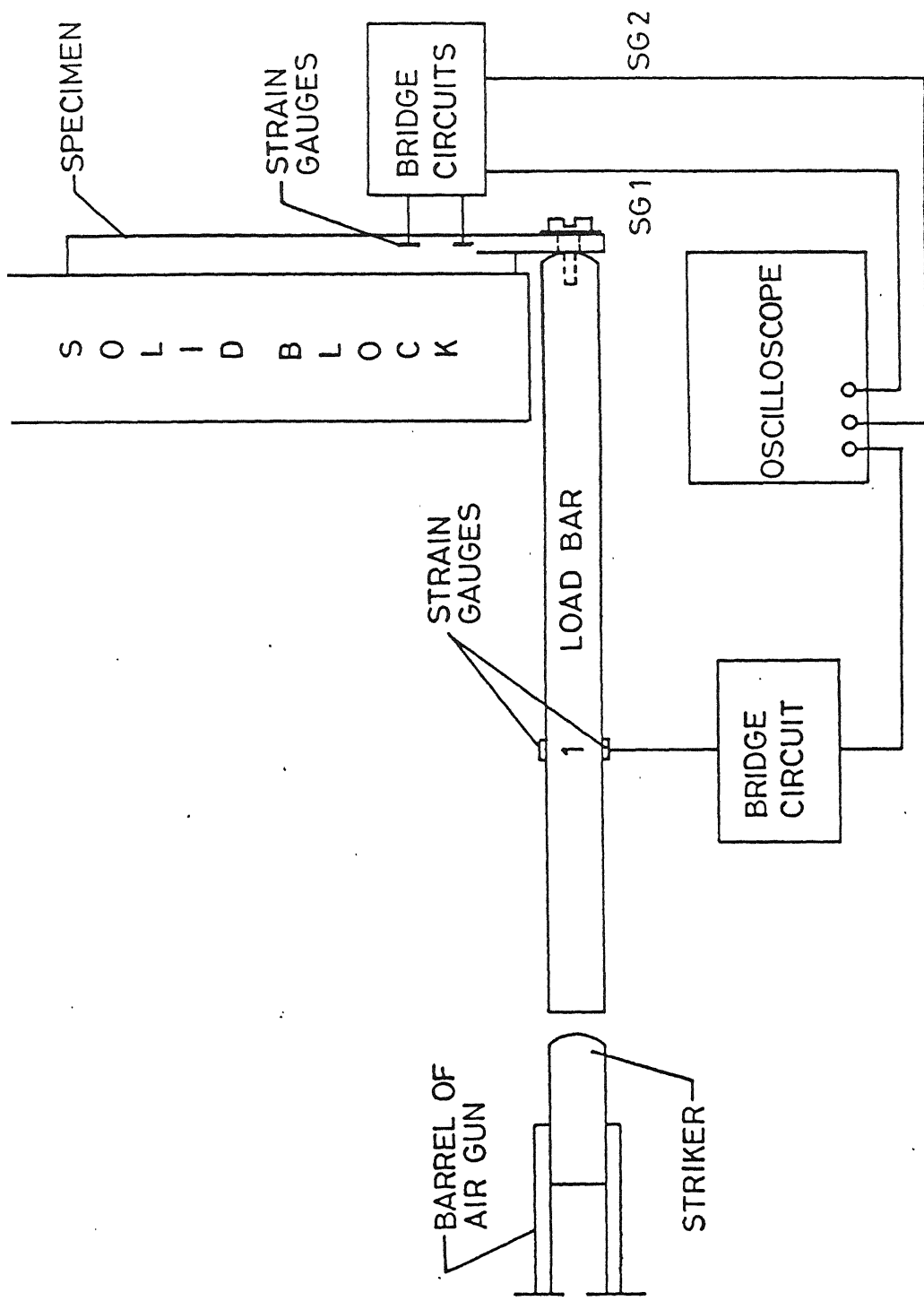


Fig. 2.3 Schematic diagram of the Impact loading setup.



Figure 2.4 : Photograph of the experimental setup

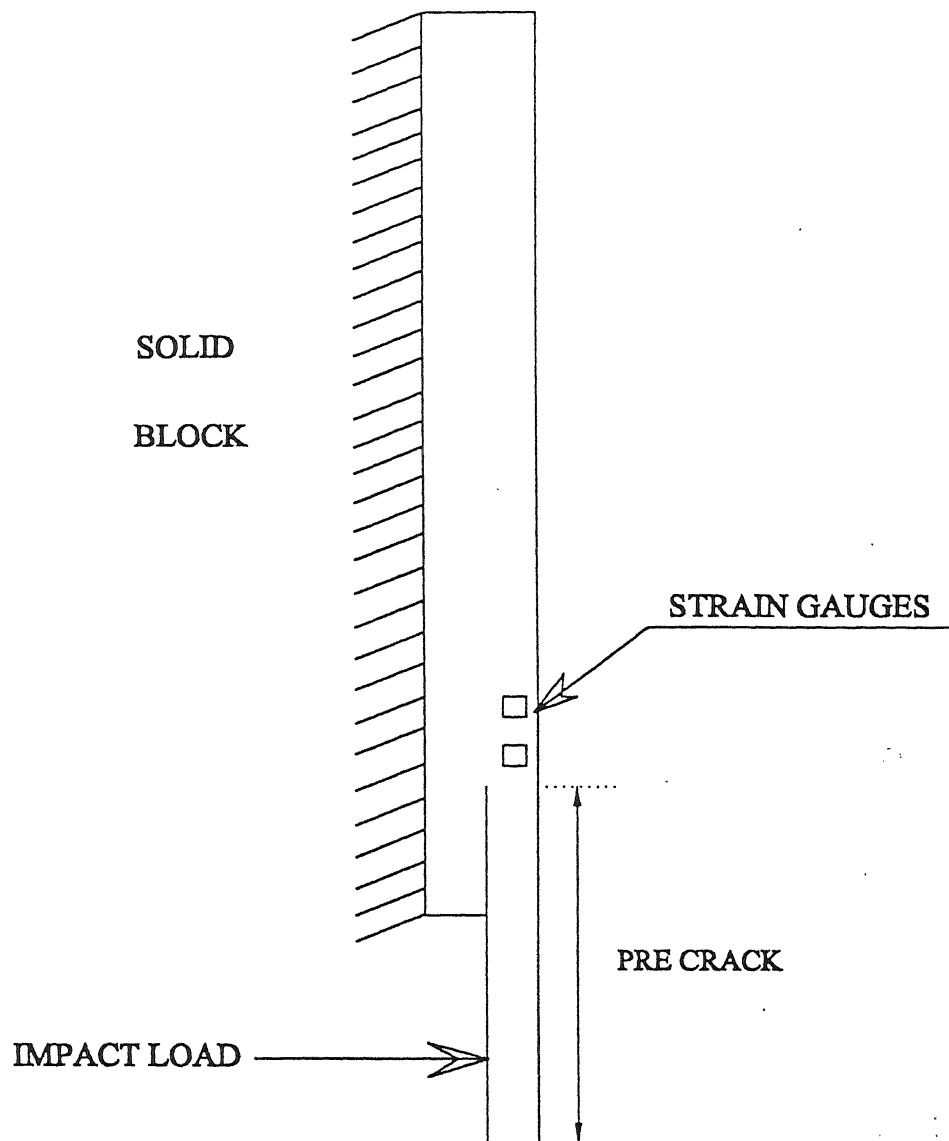


Figure 2.5 : Specimen fastened to the block

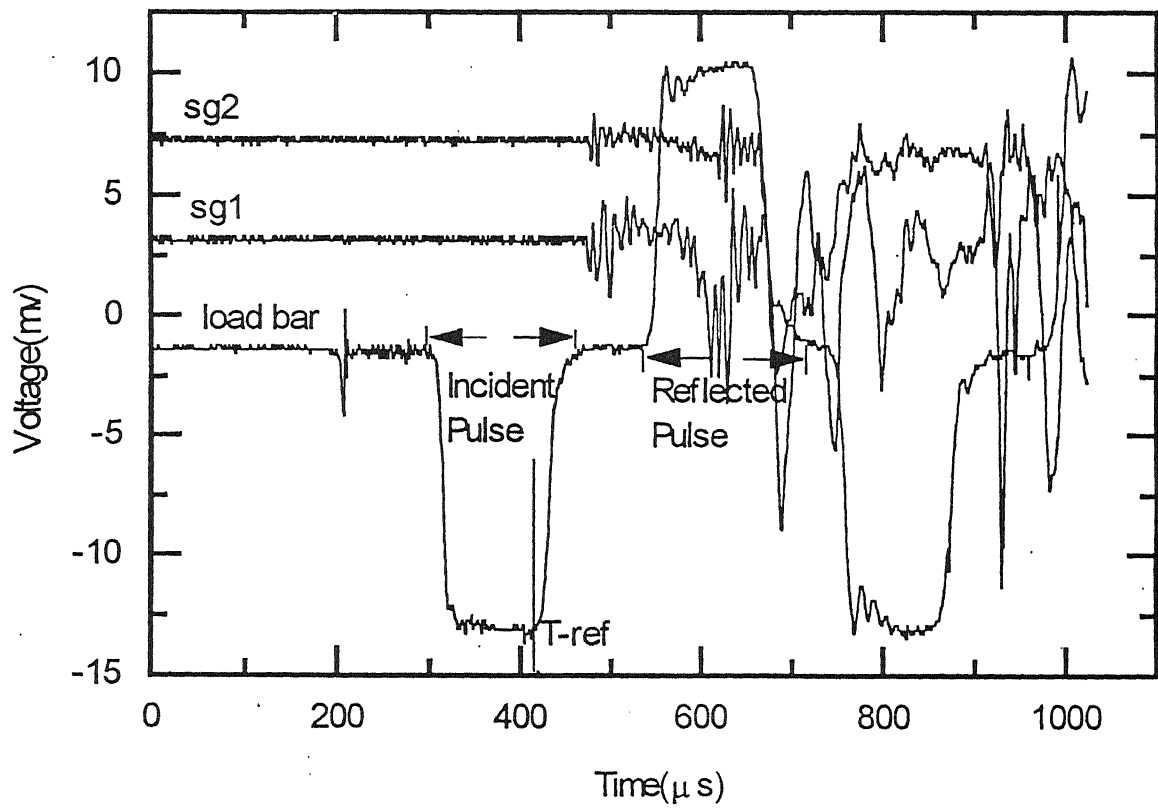


Fig.2.6: A typical Response of Stress Pulses in the Load bar

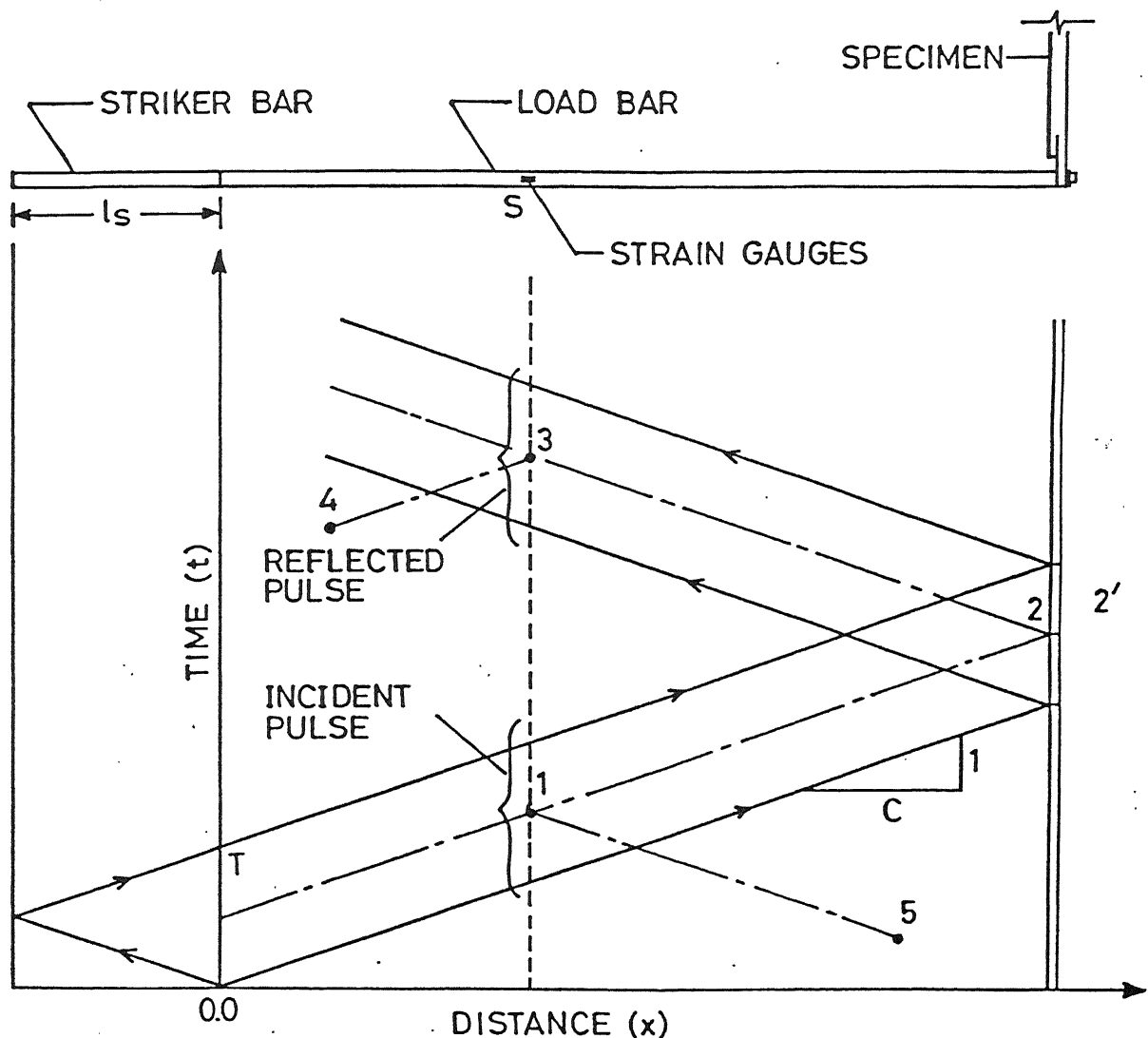


Fig. 2.7 Time-distance (t - x) diagram.

R_1, R_3 : ACTIVE GAUGES

R_2, R_4 : DUMMY GAUGES

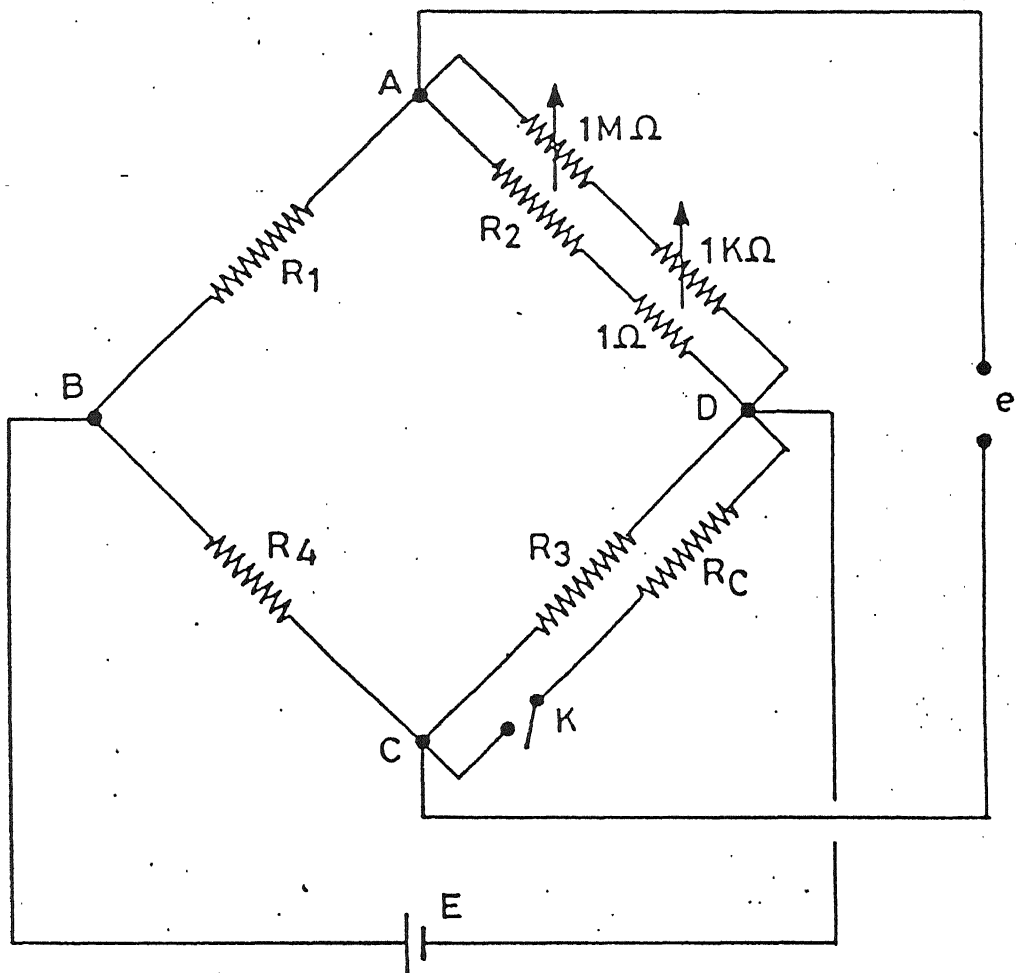


Figure 2.8 : Configuration of bridge circuit

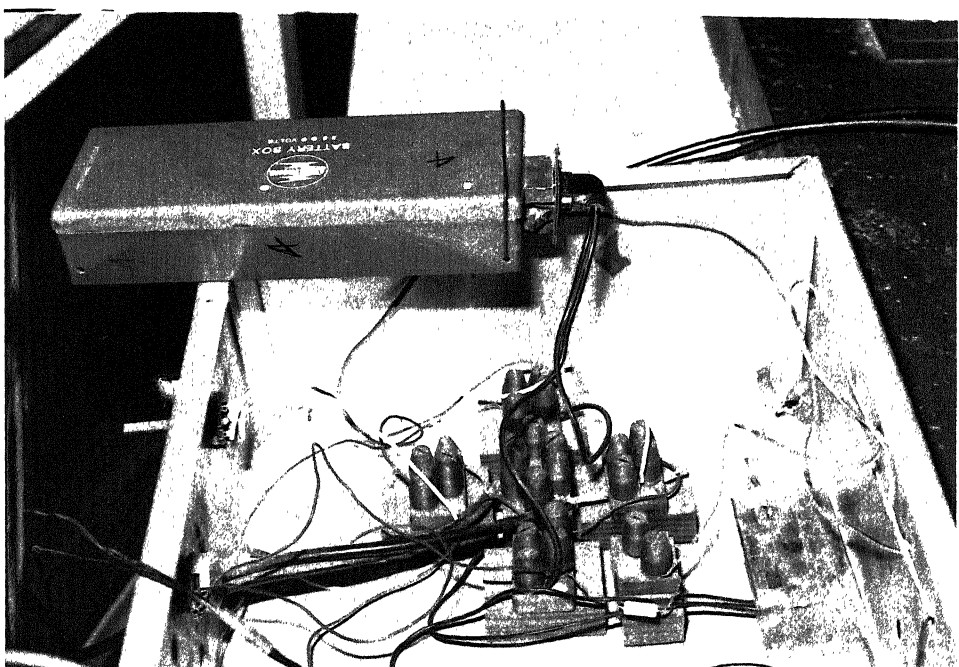
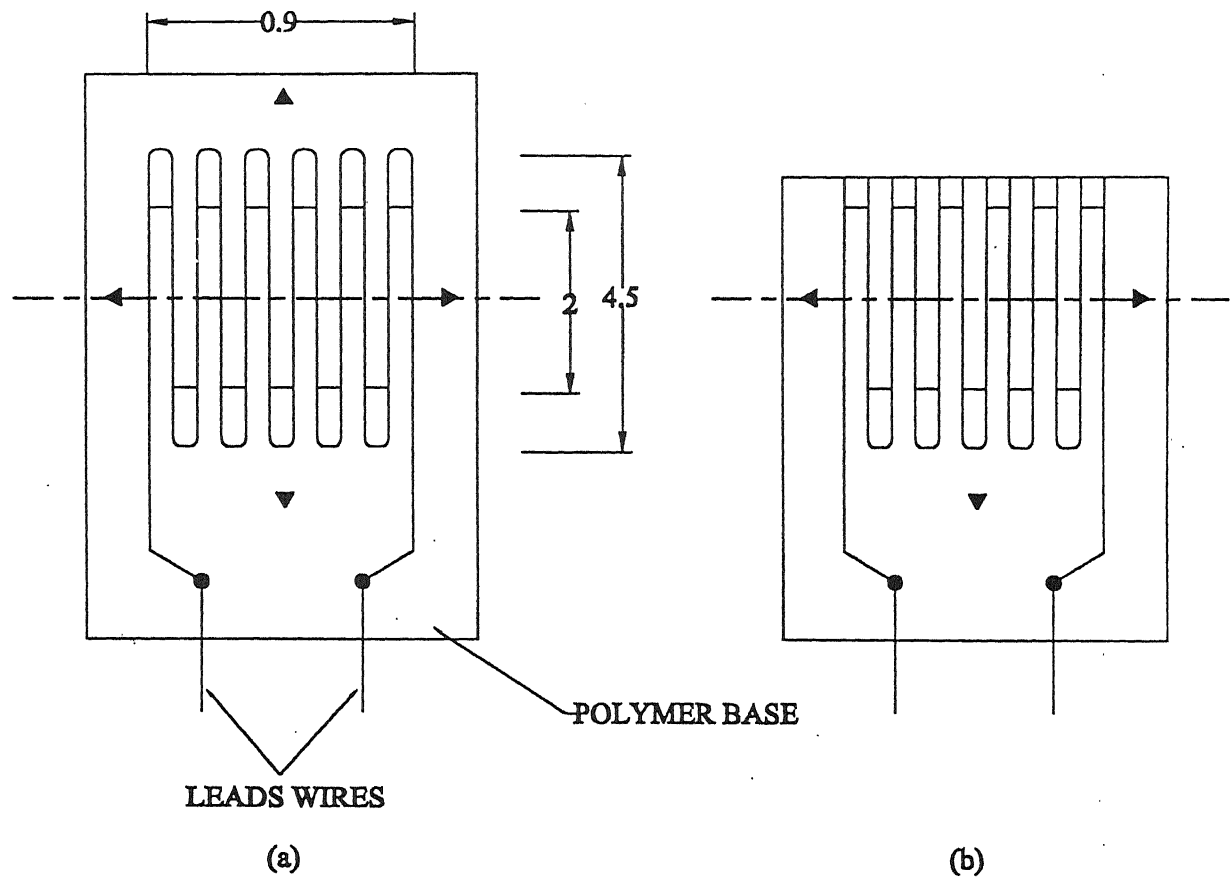


Figure 2.9 : Photograph of the bridge circuit



All dimensions in mm

Fig 2.10(a) : Schematic diagram of Strain Gauges

(b) : Schematic diagram of Strain Gauges
after trimming

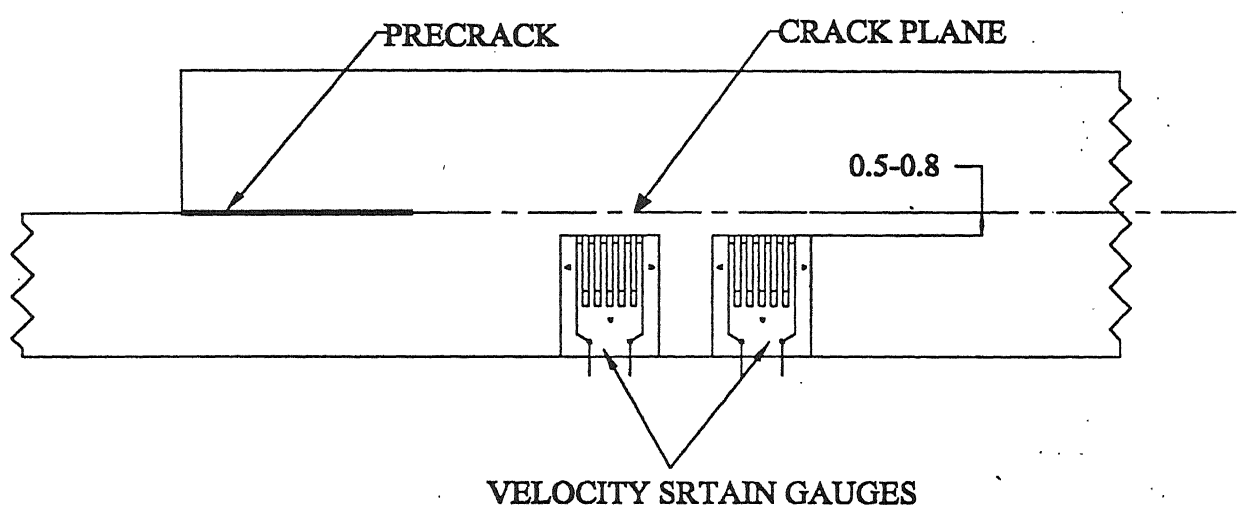


Figure 2.11 : Placement of the Strain Gauges

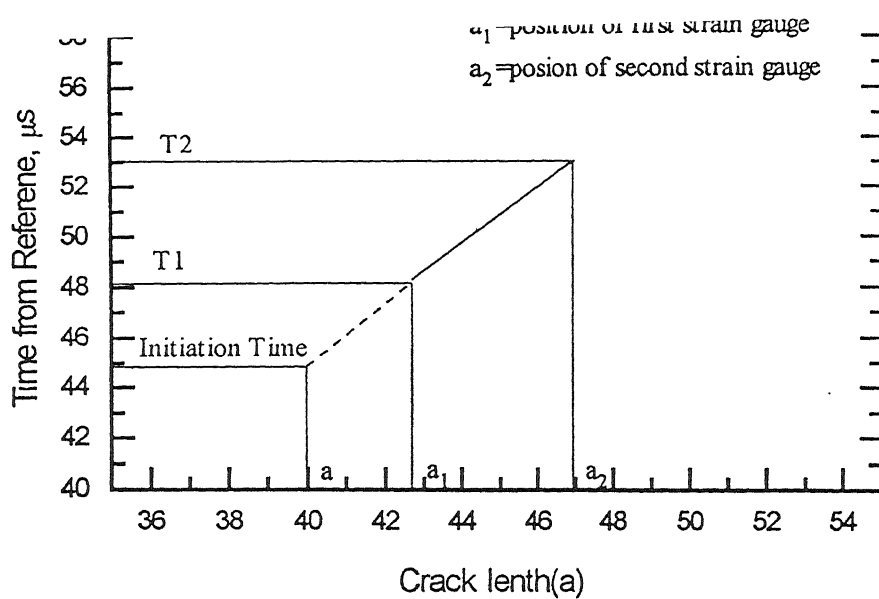


Fig. 2.12 : Details of extrapolation to find initiation time

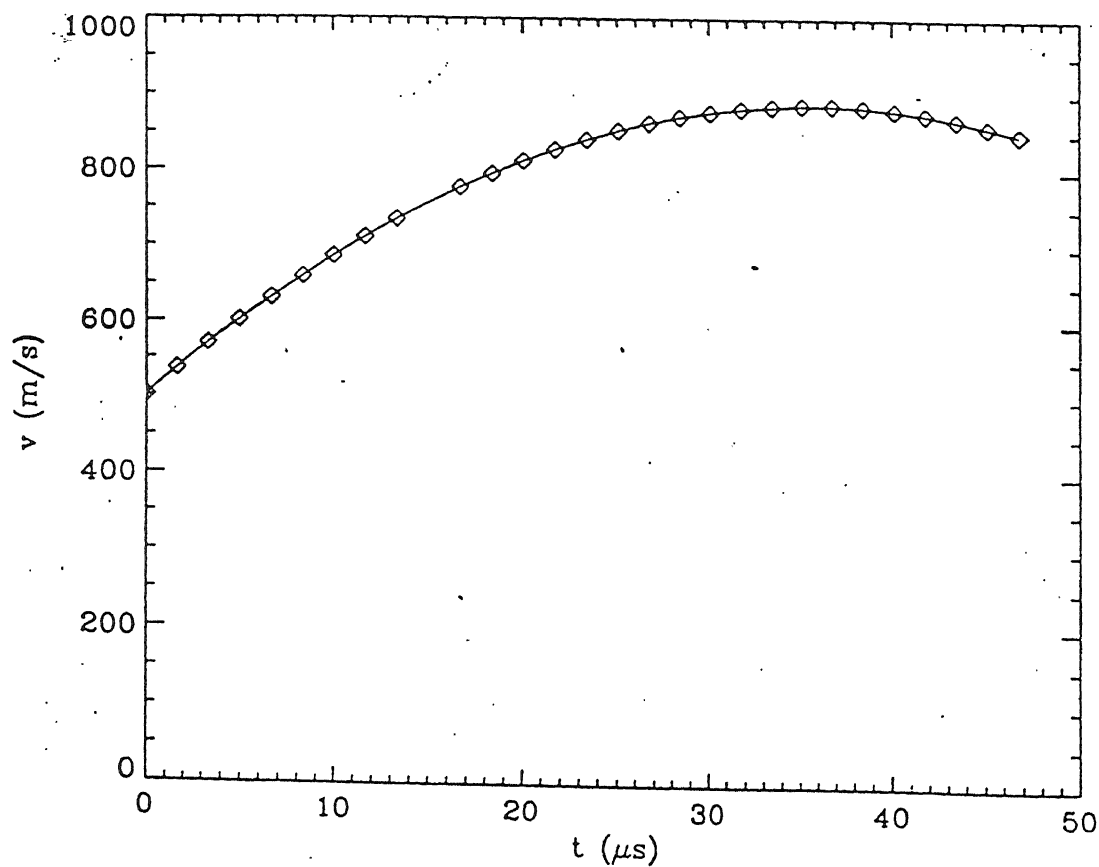


Fig. 2.13 Crack tip speed history in a 4×6 inch unidirectional graphite/epoxy Composite plate containing a sharp starter crack.(Ref:Rosakis et al.(1996))

Chapter 3

NUMERICAL AND FINITE ELEMENT ANALYSIS FOR DYNAMIC CRACK PROPAGATION

3.1 Introduction

The data obtained from the experiments needs to be further analysed to get the variation of the \hat{J} -integral at the crack tip. The analysis is done through the FE code. The FE code needs boundary conditions and initial conditions for the analysis. The inputs to FE code simulation, supplied from the experimental output as discussed in chapter 2, are

1. Displacement vs. time relation of the cantilever end,
2. Interlaminar crack velocity and
3. Initiation time of crack growth.

Verma et al. (1995) developed a program for determining the \hat{J} -integral variation with time for isotropic steel specimen. Verma's specimen was in the form of two bonded thin plates with an interlaminar crack. A modified version of Verma's program has been used in the present study for determining the initiation and propagation toughnesses of unidirectional GFRP laminates. The present chapter elucidates the outline of the FE code formulation and the modifications therein.

3.2 Finite Element Formulation

3.2.1 Formulation

The governing system of finite element equations for the linear dynamic response of an elastic body is given in the matrix form as

$$[M]\{\ddot{U}\} + [K]\{U\} = \{R\} \quad (3.1)$$

where $[M]$ and $[K]$ are the mass and stiffness matrices respectively and $\{R\}$ is the external load vector, and $\{U\}, \{\ddot{U}\}$ are the displacement and acceleration vectors of the finite element assemblage respectively. Damping forces have been neglected in the formulation.

In the above equation global matrices may be obtained as

$$[M] = \Sigma [M]^e$$

$$[K] = \Sigma [K]^e$$

$$\{R\} = \Sigma \{R\}^e$$

where elemental mass, stiffness and traction matrices are given by

$$[M]^e = \int_V \rho [N]^T [N] dV$$

$$[K]^e = \int_V [B]^T [D] [B] dV$$

$$\{R\}^e = \int_S [N]\{T\} dS$$

In these equations $[N]$ is shape function, $[B]$ derivative of shape functions, $[D]$ elastic constitutive relation matrices and $\{T\}$ traction vector.

3.2.2 Time Integration Method

The integration solves the Eq. 3.1. Basically, there are two methods to solve the above mentioned equation. One is time integration method and the other is mode superposition method. The time integration method is preferred in the present study since the wave propagation problem is being simulated in this study. Bathe (1990) gives the different methods of this integration scheme and their relative advantages and disadvantages. Verma et al. (1997) selected the Newmark integration method for the time variable and developed a FE code for 2-D finite element discretization in space analysis. Verma considered the problem as a plane strain problem, since the specimen dimension along the third direction (Z-direction in Fig. 3.1) is large with respect to the thickness of the specimen.

The front face of the specimen (Fig.3.1) remains stationary and straight because it is bonded to the rigid block. Hence the effect of this portion on the \hat{J} -integral variation was expected to be negligible. Verma (1995) and Mallikharjuna (1997) verified the above fact. Therefore, to avoid unnecessary computations, only the cantilever plate of the specimen is analysed.

3.3 \hat{J} -Integral

In the present study, in order to determine the dynamic interlaminar toughness of the unidirectional GFRP laminates, \hat{J} -integral concept is used. Nishioka and Atluri (1983) studied the use of path independent \hat{J} -integral using finite element method for dynamic crack propagation. In the present work \hat{J}_I given by Kishimoto, Aoki and Sakata (1980) is used which is defined as (Fig. 3.2)

$$\hat{J}_I = \lim_{\epsilon \rightarrow 0} \int_{\Gamma_c^- + \Gamma + \Gamma_c^+} [W n_i - T_i u_{i,1}] ds + \int_{V - V_\epsilon} \rho \ddot{u}_i u_{i,1} dV$$

where W is the strain energy density, u_i is displacement, n_i is the direction cosine of the unit outward normal, T_i is the traction, Γ_c^- , Γ , Γ_c^+ are integration paths, volume V is the volume enclosed by integration path Γ_{ϵ} and V_ϵ is the volume of a small zone in the vicinity of the crack tip.

It is noteworthy that \hat{J} -integral is independent of the choice of the path Γ (Fig. 3.2) under steady state crack growth conditions. In many cases, though these conditions are obviously not met fully yet the path independence of \hat{J} -integral can still be established within certain allowable errors. That's why the integral is evaluated over a path far away from the crack tip in order to make the analysis relatively insensitive to the finer details of crack tip region. The path is held stationary as crack tip extends in a self similar manner.

3.4 The FE Code

3.4.1 Flow Chart

The flow chart of the finite element code developed by Verma et al. (1997) is shown in Fig. 3.3. This program evaluates the variation of \hat{J} -integral with time for specified material properties (engineering constants), crack propagation history, cantilever-end-deflection history, mesh size, time step and the path of \hat{J} -integral.

3.4.2 Mesh Size

The proper working of FE code depends upon the appropriate choice of mesh size. Since the specimen is loaded in bending, C-1 continuous elements are required. It was verified by Soren et.al (1990) for dynamic problems that higher order elements are not needed for the analysis. Therefore four noded isoparametric rectangular elements are used to evaluate \hat{J} -integral with the FE code. To avoid wave reflections due to non-uniformity

in mass distribution, uniform mesh throughout the specimen is generated. To take into the consideration of bending as well, fine mesh is used. In the present study, different thicknesses of the specimen are used. One type of specimen are about 4 mm thick and the other are about 7 mm thick. For the specimen of 7 mm thickness mesh size of $h/10$ in thickness direction and $1.125h/10$ in length direction is used where ' h ' is the thickness of the cantilever end. But for the specimen of 4 mm thickness element length of $h/10$ in thickness direction is chosen to account for bending of cantilever. However, in length direction, element length of $h/5$ is selected to avoid too fine a mesh and to have manageable number of nodes.

3.4.3 Simulation of Crack Propagation

In order to simulate the crack propagation, a gradual nodal release method was used. If the actual crack tip (Fig. 3.5) is located at C between the nodes B and D the holding force F at node B is gradually reduced. In most of the studies reported in literature the force F reduces to zero when the crack reaches the next node D. However, it was found that at very high crack speeds, close to the Rayleigh wave speeds, a better model is required. For obtaining a gradual and a smooth opening of crack Verma et al. (1997) employed an alternative method. The holding back force F at the node B is linearly decreased to zero when the crack reaches the end of the next element, point E in Fig. 3.5. When the crack tip lies between nodes B and D, the holding force is given by,

$$\frac{F_B}{F_{BC}} = \left[1 - \frac{b_1}{2d} \right]$$

where F_{BC} is the force at node B when the node was not opened, b_1 is the crack extension beyond node B and d is the element length as shown in Fig. 3.5. When crack propagates beyond the node D to a point D_1

$$\frac{F_B}{F_{BC}} = \left[1 - \frac{d + b_2}{2d} \right]$$

3.4.4 Stiffness Matrix for Composite Laminates

For unidirectional composite laminates used in this study the principal directions are along the fibers L and across of the fibers T (Fig. 3.6). Elastic constants for an orthotropic composite laminates are longitudinal modulus E_L , transverse modulus E_T , rigidity modulus G_{LT} , the major Poisson ratio ν_{LT} and the minor Poisson ratio ν_{TL} . The major and minor Poisson's ratios are related with E_L and E_T as

$$\frac{\nu_{LT}}{E_L} = \frac{\nu_{TL}}{E_T}$$

Experimentally E_L and E_T can be found by conducting tension tests on 0° and 90° ply laminates respectively. For extracting G_{LT} , tension test is conducted on 45° ply laminates and E_{45° be obtained. G_{LT} is then calculated from the relation [Jones R.M. (1975)]

$$\frac{1}{E_{45^\circ}} = \frac{1}{4} \left\{ \frac{1}{E_L} + \frac{1}{E_T} + \frac{1}{G_{LT}} - \frac{2\nu_{LT}}{E_L} \right\}$$

For Glass fibers/Epoxy laminates average engineering constants are experimentally determined as

$$E_L = 39.33 \text{ GPa},$$

$$E_T = 6.6 \text{ GPa},$$

$$G_{LT} = 3.3 \text{ GPa and}$$

$$\nu_{LT} = 0.25 .$$

In the FE code developed by Verma et al. (1997) for an isotropic materials, only two engineering constants are needed to obtain stiffness matrix in the constitutive relation.

The code has been modified to accomodate the elastic properties of orthotropic GFRP laminates. The constitutive relation is written in the form

$$\{\sigma\} = [Q] \{\epsilon\}$$

where

$$[Q] = \begin{bmatrix} Q_{11} & Q_{12} & 0 \\ Q_{12} & Q_{22} & 0 \\ 0 & 0 & Q_{66} \end{bmatrix}, \{\sigma\} = \begin{Bmatrix} \sigma_L \\ \sigma_T \\ \sigma_{LT} \end{Bmatrix}, \{\epsilon\} = \begin{Bmatrix} \epsilon_L \\ \epsilon_T \\ \frac{1}{2}\gamma_{LT} \end{Bmatrix}.$$

Q_{ij} are the stiffness coefficients of the laminates and are given by

$$Q_{11} = \frac{E_L}{1 - \nu_{LT} \nu_{TL}}$$

$$Q_{22} = \frac{E_T}{1 - \nu_{LT} \nu_{TL}}$$

$$Q_{12} = \frac{\nu_{TL} E_L}{1 - \nu_{LT} \nu_{TL}} = \frac{\nu_{LT} E_T}{1 - \nu_{LT} \nu_{TL}}$$

$$Q_{66} = G_{LT}$$

3.4.5 Input Parameters

The FE code requires some input parameters as well as boundary and initial conditions. The main input parameters to the FEM code are engineering constants of composite laminates, time step, mesh size, \hat{J} -integral path, deflection history of the cantilever plate end, initiation time and crack propagation history.

3.4.6 Initiation and Propagation Toughness

For a stationary crack, a typical variation of \hat{J} -integral with time is as shown in Fig 3.7. \hat{J} -integral builds up sharply, attains a peak and then decreases to a low value. However, the experiments of this study are controlled such that the crack becomes unstable before the \hat{J} reaches the peak in Fig. 3.7. The value of \hat{J} -integral at the peak is known as J_{ini} . As soon as the crack starts propagating \hat{J} is reduced drastically to a much lower and stabilized value as shown in Fig. 3.8. This stabilized value of \hat{J} -integral is known as J_{prop} .

3.4.7 Effect of Time Step

The choice of time step (Δt) for time integration is important for an accurate solution. An optimum choice of time step is $\Delta t = a/c$ where a is the smallest mesh size and c is the fastest wave velocity. To study the effect of time step on \hat{J} -integral, the FE simulation was run for several different time steps for same boundary conditions. It is observed that up to initiation time, \hat{J} -integral does not vary much on time step. It is found there is hardly any change in the value of \hat{J} -integral for $\Delta t = 0.2 \mu s$ and $\Delta t = 0.03 \mu s$ upto initiation time. However, right after the initiation time \hat{J} -integral decreases very rapidly. Consequently response with $\Delta t = 0.2 \mu s$ shows oscillations of high amplitude. \hat{J} -integral is calculated with a time step of $0.02 \mu s$ there after. Thus, FE analysis is made with the time step of $0.2 \mu s$ up to the initiation of the crack propagation; once the crack propagation is invoked, the time step of $0.02 \mu s$ is employed.

3.5 Closure

This chapter describes the technique developed by Verma in order to evaluate \hat{J} -integral of interlaminar crack growth at very high speeds. Verma used this simulation technique for isotropic steel specimen. In the present study, the methodology adopted for crack

propagation simulation by Verma has been modified. The results obtained after combining the experimental datas and FE simulation are discussed in chapter 4.

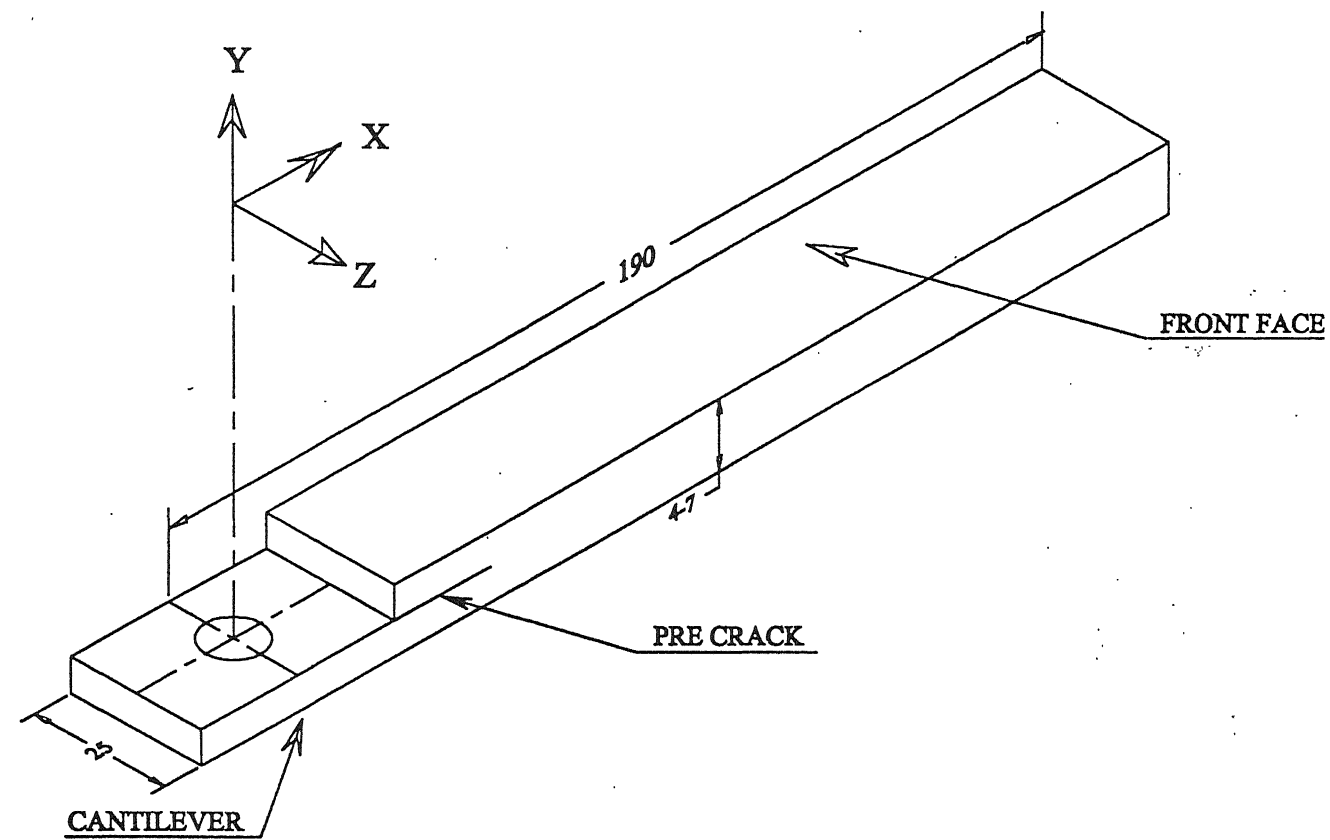


Fig. 3.1 : Isometric View of the specimen

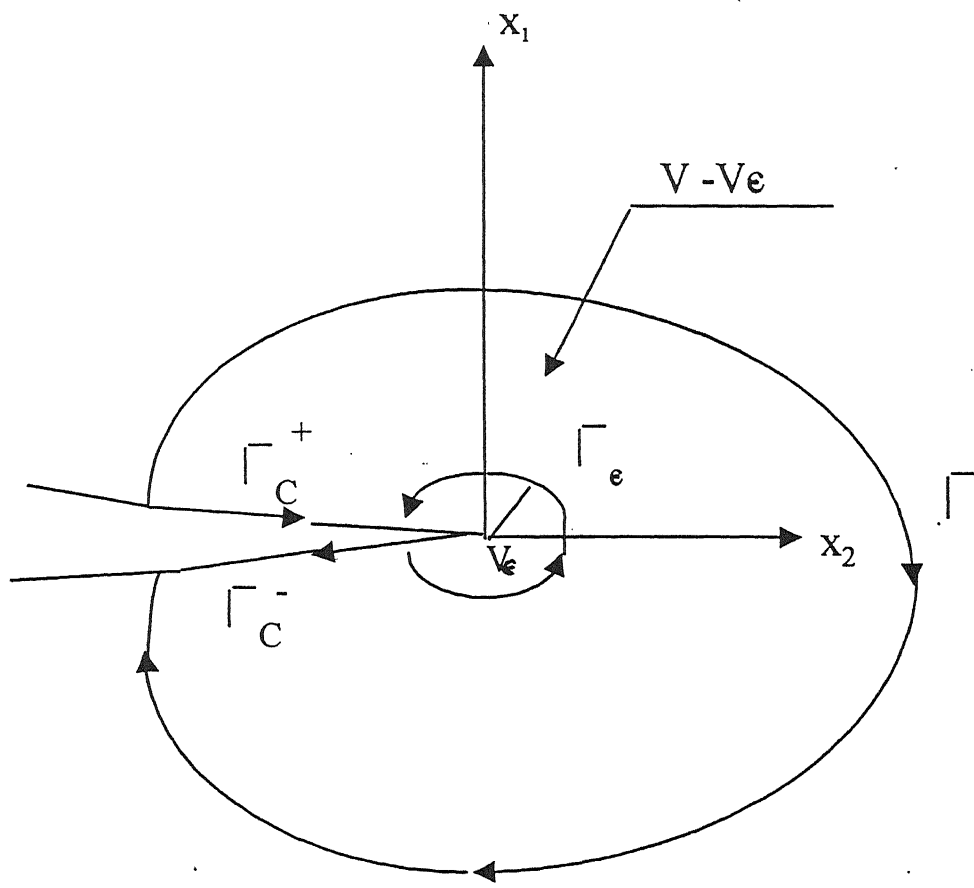


Fig 3.2:Contour for J-Integral

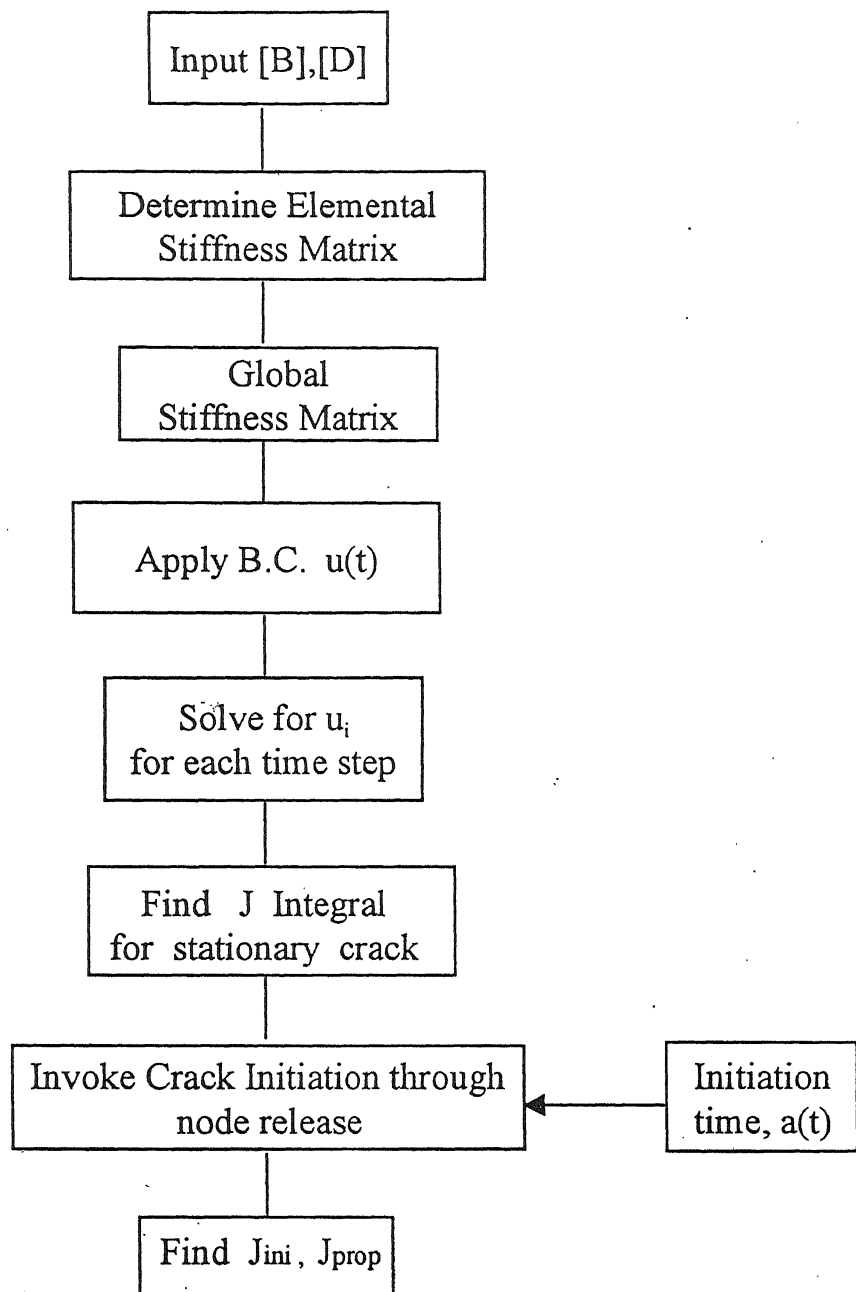
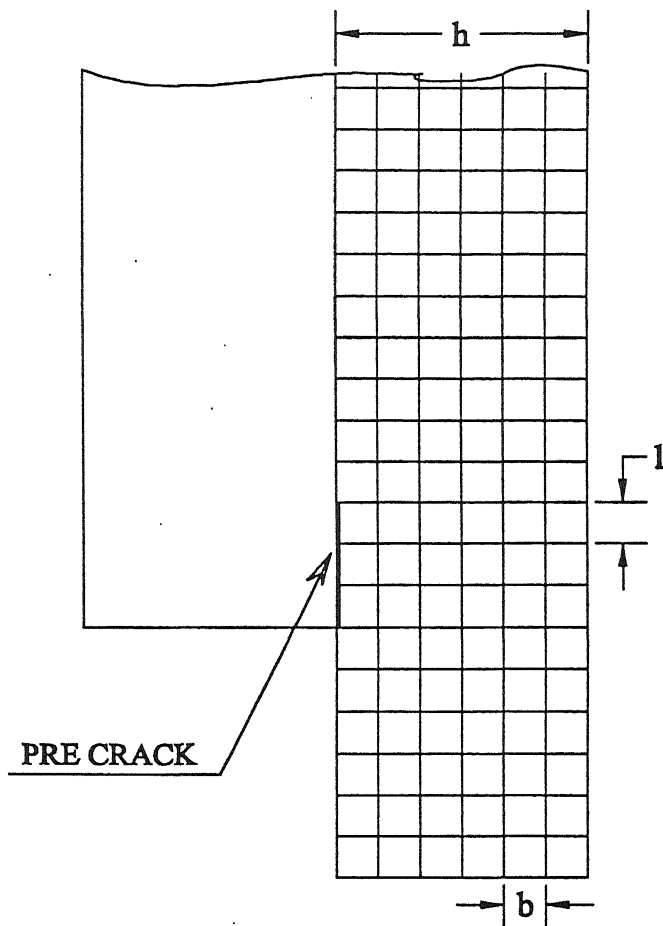


Figure 3.3: Flow chart of FE code



	1	b
THICK SPECIMEN ($h=3.5\text{mm}$)	$h/10$	$h/(10/1.125)$
THIN SPECIMEN ($h=2.0\text{mm}$)	$h/10$	$h/5$

Fig 3.4 : Mesh Generation

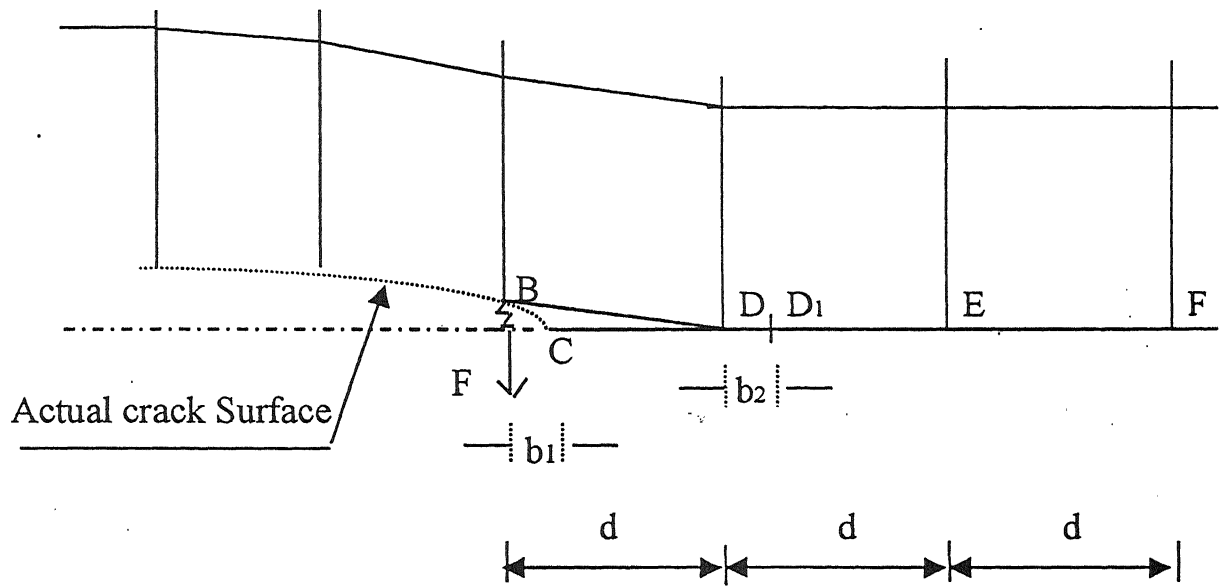


Figure 3.5: Crack opening scheme

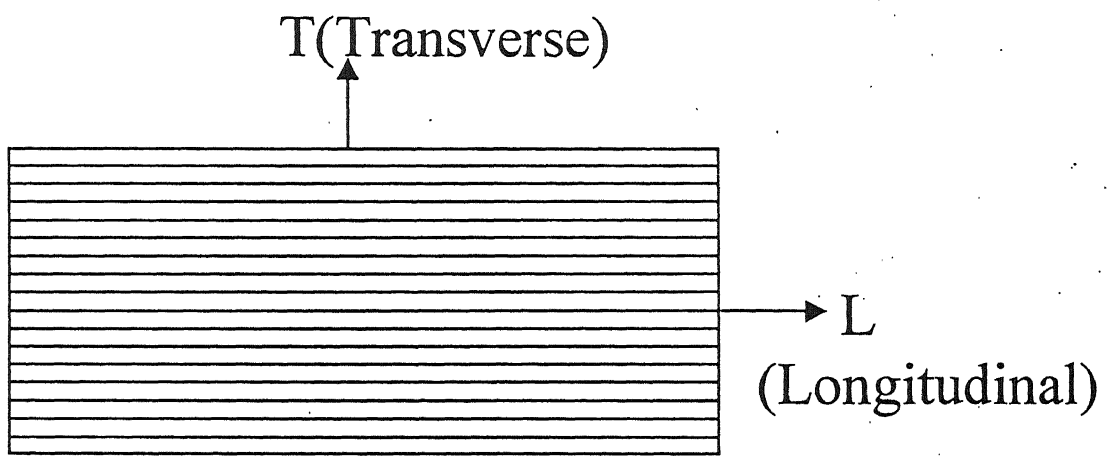


Figure 3.6: Principal directions of the specimen

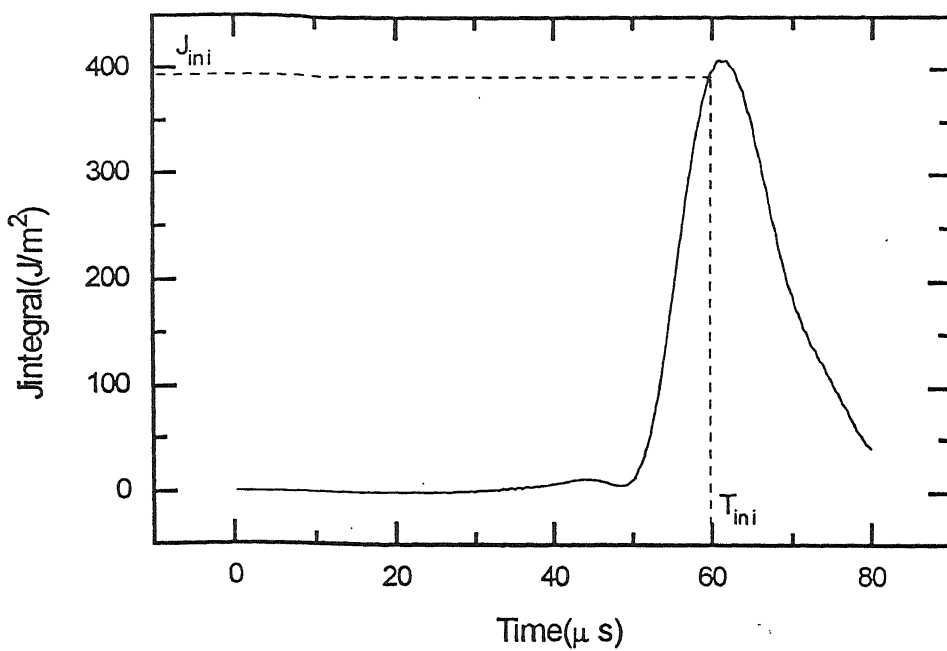


Fig.3.7: A typical variation of J-integral for stationary crack

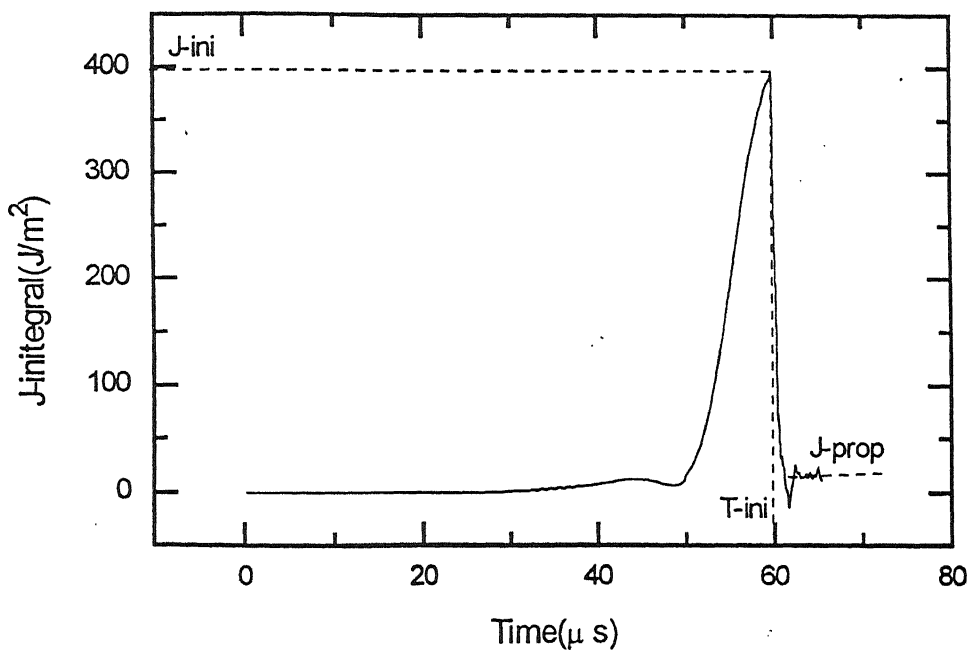


Fig.3.8: A typical variation of J-integral for propagating crack

Chapter 4

RESULTS AND DISCUSSION

4.1 Introduction

As described in Chapter 2, the experiments are performed for determining initiation and propagation toughnesses of unidirectional GFRP laminates. The experimentation yields following inputs to simulate stress wave propagation inside the specimen and to evaluate \hat{J} -integral;

1. Deflection history of cantilever-end,
2. Crack initiation time, and
3. Crack velocity.

As elucidated in Section 2.3.3, incident and reflected stress pulses give particle velocity of load bar end; with integration it yields displacement history of the load-bar-end. The cantilever-plate-end deflection is same as that of load-bar-end, since it is screwed to the cantilever plate. The velocity strain gauge responses, as recorded in the digital storage oscilloscope yield the crack velocity. By extrapolating the crack propagation velocity to precrack length, initiation time is calculated.

The present chapter presents results obtained by finite element code and compares dynamic interlaminar toughness with quasistatic interlaminar toughness.

4.2 Dynamic Interlaminar Initiation Fracture Toughness

Initiation fracture toughness is the fracture resistance of the material under dynamic loading conditions for a specific crack length and specified boundary conditions. Interlaminar initiation fracture toughness represents the toughness of the material when the interlaminar crack begins to propagate.

In the present study, two types of specimen as explained in Chapter 2 are used. The specimens having thickness 3.5 - 4.5 mm are being called as thin specimens and the specimens having thickness 6.0 - 7.5 mm are being called as thick specimens. In the present Chapter, results of experimental and FE analysis for 5 thin specimens and 9 thick specimens are presented.

4.2.1 Initiation toughness for thin specimens

The details of experimental measurements for the five experiments A1 to A5 are shown in Table 4.1. Experiment A1 is described in detail; other experiments being similar are presented only briefly.

CENTRAL LIBRARY
I.I.T., KANPUR
132016

Table 4.1 : Experimental measurements for Expt.A1 to A5.

Expt. No.	Cantilever Thickness (mm)	Specimen Width (mm)	Prcrack Length (mm)	Strain gauge locations	
				SG1 (mm)	SG2 (mm)
A1	1.8	25.0	45.0	46.5	49.8
A2	1.6	25.0	36.5	38.0	41.6
A3	2.1	25.0	39.9	41.3	44.8
A4	2.1	25.1	40.3	41.7	45.2
A5	2.1	25.0	39.8	41.4	45.7

Experiment A1

In Experiment A1, the GFRP specimen is prepared with a unsharpened precrack length of 41.0 mm. The oscilloscope records the responses of the load bar strain gauges and velocity strain gauges as shown in Fig. 4.1a. The load bar strain gauges record the incident and reflected pulses. Figure 4.1b shows the zoomed view of the oscilloscope record. The duration of each square pulse is nearly 130 μ s. From these pulses the velocity history (Fig. 4.2) of the load bar end is determined using one dimensional wave propagation theory as explained in Section 2.3.2. By integrating the velocity history, the displacement history (Fig. 4.3) is obtained. Since the cantilever end of the specimen is screwed to the load bar, the cantilever-end displacement history is same as that of the load-bar-end. The actual loading on the specimen starts at the mid point of the head of the incident pulse and head of the reflected pulse. This is denoted as 'T - ref' as shown in Fig. 4.1a.

The crack velocity strain gauge gives a peaked strain when the crack tip crosses the strain gauge. A blown up view of the two strain gauge responses for determining velocity of crack tip is shown in Fig. 4.4. Initiation time (T_i) is the actual time with respect to

' $T - \text{ref}$ ' when the crack tip crosses the first strain gauge. T_2 is the corresponding time for second strain gauge. Knowing the time interval ($T_1 - T_2$) between the corresponding peaks of the two strain gauges and the separation distance of the two velocity strain gauges already measured, crack velocity is calculated. The velocity of crack propagation comes out to be 1650 m/s . The first strain gauge is bonded 1.5 mm away from the crack tip. Actual crack initiation time is obtained by extrapolating crack length vs. time plot linearly to precrack length (Fig. 4.5). Initiation time T_{ini} for the first experiment comes out to be 56 μs .

The FE code as explained in Chapter 3, is invoked with displacement and initial boundary conditions. The FE program is executed for the stationary crack and the variation of \hat{J} - integral with time is obtained as shown in Fig. 4.6. It is observed from the Fig. 4.6 that the \hat{J} - integral increases to a certain value and starts decreasing; it decreases to almost zero value and again increases later to a larger value. This happens because the nature of the loading pulse is reversed when it starts reflecting from the crack tip. This pulse again reflects from the loading end and the \hat{J} - integral again starts increasing. If the \hat{J} - integral corresponding to the first peak is not sufficient to grow the crack, then the crack will open only after the \hat{J} - integral value shows an increasing trend again and exceeds the previous peak value.

Now the FE program is executed for the propagating crack. The \hat{J} - integral record obtained is shown in Fig. 4.6. As discussed earlier, when the cantilever-end is loaded, the stress waves start propagating towards the crack tip. After sometime (depending upon the crack length), the stress intensity at the crack tip (\hat{J} - integral) starts increasing as shown in Fig. 4.6. When \hat{J} - integral attains a certain value, the crack initiation occurs. The value of \hat{J} - integral corresponding to this time (initiation time) is defined as the initiation toughness (\hat{j}_{ini}). The value of \hat{j}_{ini} for Expt.A1 comes out to be $67 J/m^2$.

Experiments A2 - A5

Four more experiments were conducted on the thin specimens and details of the results obtained are given in Table 4.2.

Table 4.2 : Precrack length, time of peak strain at different strain gauges, initiation time and initiation toughness for Expt. A1 to A5.

Expt. No.	Pprecrack Length (mm)	SG1 from Cracktip (mm)	SG2 from Cracktip (mm)	Strain gauge peak response		Initiation Time μs	\hat{J}_{ini} J/m^2
				SG1 (mm)	SG2 (mm)		
A1	45.0	1.5	4.8	57.0	59.0	56.0	67
A2	36.5	1.5	5.1	44.0	48.0	42.0	22
A3	39.9	1.4	4.9	62.5	65.5	61.5	32
A4	40.3	1.4	4.9	45.0	47.0	44.0	22
A5	39.8	1.6	5.9	61.5	64.5	60.0	119

Oscilloscope records, velocity records of load bar end, displacement records of cantilever end and \hat{J} -integral records for stationary and propagating crack for Expt. A2 to A5 are presented in Appendix 1.

From the results, it is clear that \hat{J}_{ini} for thin specimen varies from $22 J/m^2$ to $119 J/m^2$ for crack velocity ranging between $900- 1750 m/s$.

4.2.2 Initiation toughness for thick specimens

The details of the experimental measurements for the ten experiments from B1 to B9 are shown in Table 4.3. The details of strain gauge peak response time, initiation time, crack velocity and initiation toughness (\hat{J}_{ini}) are given in Table 4.4.

Table 4.3 : Experimental measurements for Expt.B1 to B9.

Expt. No.	Cantilever Thickness (mm)	Specimen Width (mm)	Precrack Length (mm)	Strain gauge locations	
				SG1 (mm)	SG2 (mm)
B1	3.2	25.1	40.0	41.2	44.4
B2	3.2	25.0	40.7	42.4	46.3
B3	3.2	25.1	43.5	45.2	49.7
B4	4.0	25.2	41.0	43.0	47.3
B5	3.2	25.0	42.3	44.3	48.6
B6	3.7	25.1	44.2	46.2	50.2
B7	3.0	25.0	39.7	41.2	44.6
B8	3.1	25.0	40.4	42.5	47.4
B9	3.2	25.0	40.2	42.0	45.0

Table 4.4 : Precrack length, time of peak strain at different strain gauges, initiation time and initiation toughness for Expt. B1 to B9.

Expt. No.	Pprecrack Length (mm)	SG1 from Cracktip (mm)	SG2 from Cracktip (mm)	Strain gauge peak response		Initiation Time μs	\hat{J}_{ini} J/m^2
				SG1 (mm)	SG2 (mm)		
B1	40.0	1.2	4.4	46.0	51.0	44.0	217
B2	40.7	1.7	5.6	55.5	57.5	54.0	94
B3	43.5	1.7	6.2	57.0	60.0	56.0	132
B4	41.0	2.0	6.3	59.0	69.0	55.0	590
B5	42.3	2.0	6.3	51.5	55.5	50.0	46
B6	44.2	2.0	6.0	62.0	65.0	60.0	395
B7	39.7	1.5	4.9	59.5	67.5	56.0	270
B8	40.4	2.1	7.0	58.0	61.0	56.0	550
B9	40.2	1.8	4.8	58.0	62.0	56.0	440

The corresponding records of Expt. B1 to B9 are presented in Appendix 1. From the results it is clear that \hat{J}_{ini} for thick specimen varies from $46 J/m^2$ to $590 J/m^2$ for crack velocity ranging between 487 - $1700 m/s$.

4.3 Dynamic Interlaminar Propagation Fracture Toughness

After the initiation time, the crack starts propagating. \hat{J} -integral record after the initiation time yields propagation fracture toughness (\hat{J}_{prop}). For evaluating \hat{J}_{prop} , finite element algorithm is called for crack propagation analysis after the initiation time. The

results of Expt.A1 are discussed in detail and for other experiments are presented briefly.

4.3.1 Propagation toughness for thin specimens

Experiment A1

Once the FE code is executed upto the time of crack initiation, then the crack propagation module is called. The advancement of crack in each iteration is to be known so that an appropriate factor can be applied to the holding back force for modelling the crack propagation. The advancement of crack in each iteration is calculated, as discussed in Section 4.2.1, by a straight line fitted through the data points of peak response of the velocity strain gauges. With the load input and the crack propagation data, the FE analysis determines the stress/strain field in the specimen in successive time steps. Using this, the variation of \hat{J} - integral with time is obtained as shown in Fig. 4.7. In the inception, the crack remains stationary and \hat{J} - integral increases. A stage is reached at the initiation time when the crack starts growing under the given dynamic displacement boundary conditions. The computer code provides the \hat{J} - integral for the measured crack velocity. Figure 4.8 shows the zoomed view of \hat{j}_{prop} . It is visible that the drop in \hat{J} - integral at initiation time is very sharp and substantial. Figure 4.8 shows the zoomed view of \hat{j}_{prop} . For Expt.A1 the value of \hat{J} -integral for the propagating crack varies between $7 - 10 \text{ J/m}^2$. A few seconds after T_{ini} , \hat{J} is stabilized. This stabilized \hat{J} -integral value is taken as \hat{J}_{prop} and it comes out to be 8 J/m^2 for Expt. A1.

The fast drop in the \hat{J} - integral value as the crack starts moving, occurs because a large amount of energy is consumed to accelerate the crack. The faster the crack speed, the more is the radiated kinetic energy and the bigger is the drop in the \hat{J} - integral value. If the crack velocity is constant then the \hat{J} - integral starts increasing after initial drop

because the input energy is increasing but the energy required to drive the crack is negligible. If the crack velocity keeps on increasing after the initiation, more and more energy is required to accelerate the crack and the \hat{J} - integral will decrease further. On the other hand, with decreasing crack velocity the energy required to move the crack is less and hence the \hat{J} - integral remains almost constant or increases depending upon the energy input.

Figure 4.8 shows that there are oscillations of low magnitude superposed on the stabilized behaviour. Two reasons are being attributed to this oscillatory behaviour of the \hat{J} -integral after the initiation time;

- (1) The free surfaces of the specimen are very close to the cracktip. In fact the propagation time for some stress waves to emanate from the crack tip and return to the tip as smaller as $3-6\mu s$. The superposition of these waves and their effect on \hat{J} -integral would provide oscillation.
- (2) In the Finite Element Modelling, the crack tip is moved from one point to other point by decreasing the holding back force linearly. Thus the FE code may not be simulating the crack propagation behaviour very accurately. Some improvement in the direction of better modelling may decrease the noisy fluctuations.

Experiments A2 to A5

The records for \hat{J}_{prop} for Expt. A1 to A5 are shown in Fig. 4.9. The average crack velocity, initiation toughness (\hat{J}_{ini}) propagation toughness (\hat{J}_{prop}) for Expt. A1 to A5 are given in Table 4.5

Table 4.5 : Crack velocity, initiation toughness (\hat{J}_{ini}) and propagation toughness (\hat{J}_{prop}) for Expt. A1 to A5.

Expt. No.	Cantilever Thickness (mm)	Precrack Length (mm)	Crack velocity m/s	\hat{J}_{ini} J/m ²	\hat{J}_{prop} J/m ²
A1	1.8	45.0	1650	67	8
A2	1.6	36.5	900	22	7
A3	2.1	39.9	1166	32	6
A4	2.1	40.3	1750	22	5
A5	2.1	39.8	1433	119	8

It is clear that \hat{J}_{prop} for thin specimens is varying between 5 and 8 J/m² for crack speed ranging in 900-1750 m/s.

4.3.2 Propagation toughness for thick specimen

The zoomed views of \hat{J}_{prop} for Expt. B1 to B9 are shown in Fig. 4.9 The average crack velocity, initiation toughness (\hat{J}_{ini}) propagation toughness (\hat{J}_{prop}) for Expt. B1 to B9 are given in Table 4.6

Table 4.6 : Crack velocity, initiation toughness (\hat{J}_{ini}) and propagation toughness (\hat{J}_{prop}) for Expt. B1 to B9.

Expt. No.	Cantilever Thickness (mm)	Precrack Length (mm)	Crack velocity m/s	\hat{J}_{ini} J/m ²	\hat{J}_{prop} J/m ²
B1	3.2	40.0	980	217	6.0
B2	3.2	40.7	1700	94	6.5
B3	3.2	43.5	1334	132	6.0
B4	4.0	41.0	430	590	25.0
B5	3.2	42.3	1075	46	10.0
B6	3.7	44.2	1500	395	16.0
B7	3.0	39.7	487	270	22.0
B8	3.1	40.4	1060	550	30.0
B9	3.2	40.2	1300	440	30.0

4.4 Comparison of Dynamic Interlaminar Fracture Toughness with Quasistatic interlaminar Fracture Toughness

Four experiments to determine the quasistatic interlaminar toughness (G_{Ic}) of thin specimen and three experiments to determine the same for the thick specimen are performed. Table 4.7 and 4.8 give the value of average quasistatic interlaminar toughness (G_{Ic}) obtained for thin and thick specimens respectively.

Table 4.7 : Quasistatic Interlaminar Toughness (G_{Ic}) for thin specimens

Expt. No.	Quasistatic Interlaminar Toughness, G_{Ic} J/m^2	Average Quasistatic Interlaminar Toughness J/m^2
P1	419	
P2	389	432
P3	457	
P4	466	

Table 4.8 : Quasistatic Interlaminar Toughness (G_{Ic}) for thick specimens

Expt. No.	Quasistatic Interlaminar Toughness, G_{Ic} J/m^2	Average Quasistatic Interlaminar Toughness J/m^2
Q1	580	
Q2	620	613
Q3	638	

It is observed that average quasistatic interlaminar toughness (G_{Ic}) of thin and thick specimens are 432 J/m^2 and 613 J/m^2 . These values are significantly higher than the values obtained for the initiation fracture toughnesses for both the specimens.

4.5 Discussion

In this study, fourteen experiments have been presented. Expt. A1 to A5 are for thin specimen and Expt. B1 to B9 are for thick specimen. The variation of \hat{J}_{ini} with the

of plies is enhance in the laminates used in the present study.

(2) Ramakrishna used to sharpen the precrack tip of the specimen before conducting the experiments. Due to this, the chances of crack front to be inclined to the axis of the specimen were high while in an ideal case the crack front has to be normal to the axis of the specimen. In the present study, the as cast unsharpened precrack is used so the crack front remains normal to the axis of the specimen.

(3) Ramakrishna used strain gauges of FLA series which are not suited to heterogenous composite laminates. In the present work BFLA series strain gauges are used which are specially designed for composite laminates.

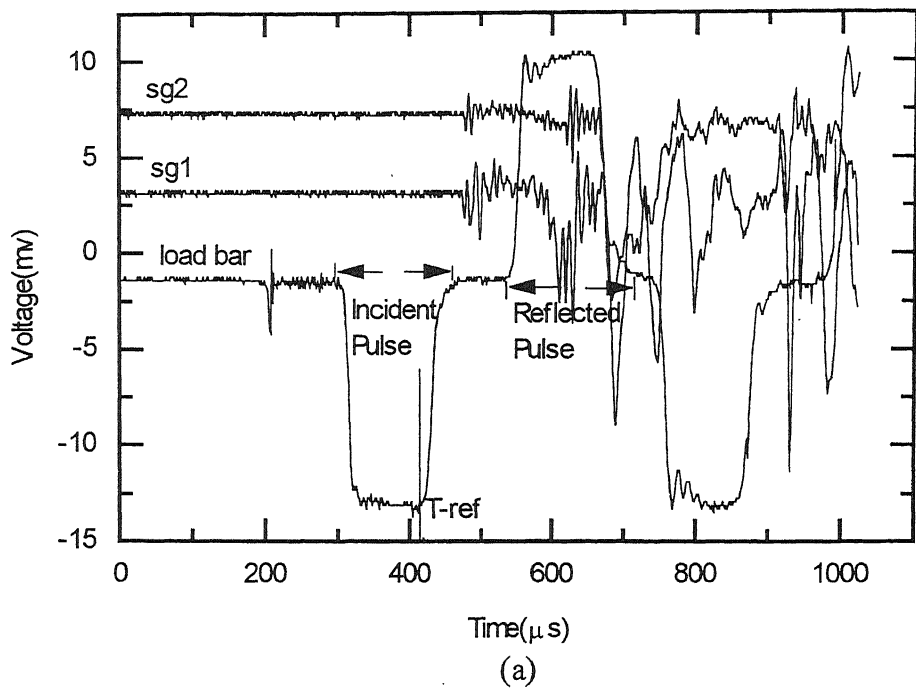
4.5.2 Comparison with Babu & Mallikharjuna's work

The laminates used by Babu & Mallikharjuna were prepared through almost the same cold technology as in the present study. In their work, the quasistatic interlaminar toughness is 1055 J/m^2 , average initiation toughness is 342 J/m^2 and average propagation toughness is 65 J/m^2 . The comparison of \hat{J}_{ini} and \hat{J}_{prop} of present work to the Babu & Mallikharjuna's work are shown in Fig. 4.15 and Fig. 4.16 respectively.

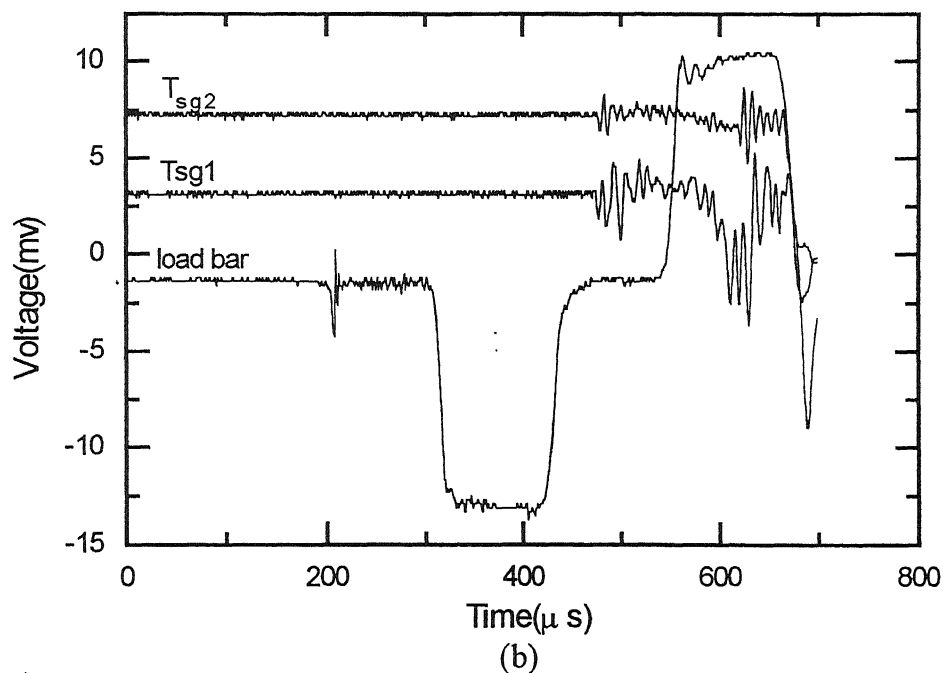
The reason for the values of \hat{J}_{ini} and \hat{J}_{prop} in the present study to be lower than that of Babu & Mallikharjuna's study may be justified on the grounds that the quasistatic interlaminar toughness in the present study is also lower than that of Babu & Ramakrishna's study. This difference in the values of quasistatic interlaminar toughnesses is due to some difference in the technique of the specimen preparation used in the present study and the Babu & Mallikharjuna's study.

4.6 Closure

The present Chapter presents the record of \hat{J} -integral obtained through FE analysis using experimental data on GFRP laminates. The average interlaminar quasistatic toughnesses for the thin and thick specimens are 432 J/m^2 and 613 J/m^2 respectively. The initiation toughness (\hat{J}_{ini}) and propagation toughness (\hat{J}_{prop}) for the thin specimen are in the range of $22 - 119 \text{ J/m}^2$ and $5 - 8 \text{ J/m}^2$ respectively for the crack velocity ranging between $900-1750 \text{ m/s}$. The initiation toughness (\hat{J}_{ini}) and propagation toughness (\hat{J}_{prop}) for the thick specimen ranges in $46 - 590 \text{ J/m}^2$ and $6 - 30 \text{ J/m}^2$ respectively for the crack velocity ranging between $430-1700 \text{ m/s}$.



(a)



(b)

Fig. 4.1(a): Oscilloscope Record and,
 (b): Zoomed View of Oscilloscope Record for Expt. A1

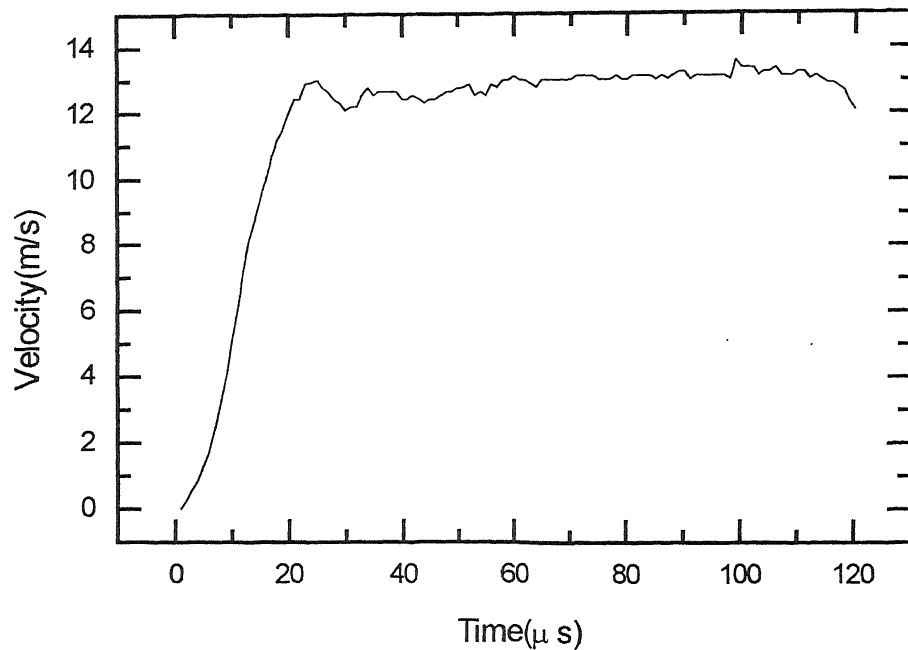


Fig4.2: Velocity Record of Load Bar End for Expt. A1

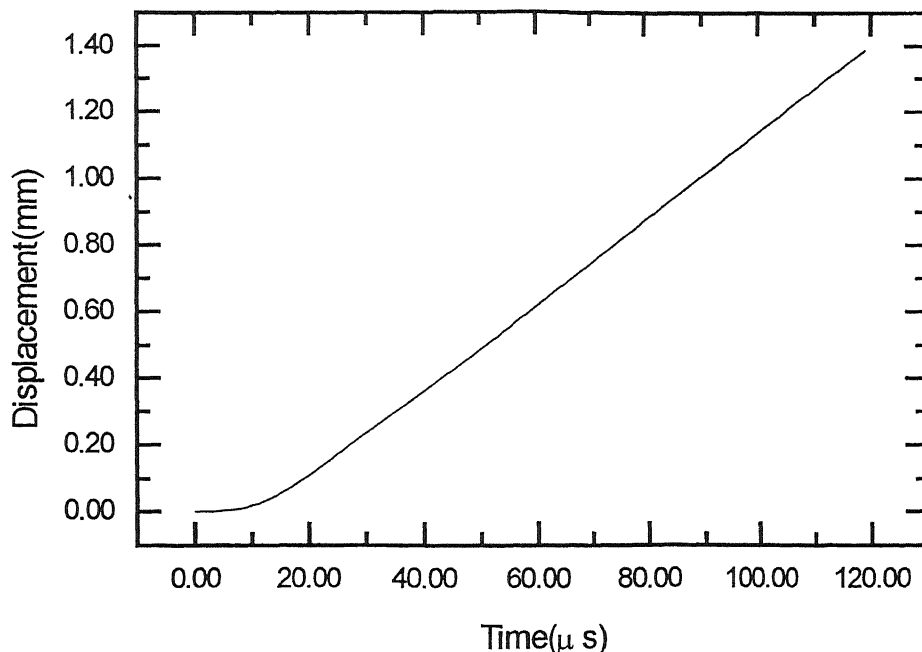


Fig.4.3: Displacement Record of Cantilever End for Expt. A1

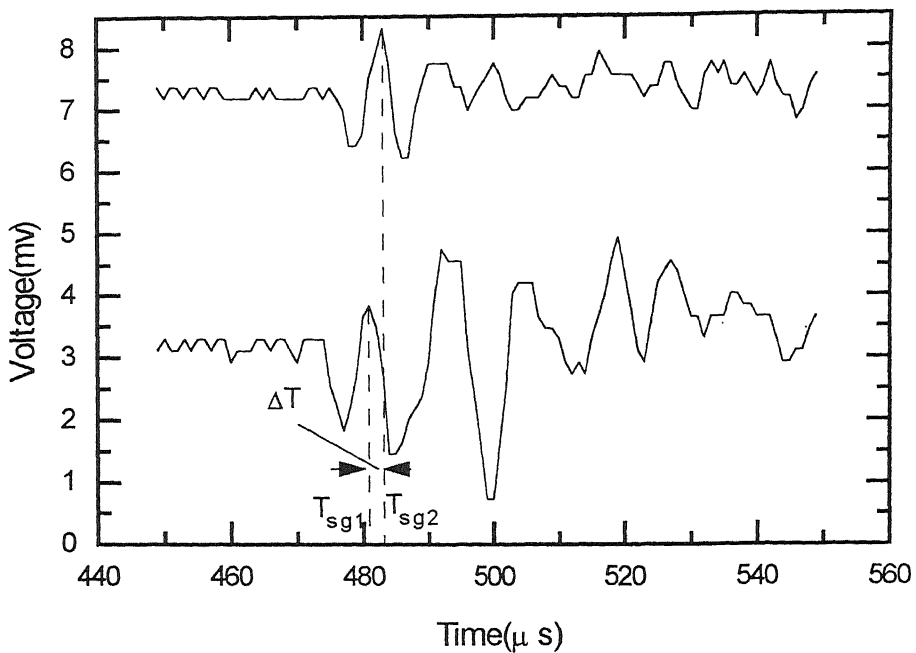


Fig.4.4: Blown up View of Peaks of Velocity Strain Gauges for Expt.A1

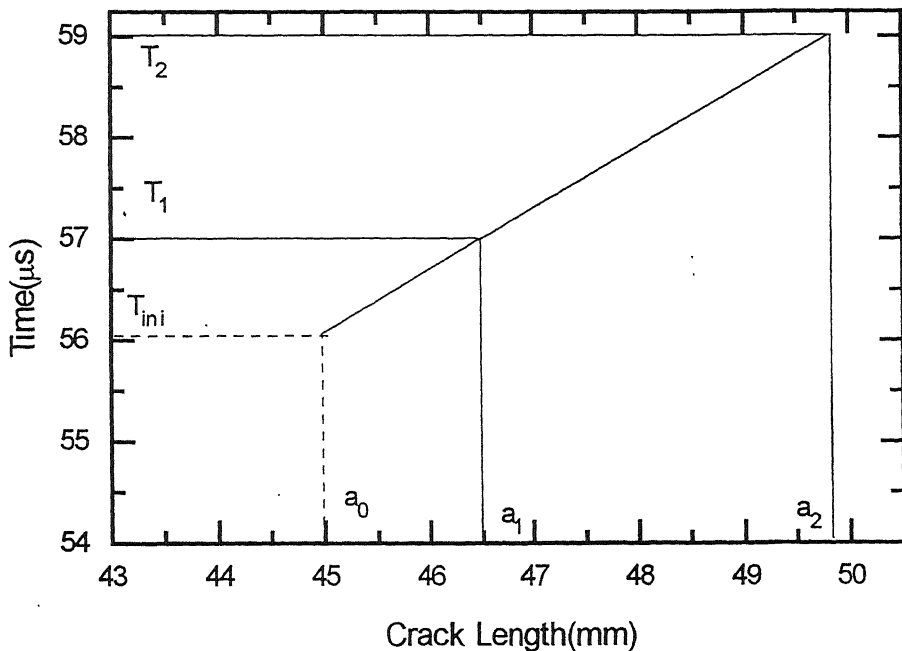


Fig.4.5: Extrapolation of Initiation Time for Expt.A1

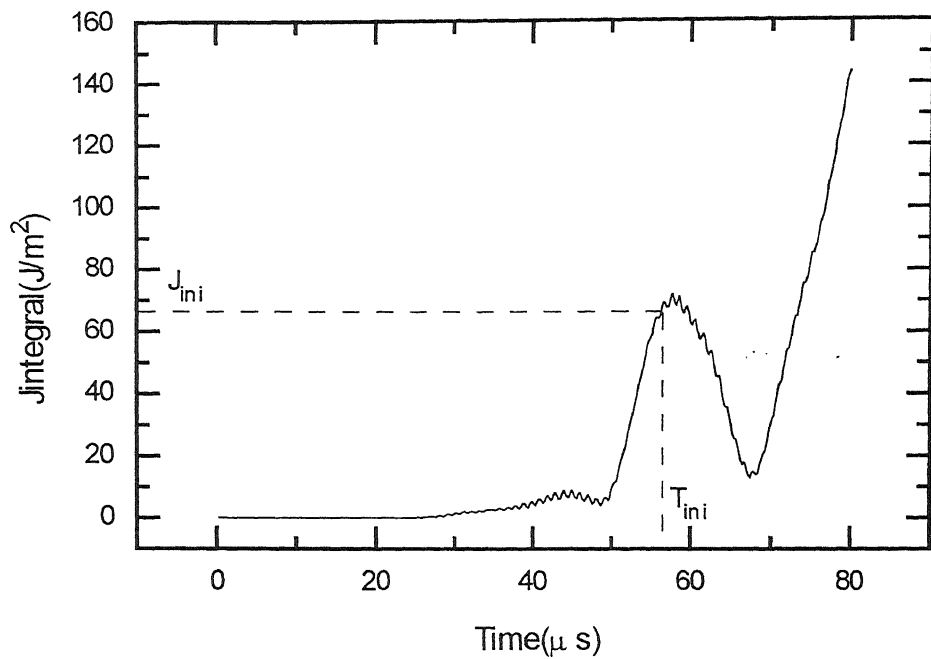


Fig.4.6: Jintegral Record for Stationary crack for Expt.A1

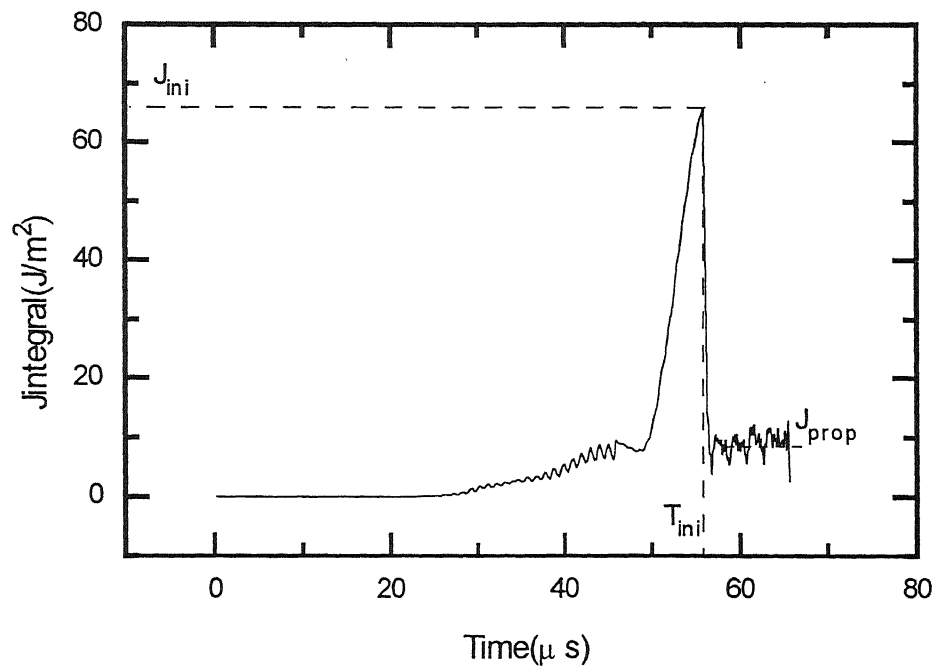


Fig.4.7: Jintegral Record for Propagating Crack for Expt.A1

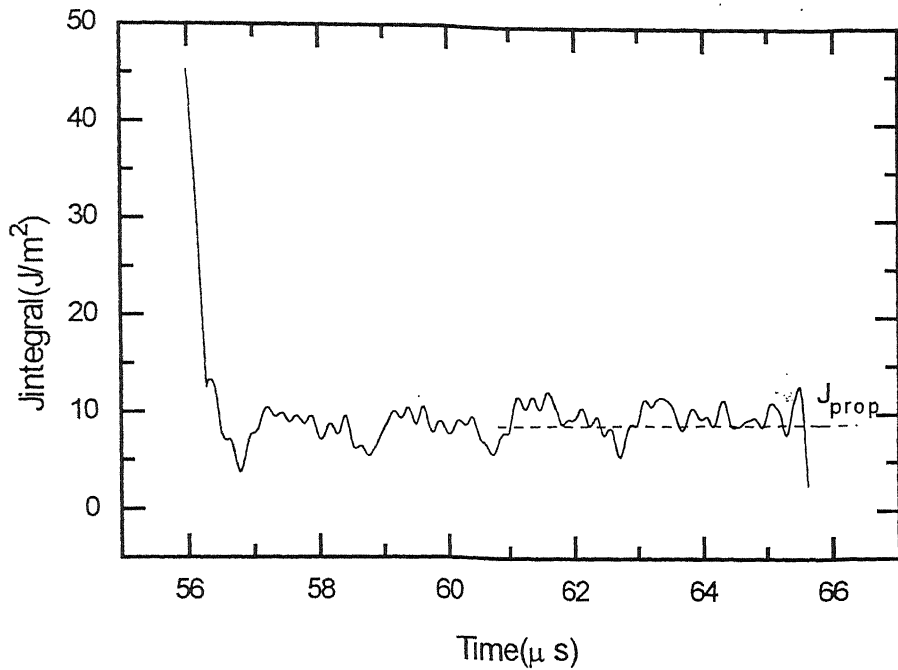
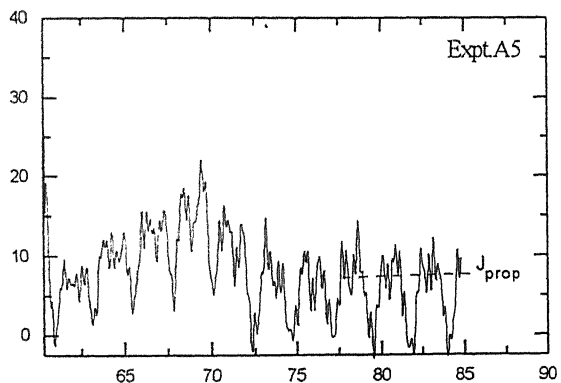
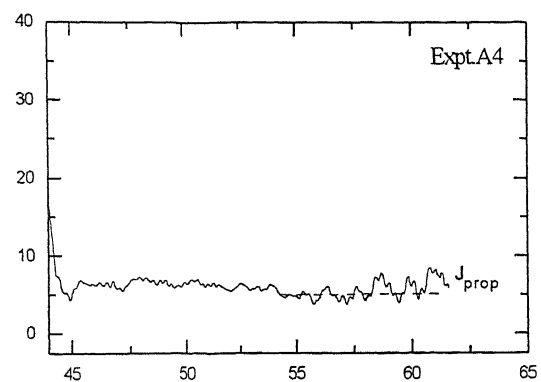
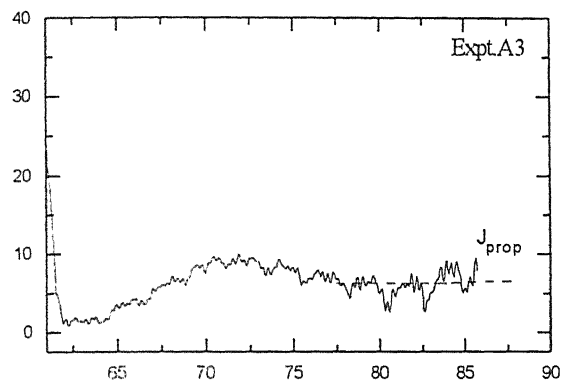
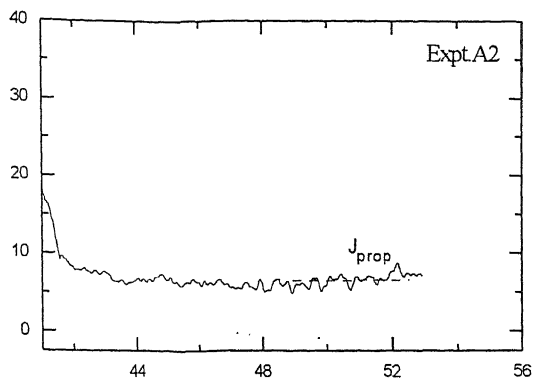
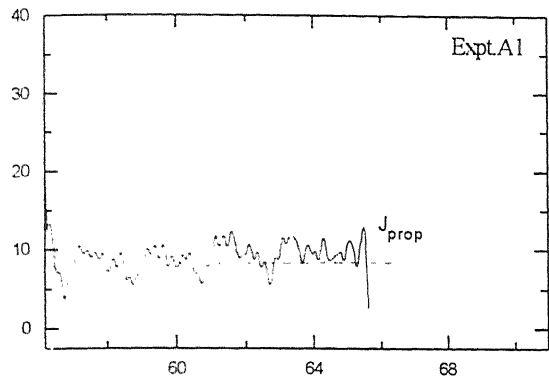
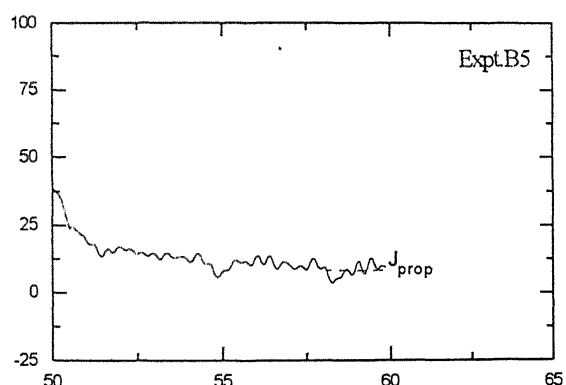
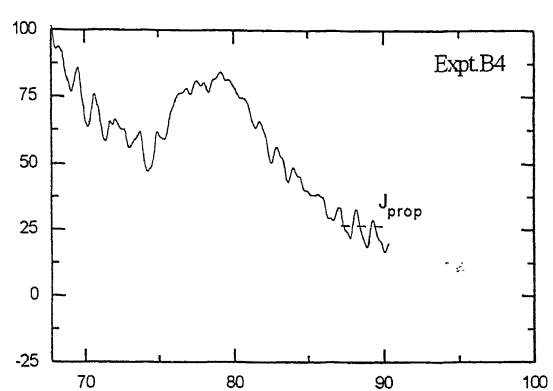
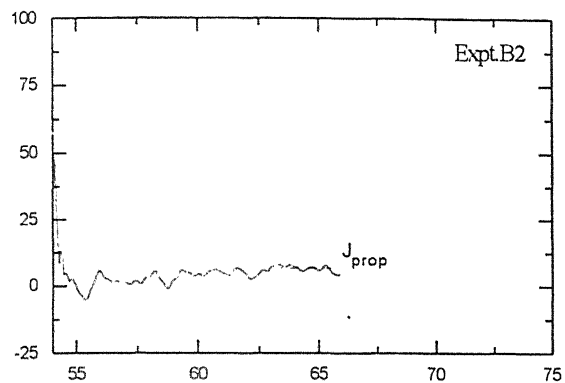
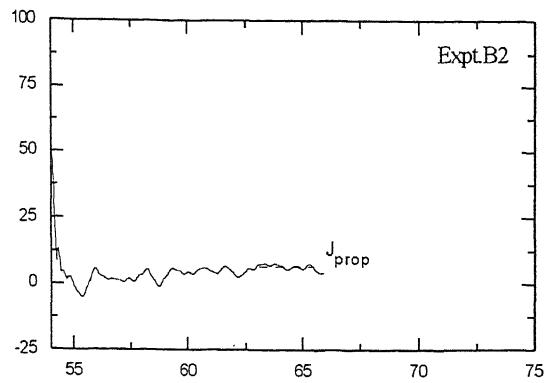
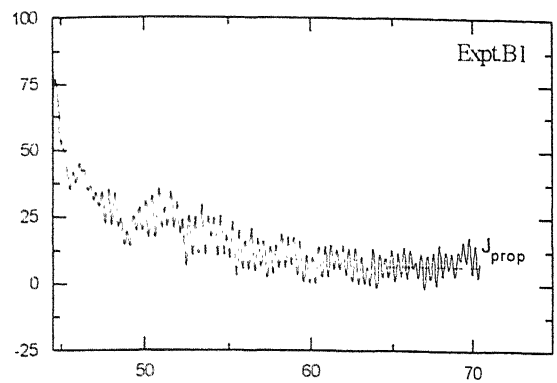


Fig. 4.8: Zoomed View of J_{prop} for Expt. A1



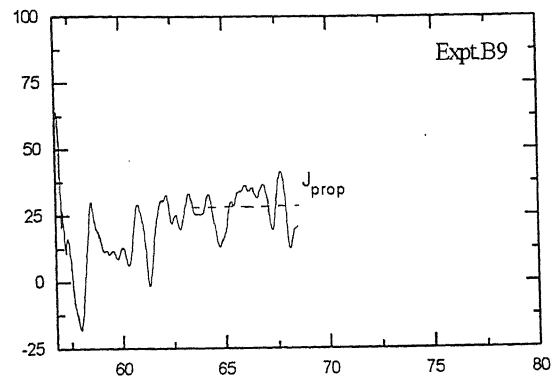
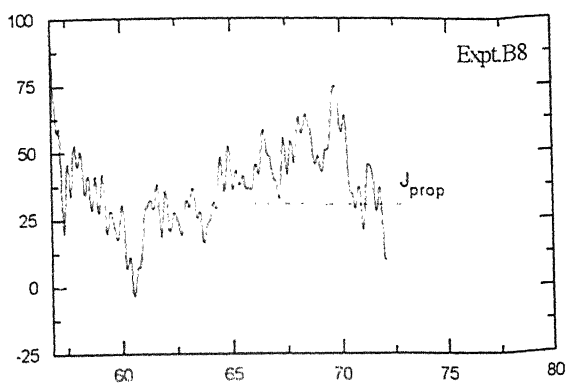
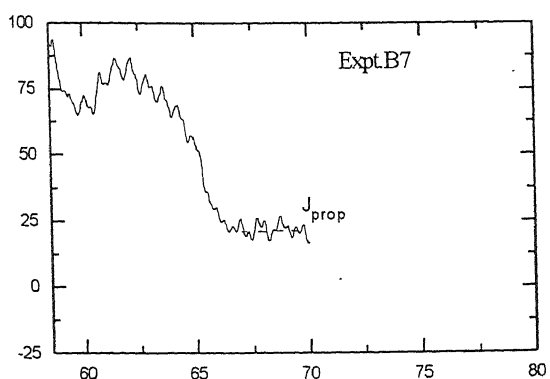
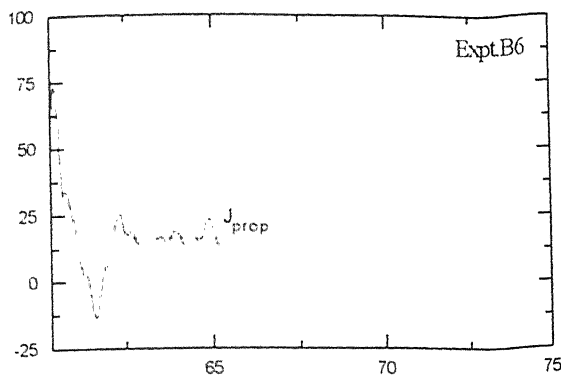
X-axis: Time(μs)
Y-axis: $\text{Jintegral}(\text{J/m}^2)$

Fig. 4.9: Zoomed views of J_{prop} for Expt1.A1 to A5.



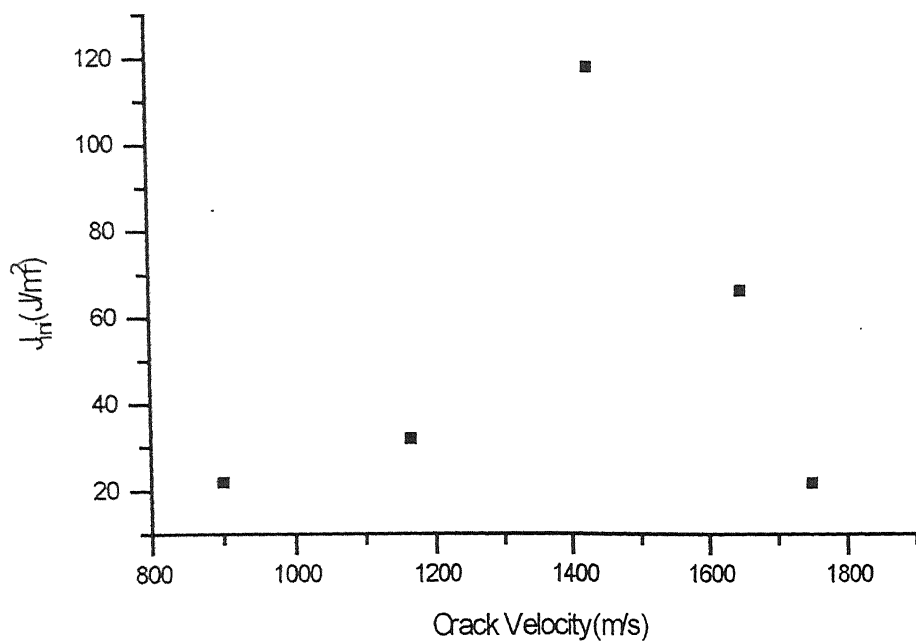
X-axis: Time(μs)
Y-axis: Jintegral(J/m^2)

Fig. 4.10a: Zoomed views of J_{prop} for Expt1.B1 to B5.

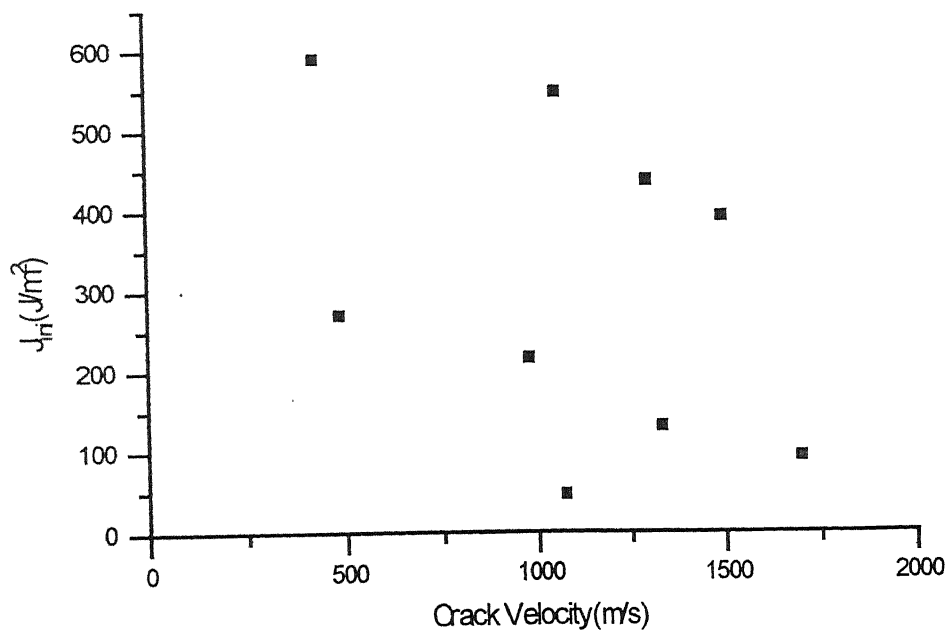


X-axis: Time(μs)
Y-axis: Jintegral(J/m²)

Fig. 4.10b: Zoomed views of J_{prop} for Expt1.B6 to B9.



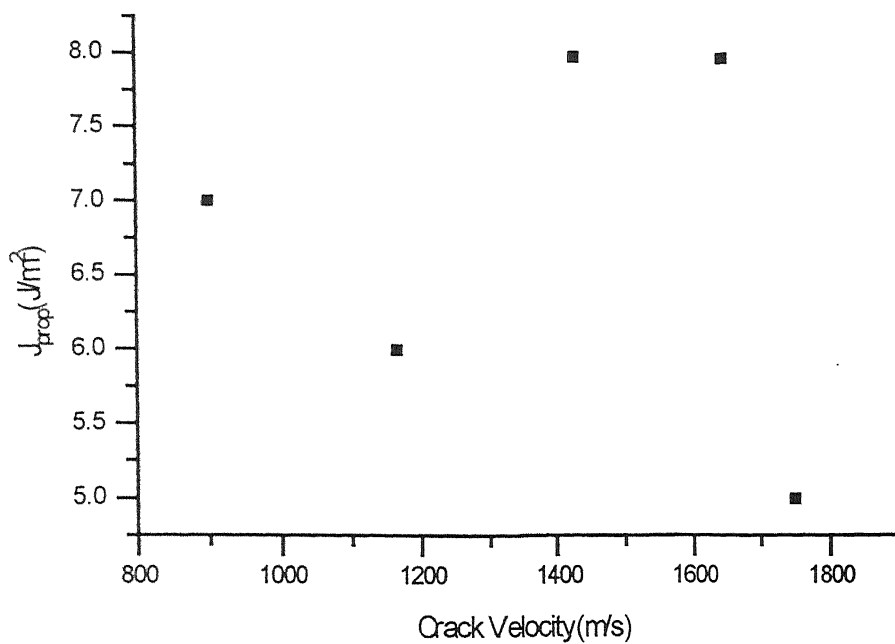
(a)



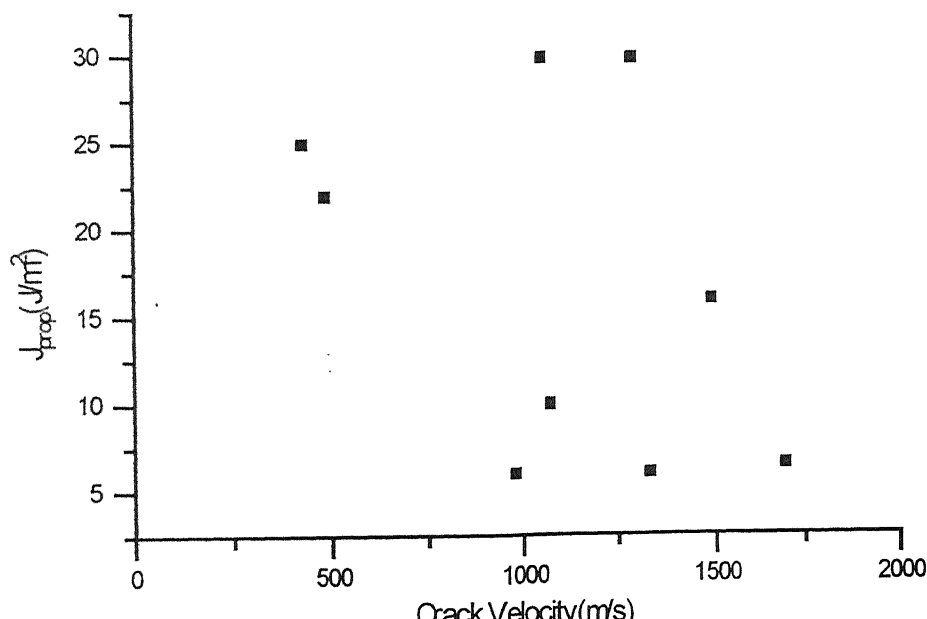
(b)

Fig. 4.11(a): Variation of J_{in} with Crack Velocity for Thin Specimen

(b): Variation of J_{in} with Crack Velocity for Thick Specimen



(a)



(b)

Fig 4.12(a): Variation of J_{prop} with Crack Velocity for Thin Specimens

(b): Variation of J_{prop} with Crack Velocity for Thick Specimens

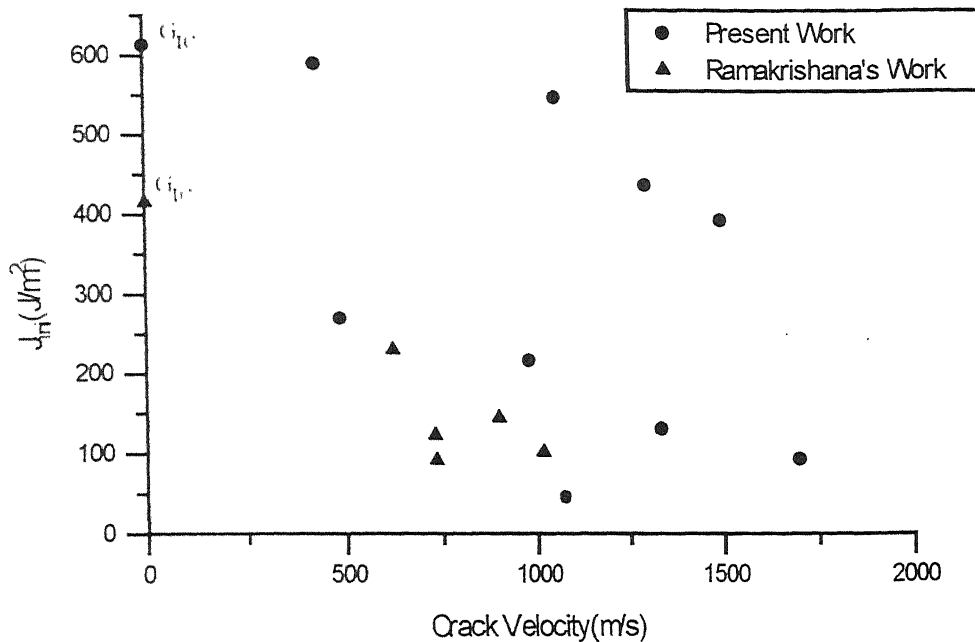


Fig. 4.13: comparison of J_{ini} for Present work and Ramakrishna's work

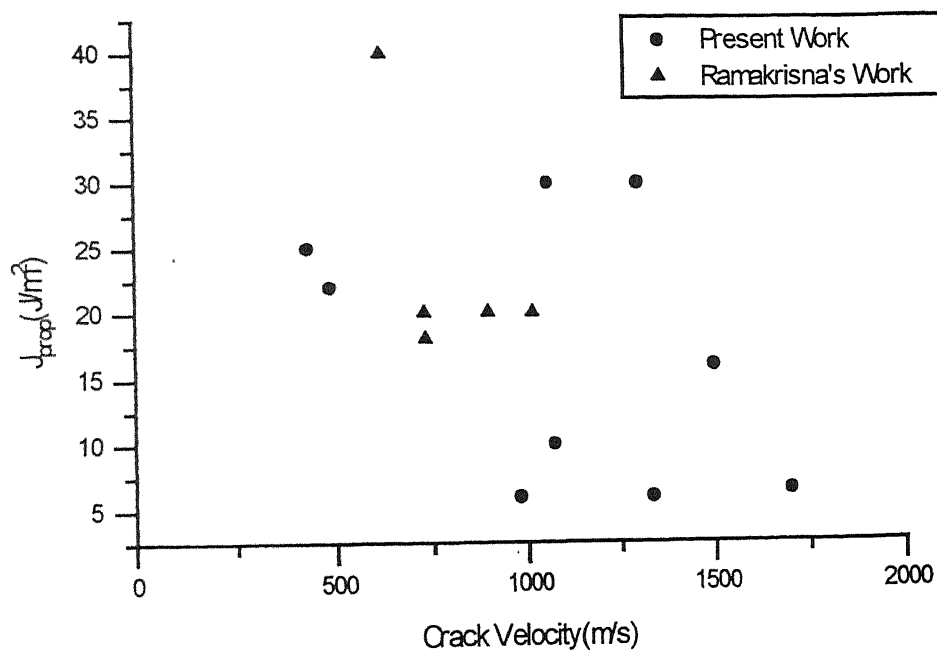


Fig. 4.14: comparison of J_{prop} for Present work and Ramakrishna's work

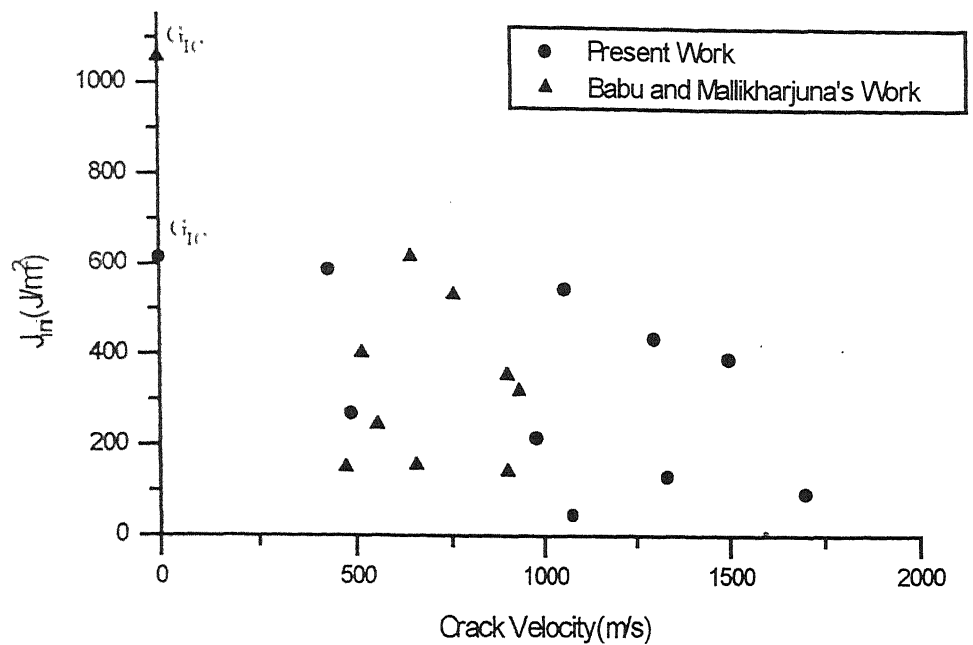


Fig 4.15: comparison of J_{inj} for Present Work and Babu & Mallikharjuna's Work

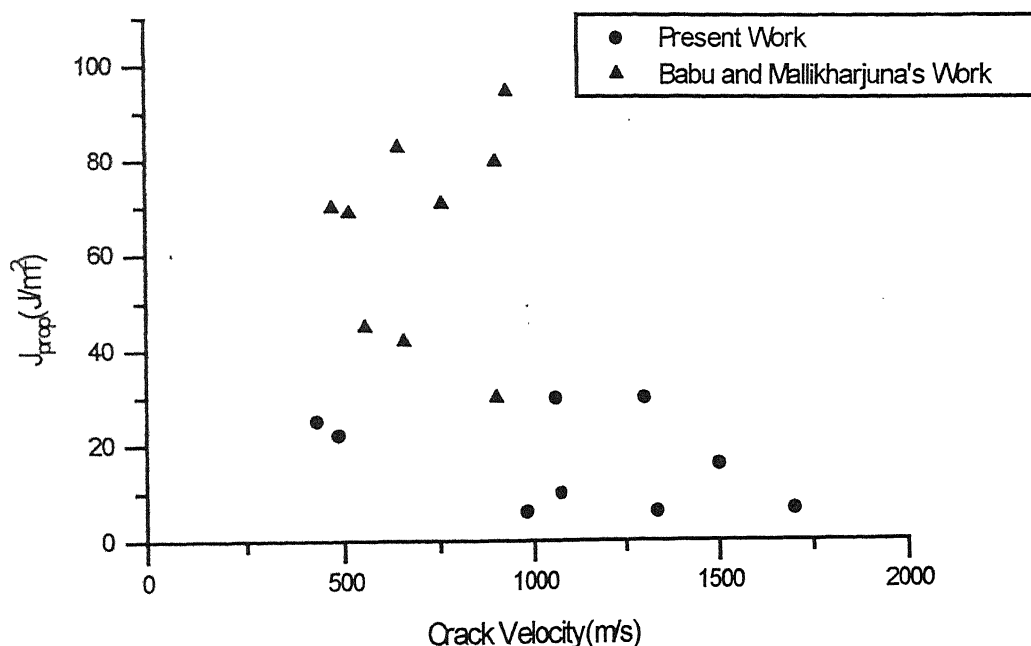


Fig 4.16: comparison of J_{prop} for Present Work and Babu & Mallikharjuna's Work

Chapter 5

CONCLUSIONS AND SCOPE FOR FUTURE WORK

5.1 Conclusions

The present work is carried on GFRP laminates for finding dynamic interlaminar toughness under impact loading by adopting the technique developed by Verma(1995). Experimentation gives (i) deflection history of cantilever-end, (ii) initiation time, and (iii) crack propagation history.

The response within the specimen after the impact is simulated using a FE code and boundary conditions determined through the experiment. After each successive time step stress and displacement fields are determined in the entire specimen. An appropriate path is chosen to find \hat{J} -integral around the crack tip. Initially the crack remains stationary and \hat{J} builds up. A stage is reached when the crack starts propagating (at initiation time); the crack growth is introduced in the numerical simulation by the gradual release of nodal forces at the crack front.

Two types of specimens are used in the present study; one about 4 mm thick and the other about 7 mm thick. The initiation toughness (J_{ini}) and propagation toughness (J_{prop}) for the 4mm thick specimen come out to be in the the range of 22-119 J/m^2 and

5-8 J/m^2 respectively for the crack velocity ranging between 900 and 1750 m/s . The initiation toughness (J_{ini}) and propagation toughness (J_{prop}) for the 7mm thick specimen come out to be in the range of 96-590 J/m^2 and 6-30 J/m^2 respectively for the crack velocity ranging between 430 and 1700 m/s .

From the present study on GFRP laminates, we can conclude the following:

- The initiation toughness (\hat{J}_{ini}) is substantially greater than the propagation toughness (\hat{J}_{prop}) for a given thickness of specimen.
- The initiation toughness (\hat{J}_{ini}) is less than the quasistatic interlaminar toughness (G_{Ic}) for a given thickness of specimen.
- A sharp and substantial drop occurs in (\hat{J}) at the crack initiation time.
- The propagation toughness (\hat{J}_{prop}) shows a decreasing trend with the increase in crack velocity.
- Both the initiation toughness (\hat{J}_{ini}) as well as the propagation toughness (\hat{J}_{prop}) decrease with the decrease in the thickness of the specimen.

5.2 Scope for Future work

- More experiments could be conducted on various thicknesses of the specimen to study the trend of dynamic interlaminar toughness with the thickness.
- More experiments could be conducted to study the effect of the crack length on the dynamic interlaminar toughness.
- From literature survey it is found that temperature is also one of the parameter, which affects the toughness of the laminates. Some more experiments can be done at different temperatures.

- Digital Oscilloscope with a capability of measuring time in smaller steps could be used to measure the crack velocity more accurately.
- Three strain gauges could be used to monitor the crack propagation so that a second degree polynomial could be fitted to the data points given by the peak responses of the velocity strain gauges. This could improve the accuracy of the results.
- A correlation between characteristics of cracked surfaces and crack velocity could be explored.

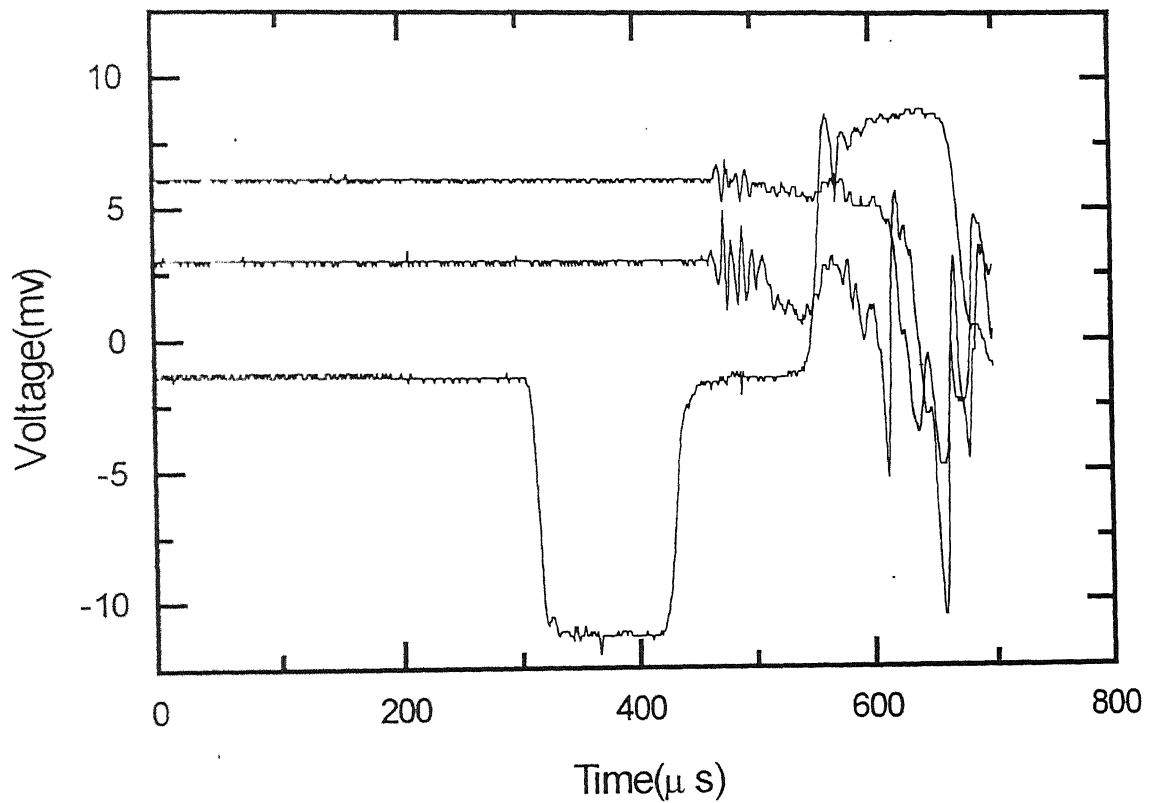


Fig.6.1a: Oscilloscope Record for Expt.A2

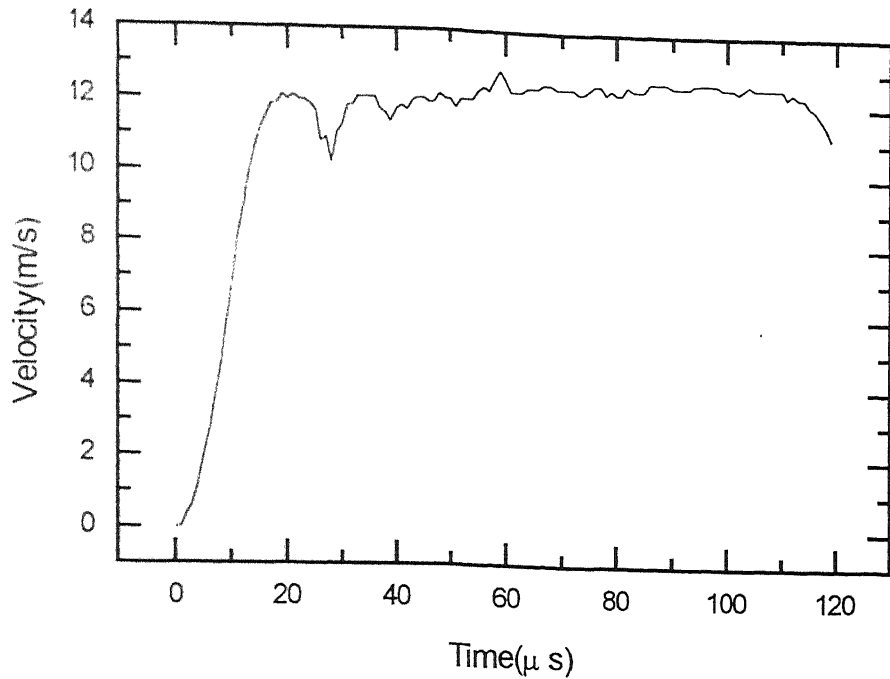


Fig. 6.1b: Velocity Record of Load Bar End for Expt. A2

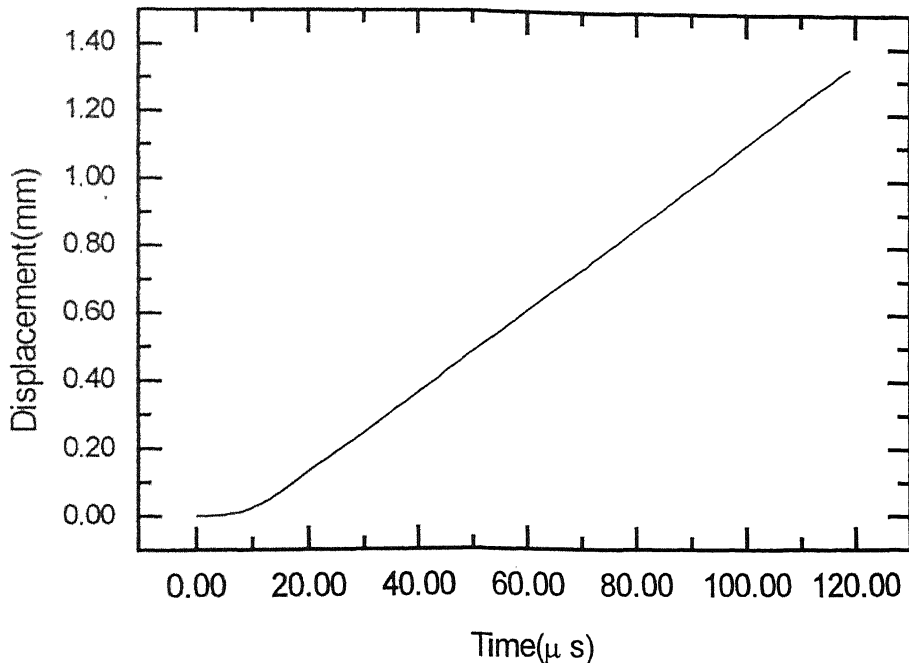


Fig. 6.1c: Displacement Record of Cantilever End for Expt. A2

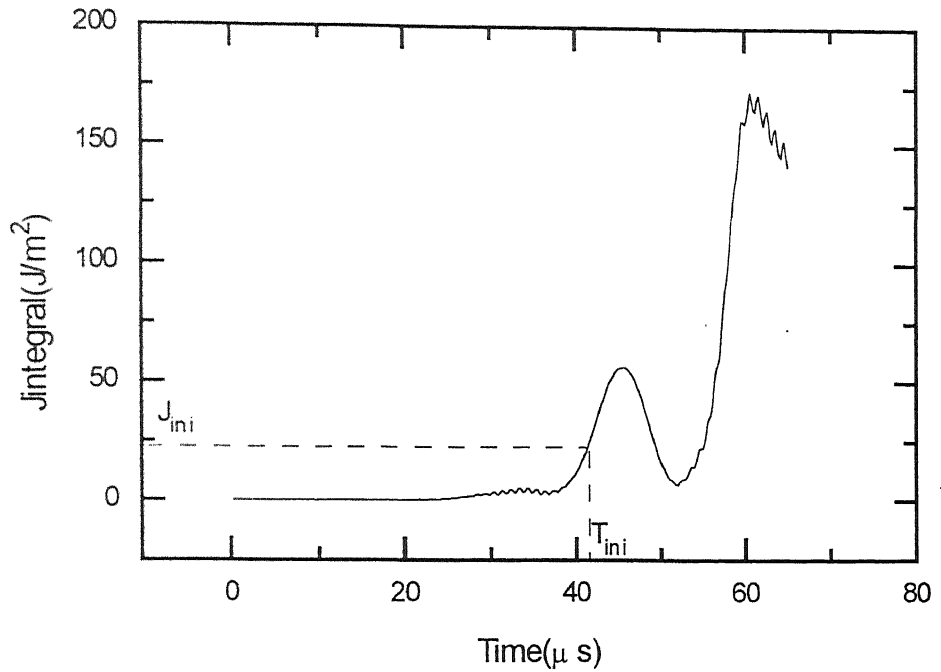


Fig.6.1d: Jintegral Record for Stationary Crack for Expt.A2

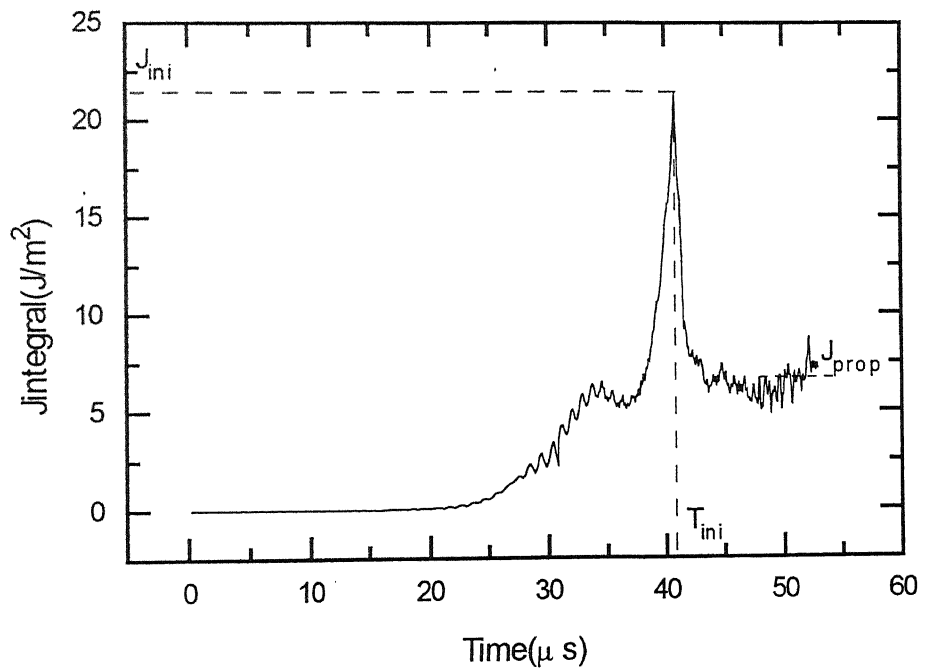


Fig.6.1e: Jintegral Record for Propogating Crack for Expt.A2

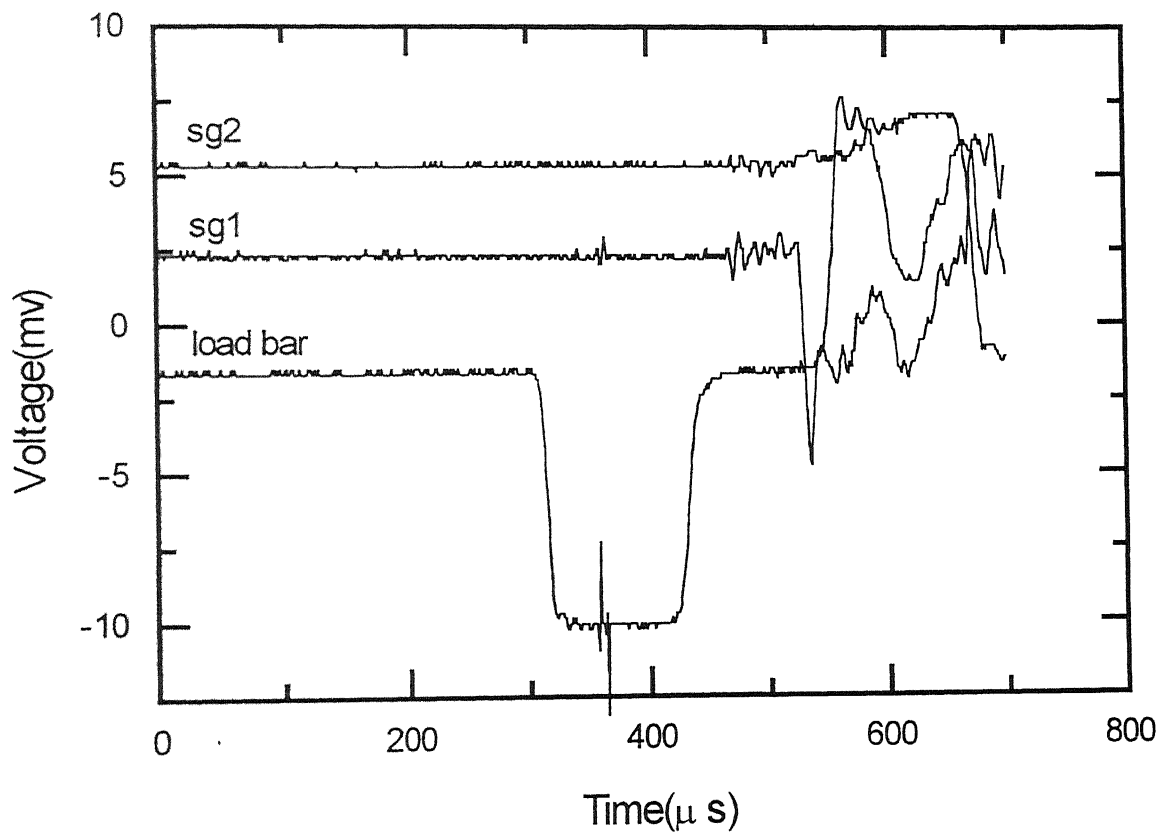


Fig.6.2a: Oscilloscope Record for Expt.A3

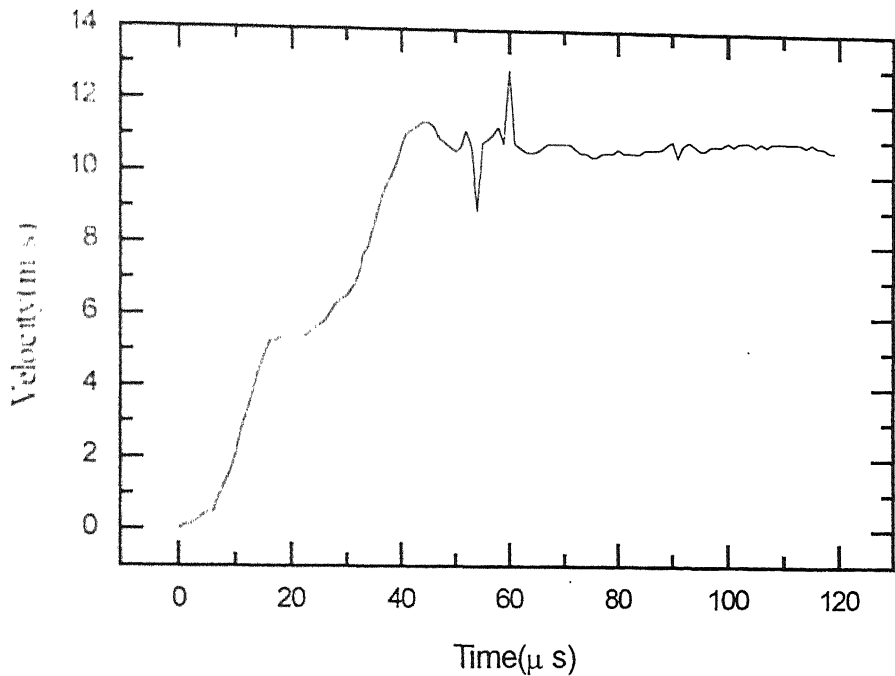


Fig. 6.2b: Velocity Record of Load bar End for Expt. A3

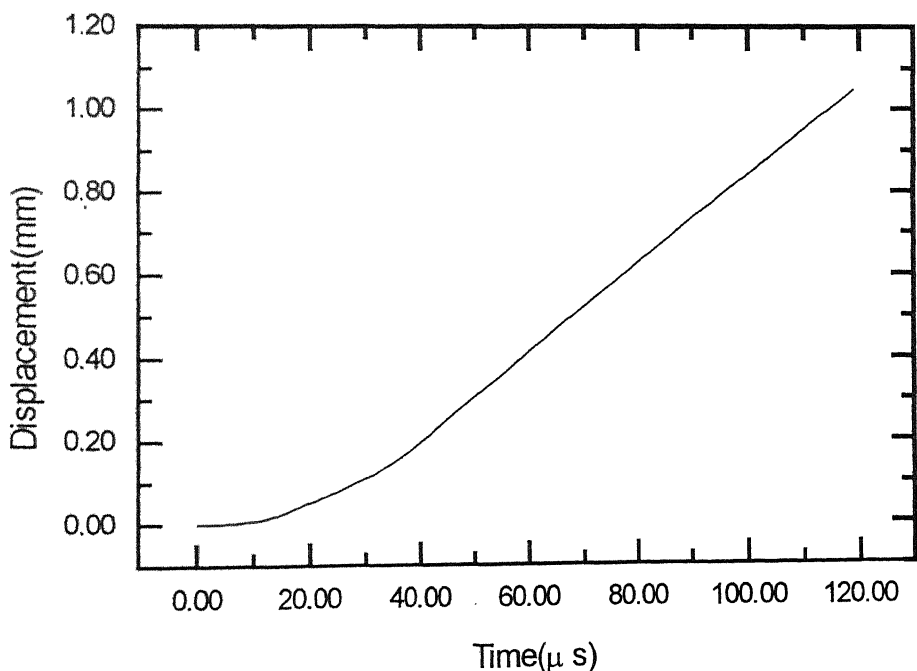
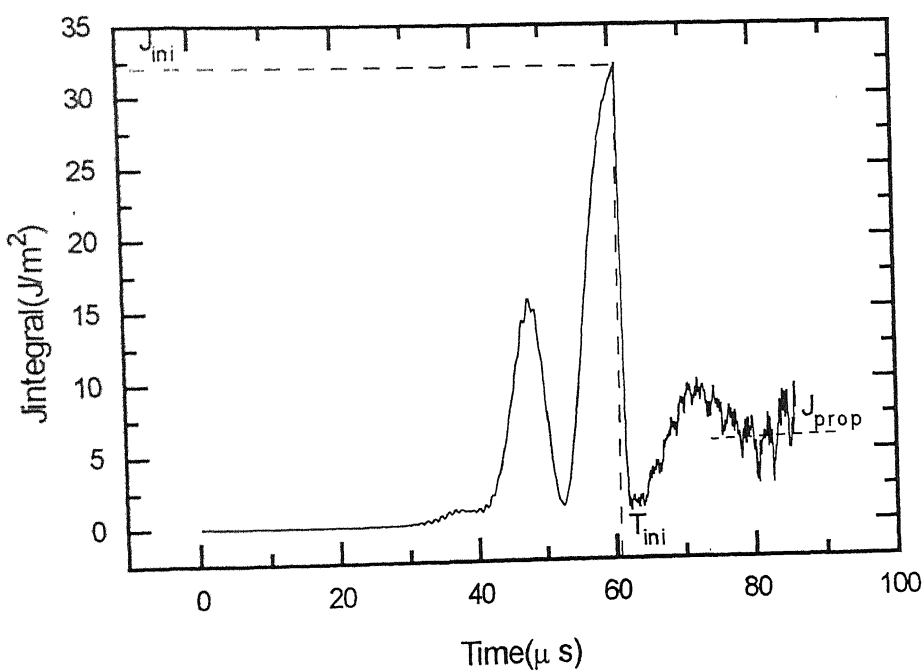
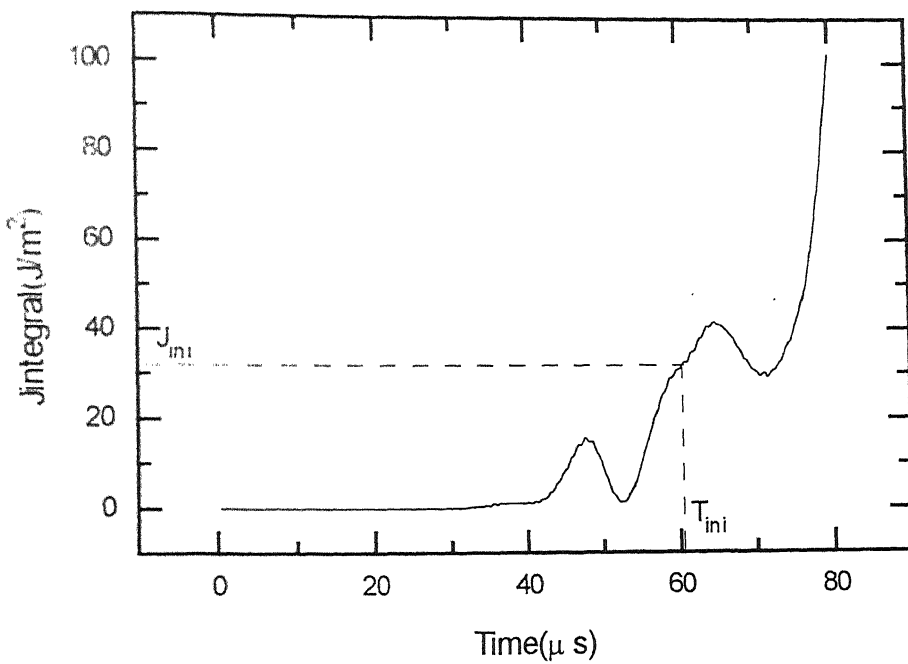


Fig. 6.2c: Displacement Record of Cantilever End for Expt. A3



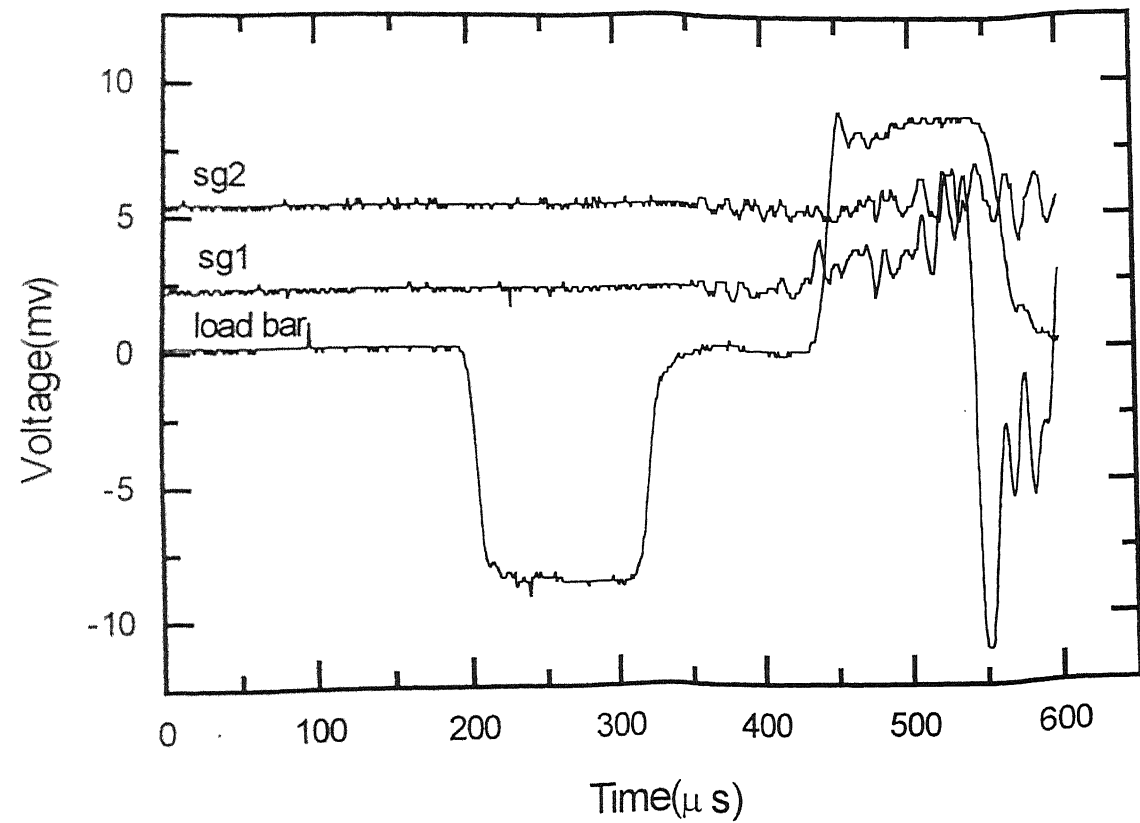


Fig. 6.3a: Oscilloscope Record for Expt. A4

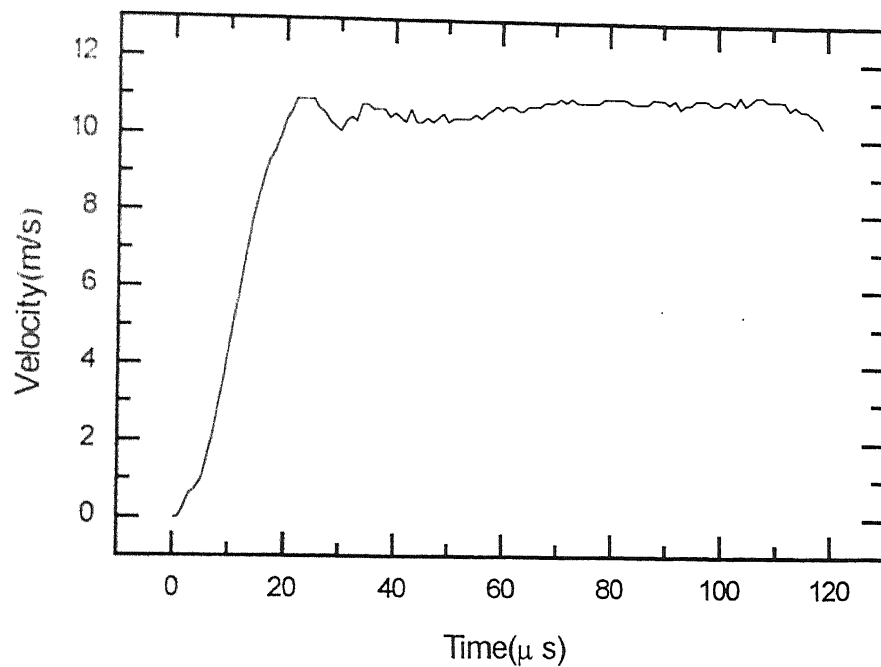


Fig. 6.3b: Velocity Record of Load bar End for Expt. A4

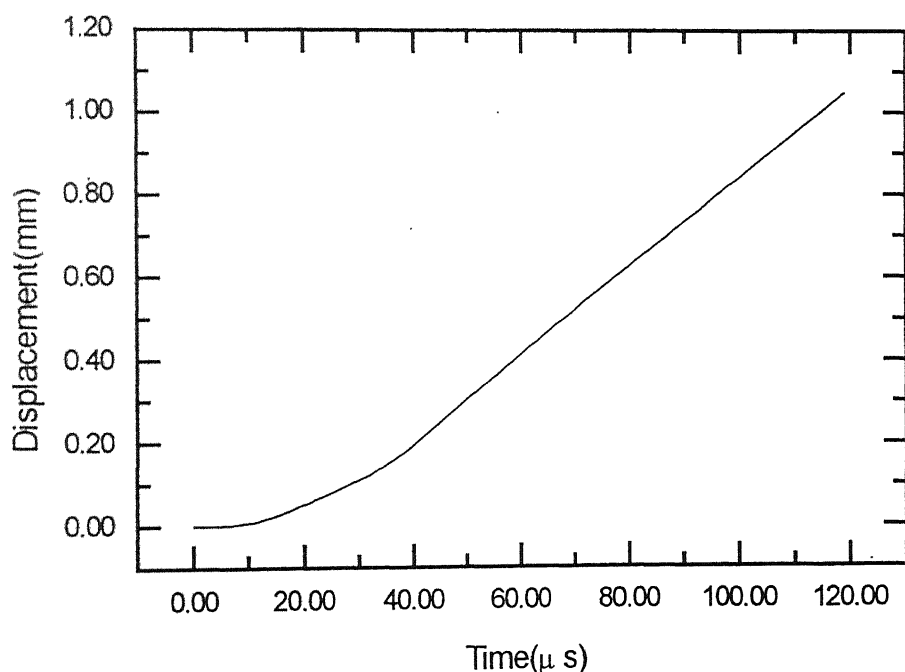


Fig. 6.3c: Displacement Record of Cantilever End for Expt. A4

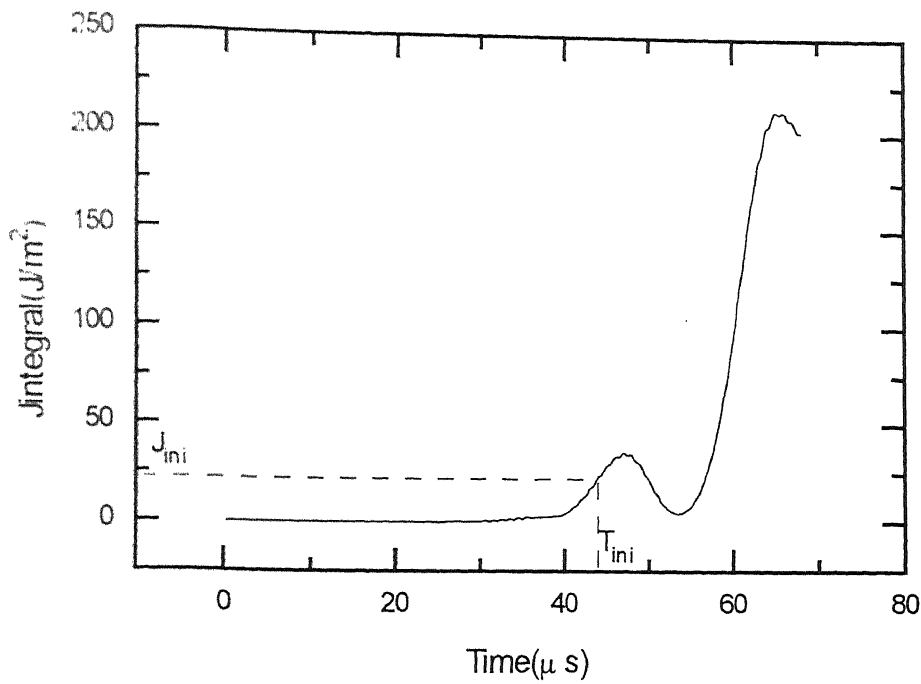


Fig.6.3d: Jintegral Record for Stationary Crack for Expt. A4

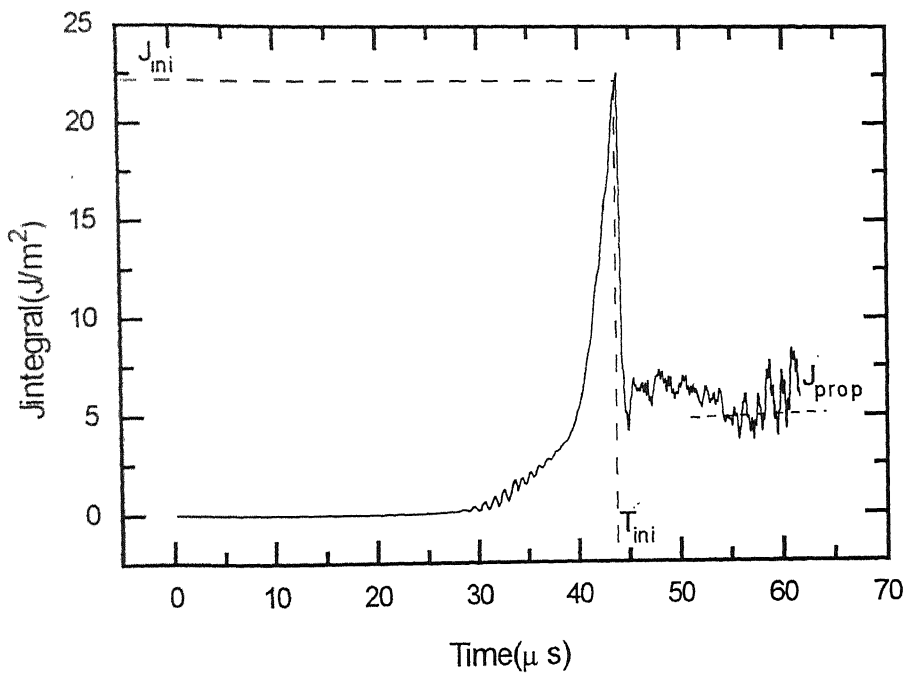


Fig.6.3e: Jintegral Record for Propogating Crack for Expt. A4

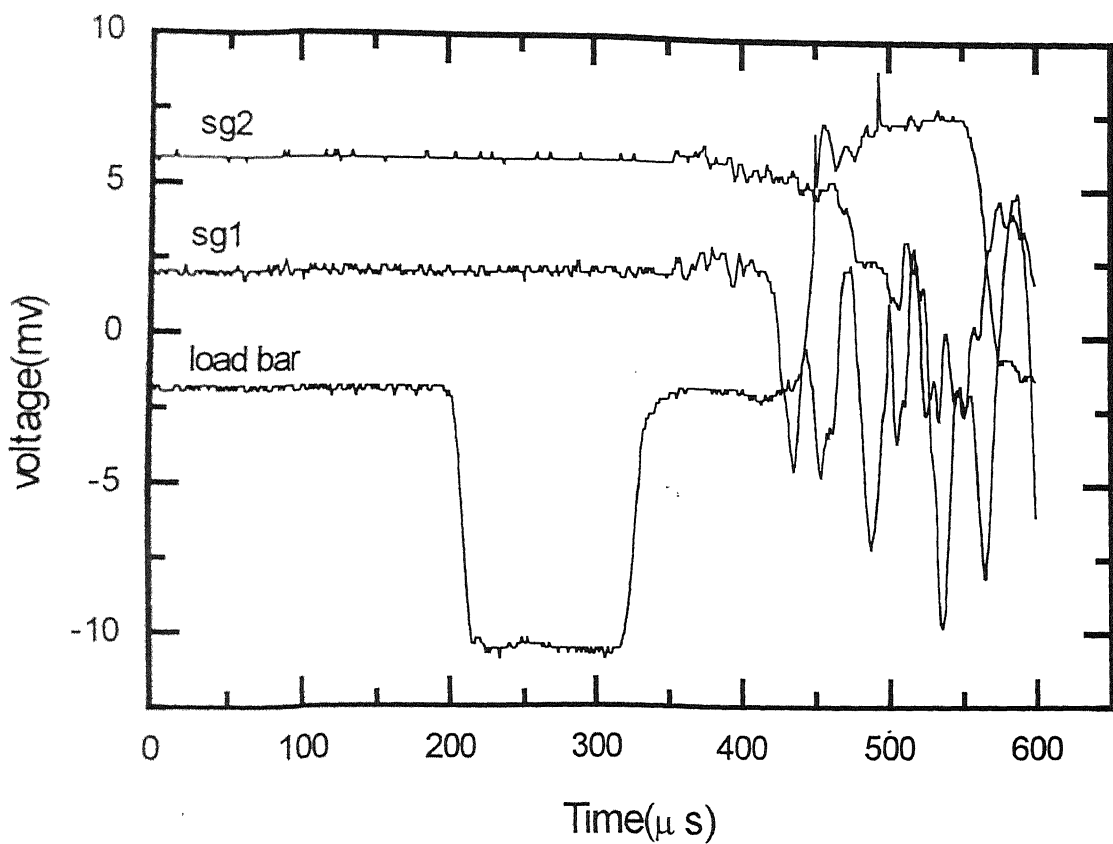


Fig. 6.4a: Oscilloscope Record for Expt. A5

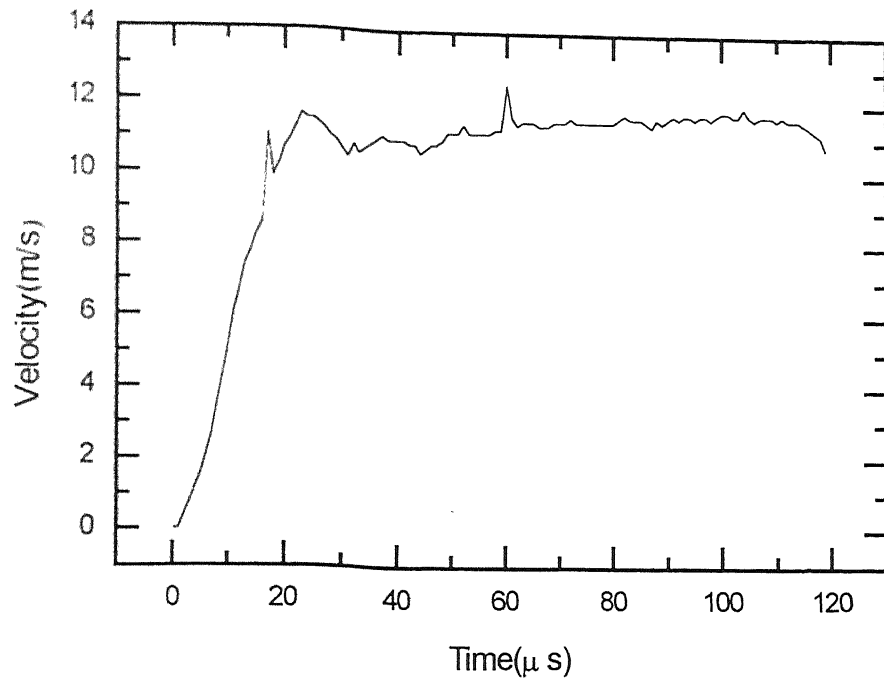


Fig.6.4b: Velocity Record of Load bar End for Expt.A5

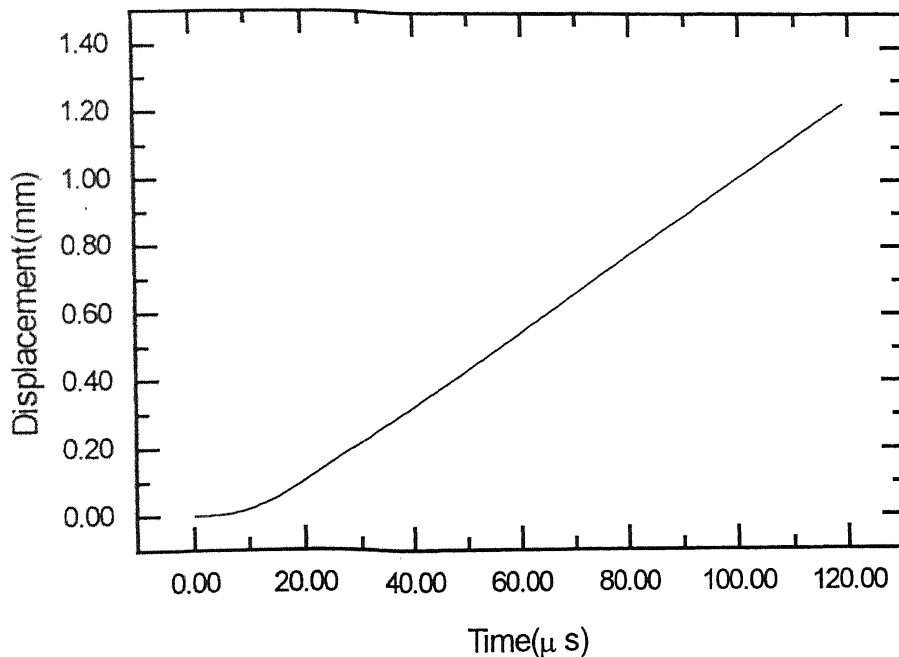


Fig.6.4c: Displacement Record of Cantilever end for Expt.A5

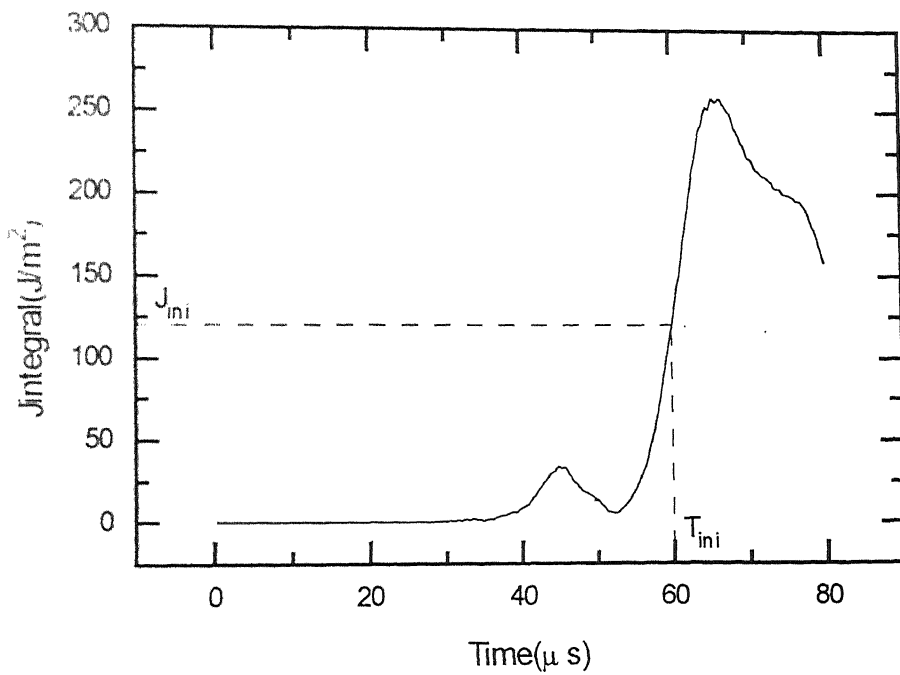


Fig. 6.4d: Jintegral Record for Stationary Crack for Expt. A5

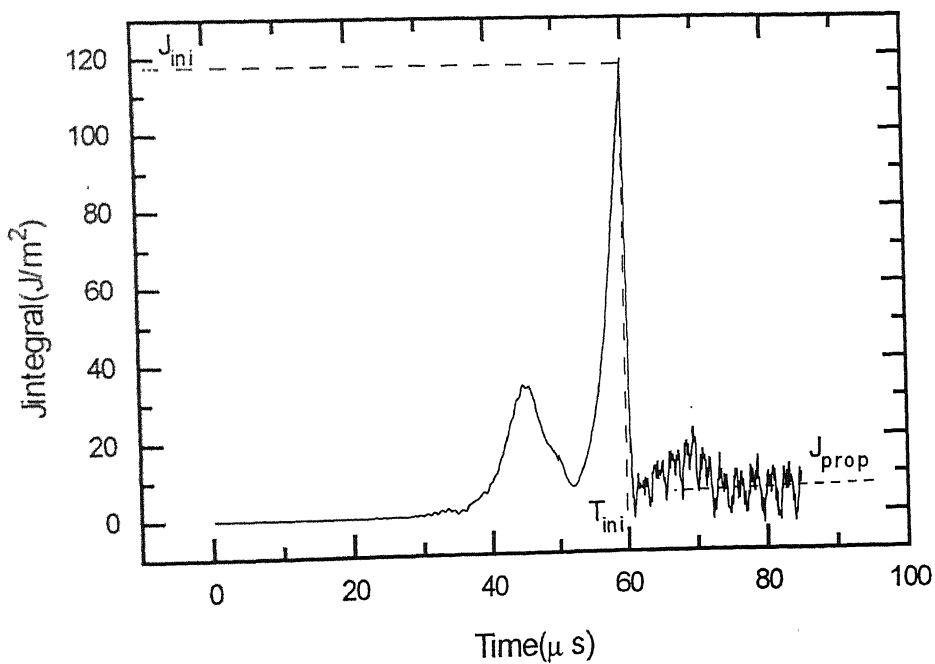


Fig. 6.4e: Jintegral Record for Propogating Crack for Expt. A5

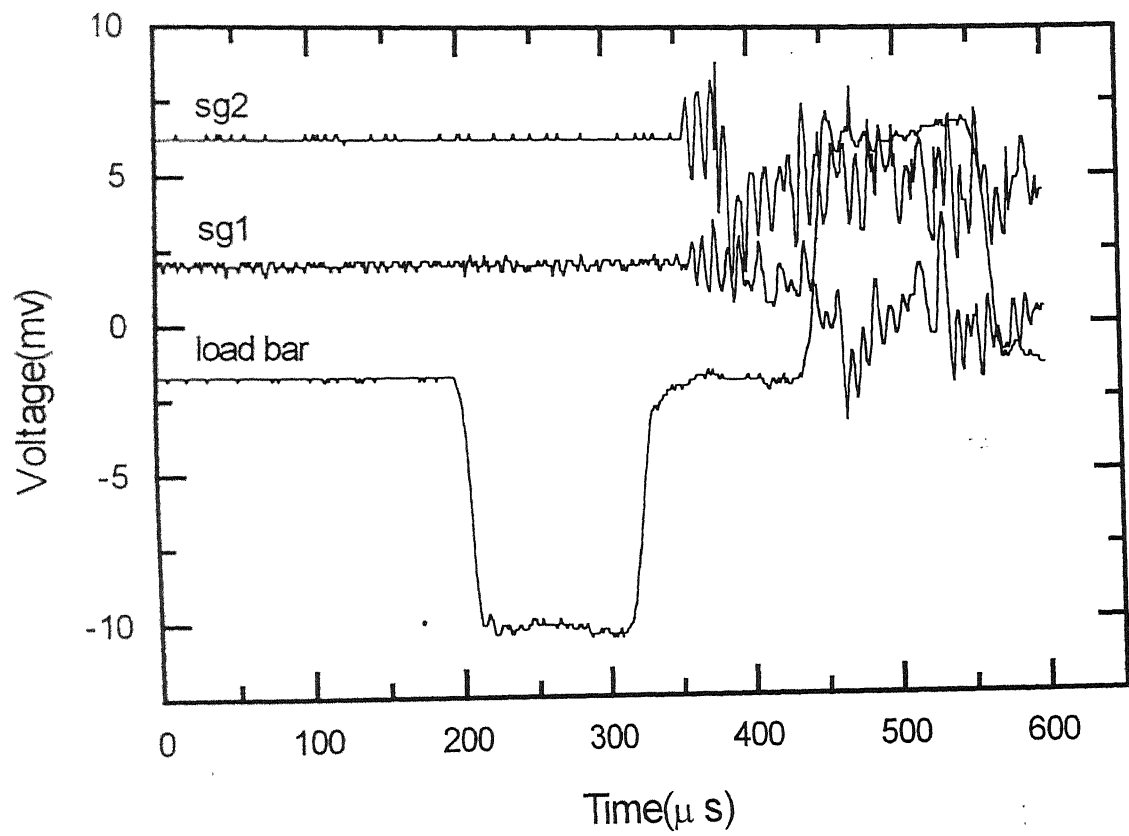


Fig. 7.1a: Oscilloscope Record for Expt.B1

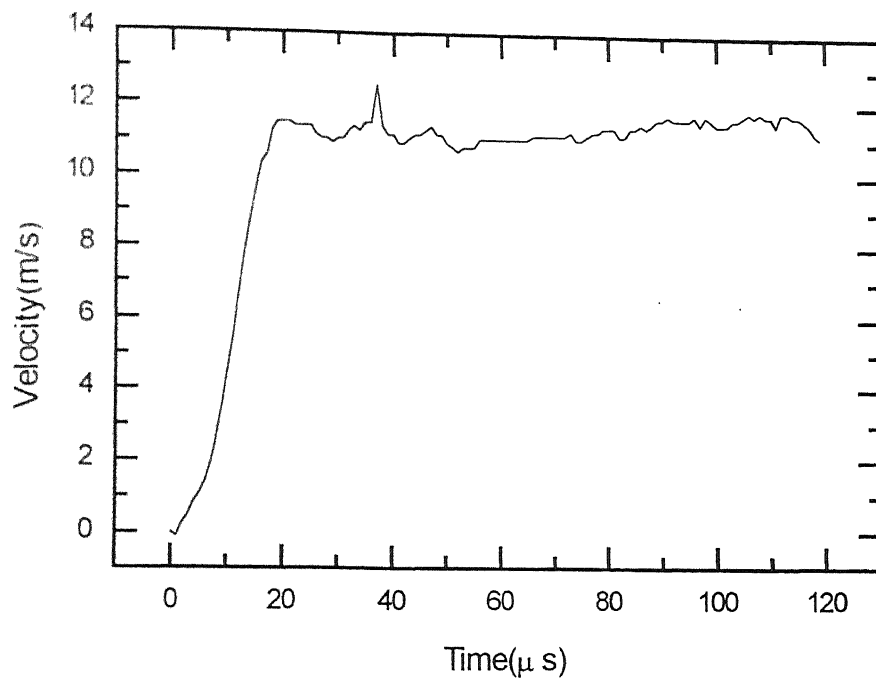


Fig. 7.1b: Velocity Record of Load bar End for Expt.B1

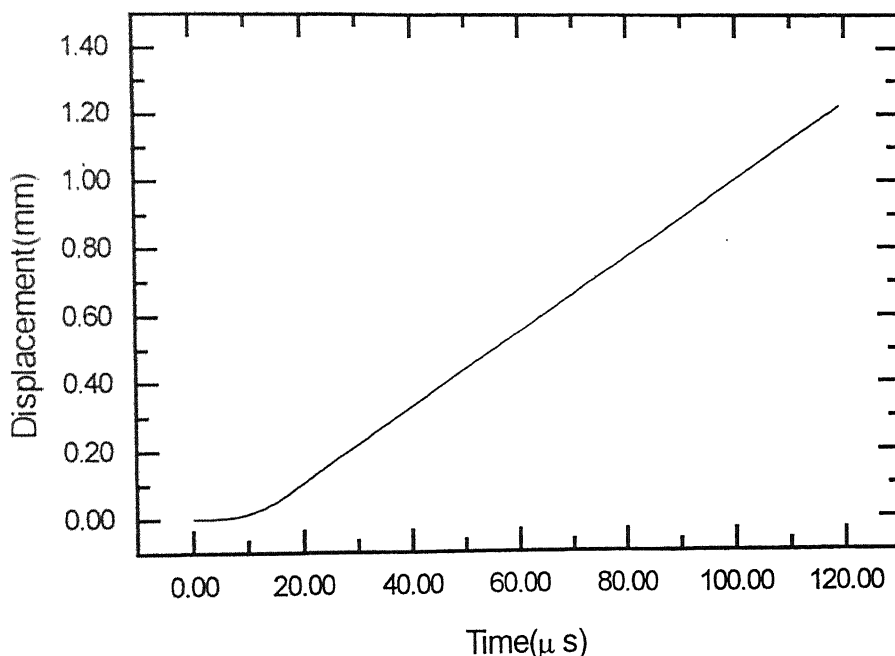
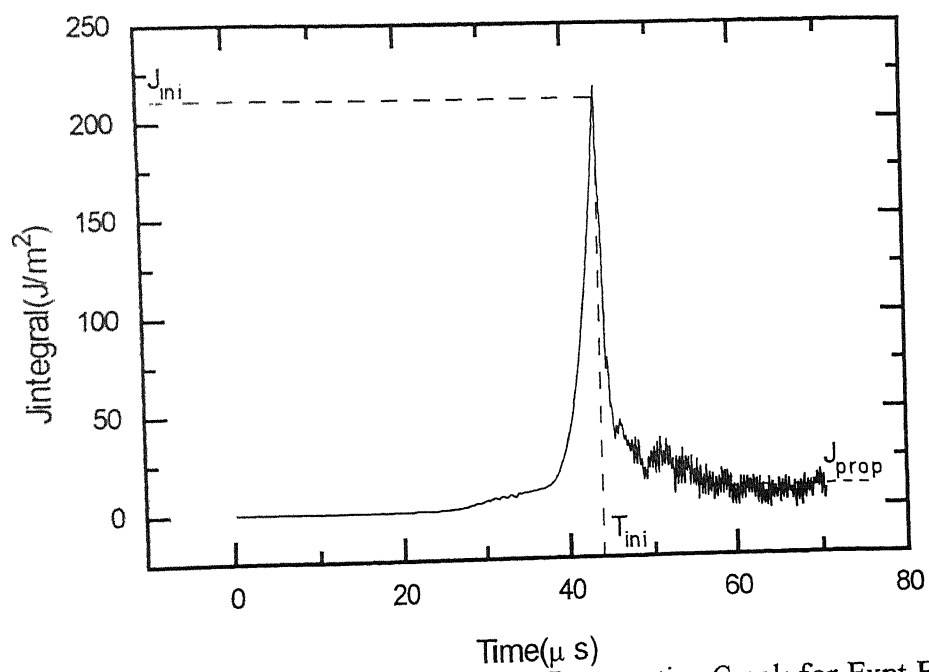
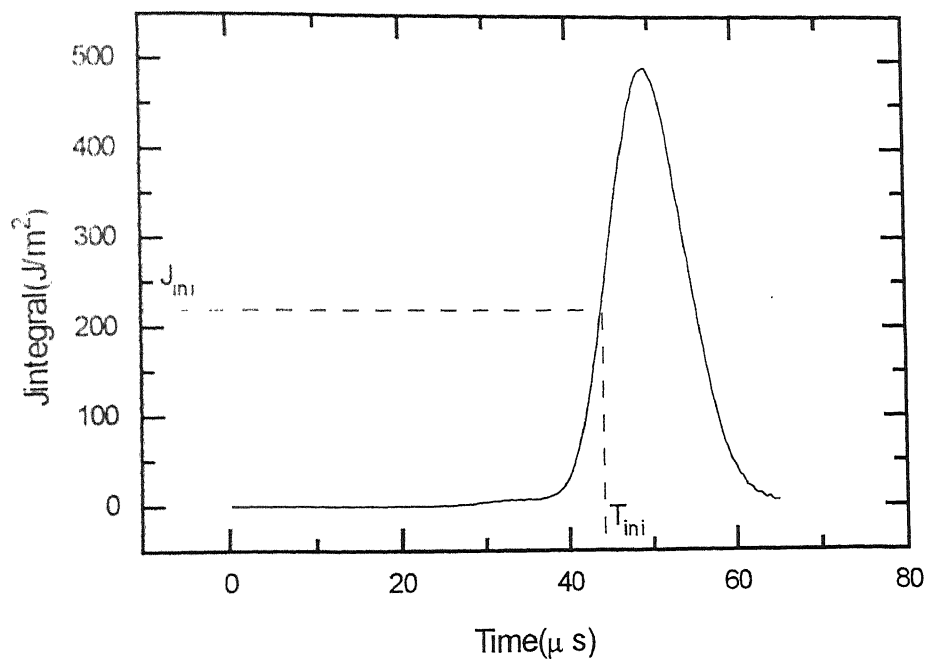


Fig. 7.1c: Displacement Record of Cantilever End for Expt.B1



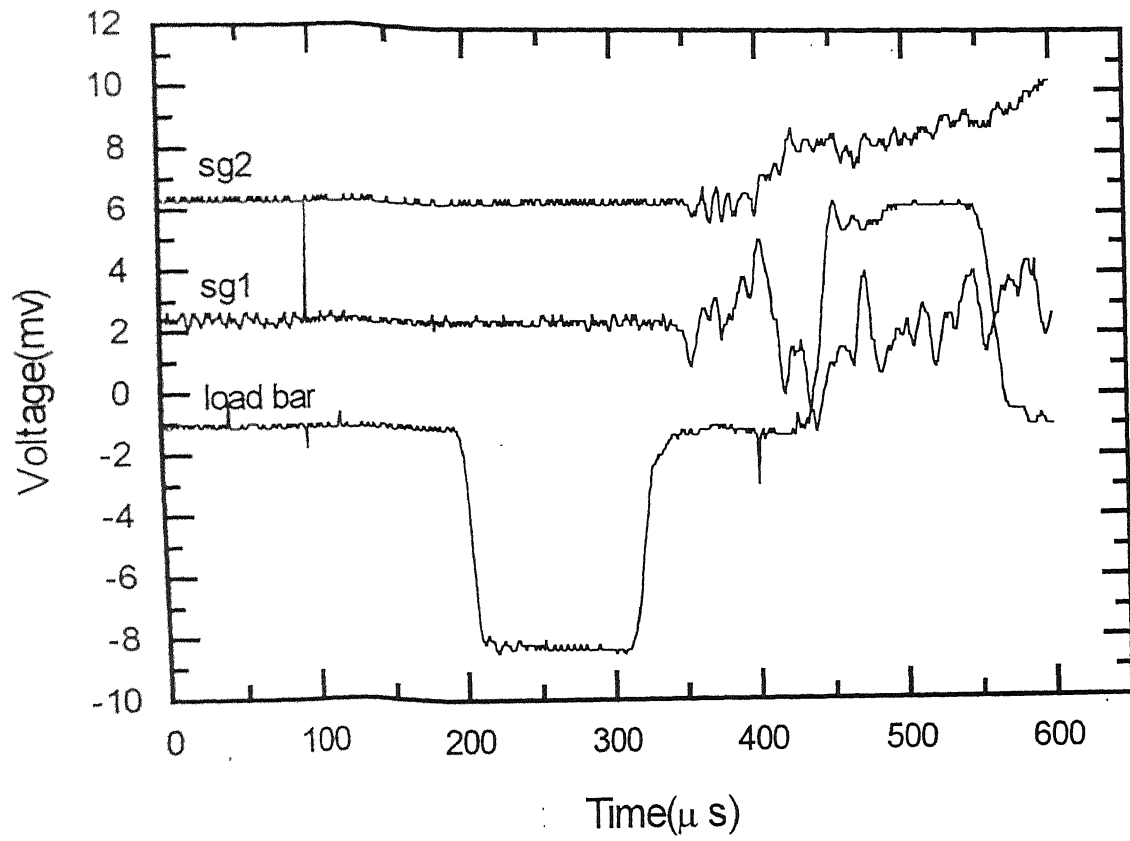


Fig. 7.2a: Oscilloscope Record for Expt. B2

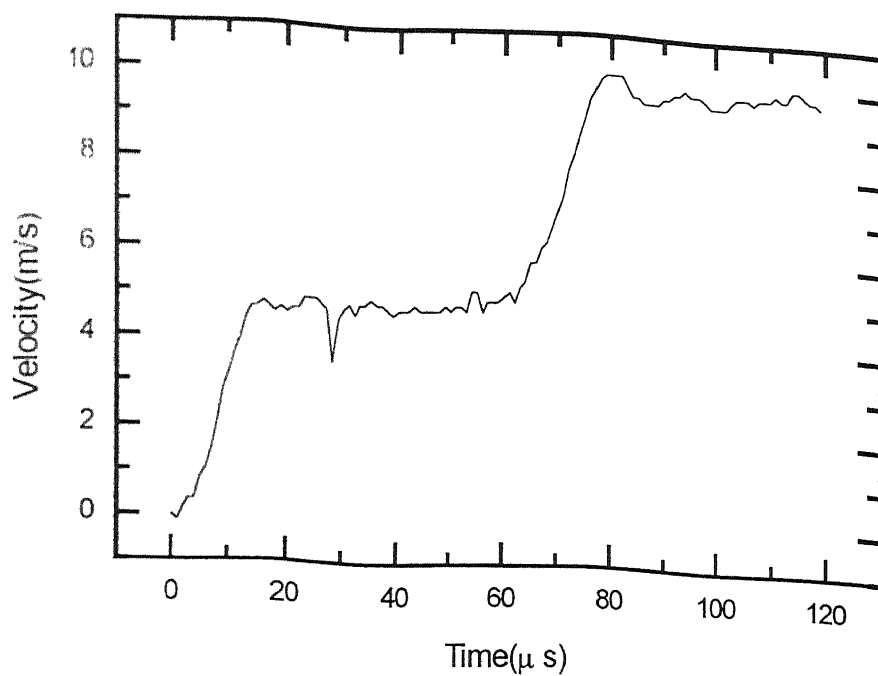


Fig. 7.2b: Velocity Record of Load bar End for Expt.B2

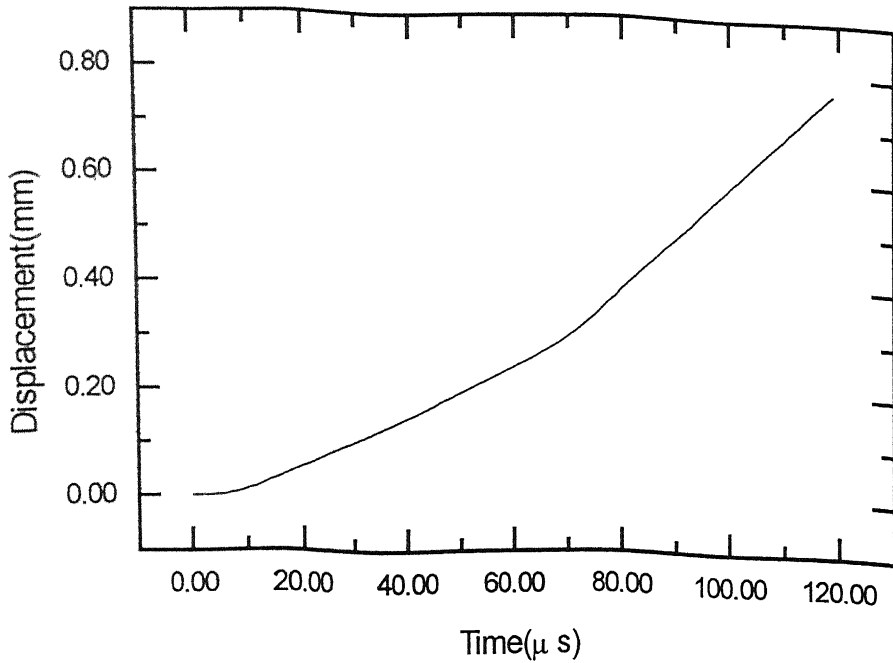


Fig. 5.2.6c: Displacement Record of Cantilever End for Expt.B2

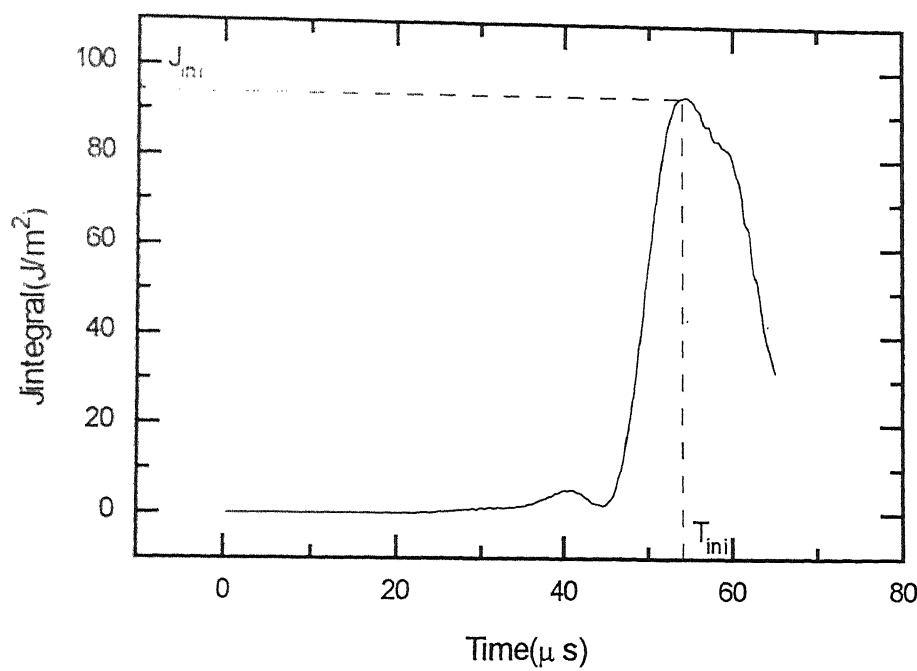


Fig. 7.2d: Jintegral Record for Stationary Crack for Expt.B2

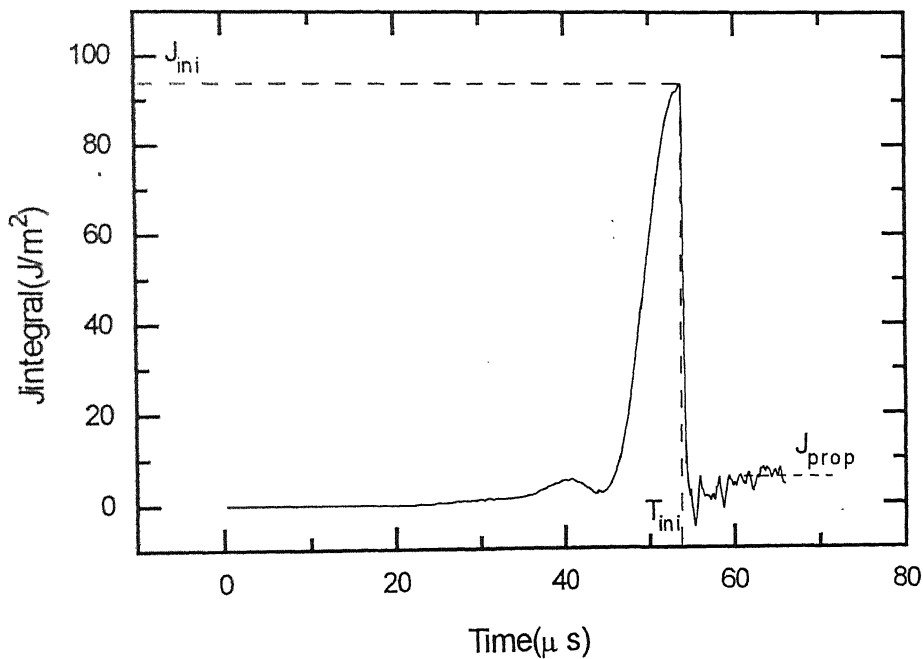


Fig. 7.2e: Jintegral Record for Propogating Crack for Expt.B2

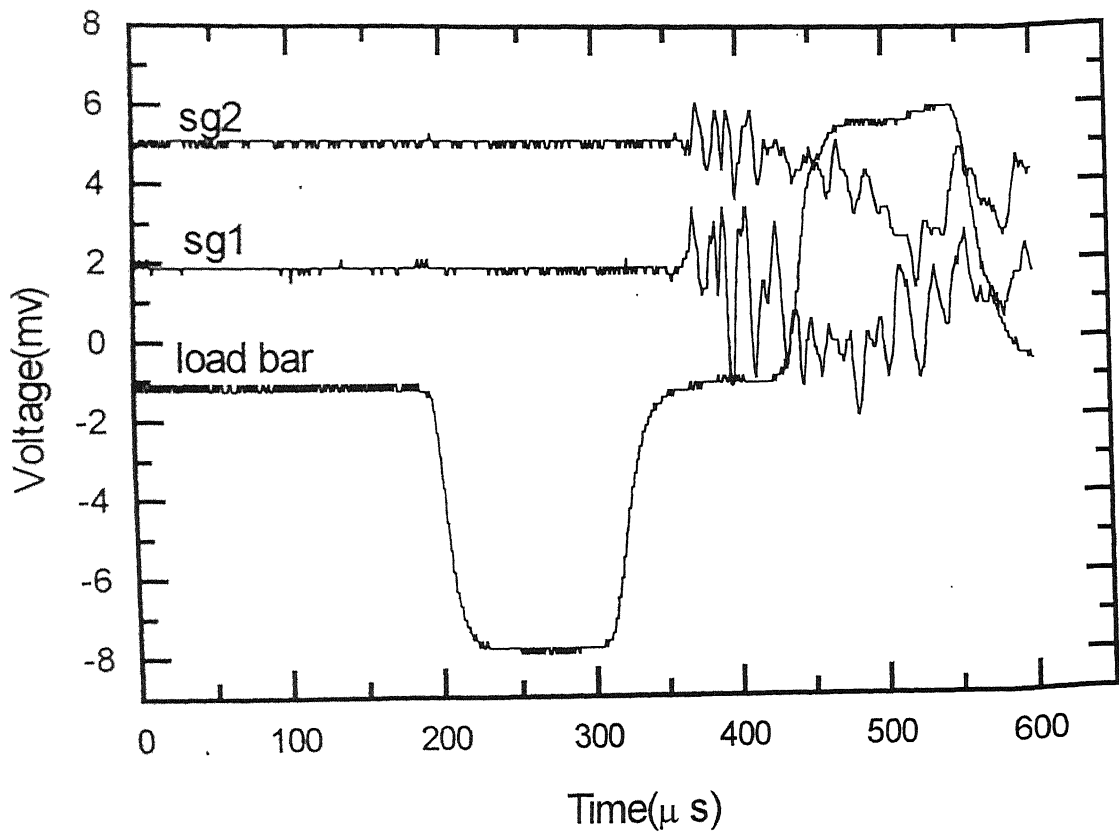


Fig. 7.2a: Oscilloscope Record for Expt. B3

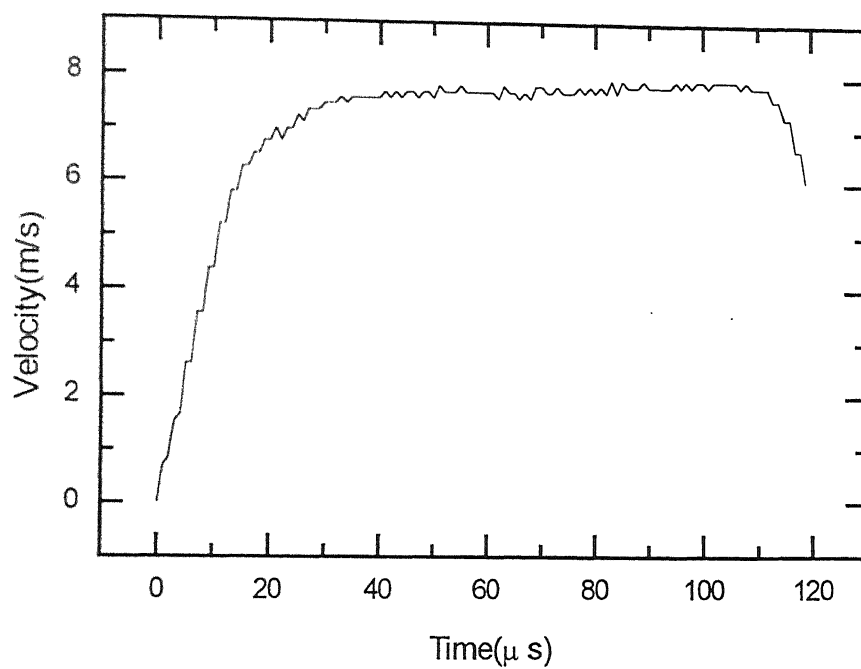


Fig. 7.3b: Velocity Record of Load bar End for Expt.B3

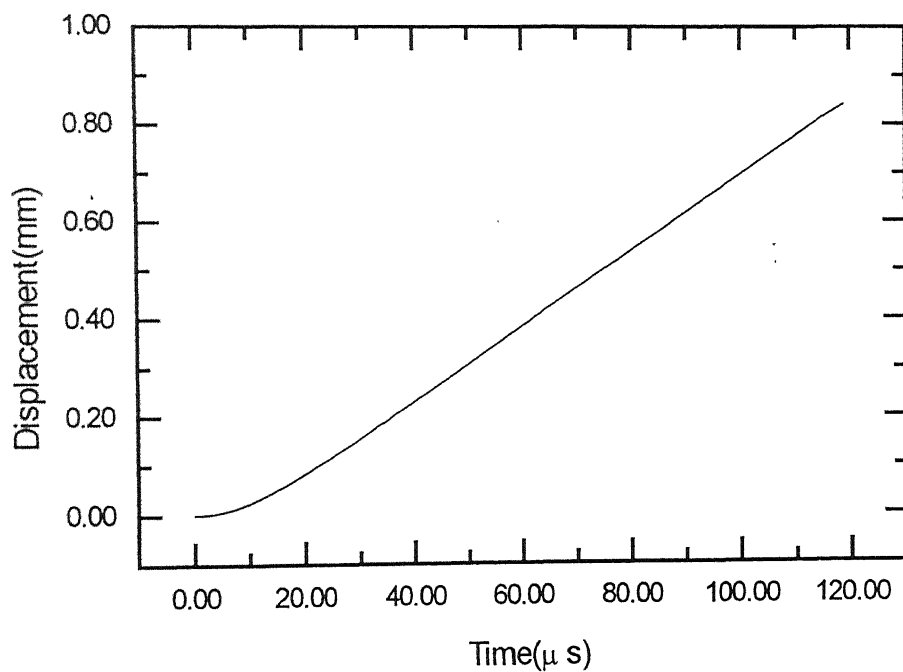


Fig. 7.3c: Displacement Record of Cantilever End for Expt.B3

Voltage(mV)

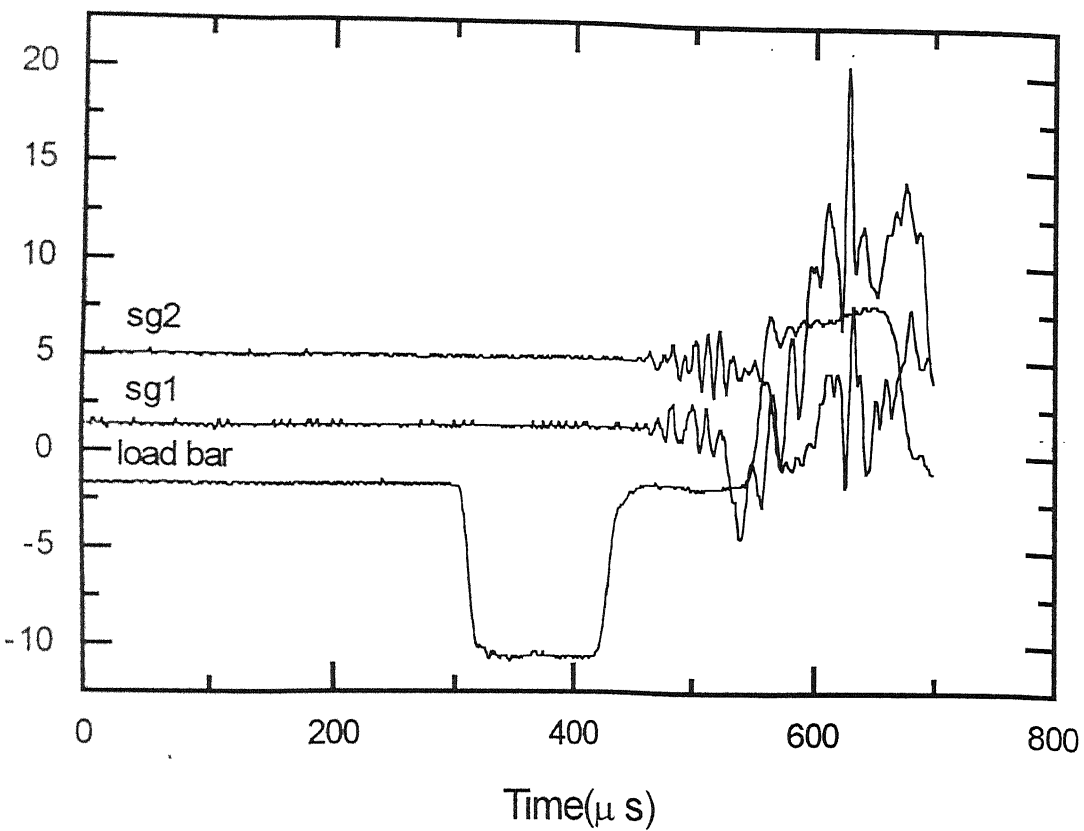


Fig. 7.4a: Oscilloscope Record for Expt. B4

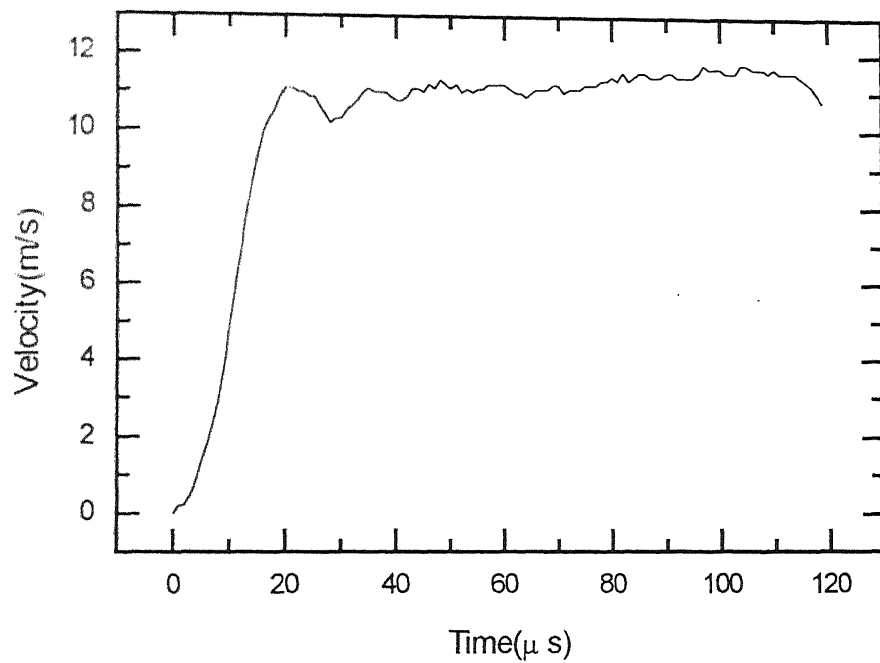


Fig. 7.4b: Velocity Record for Load bar End for Expt.B4

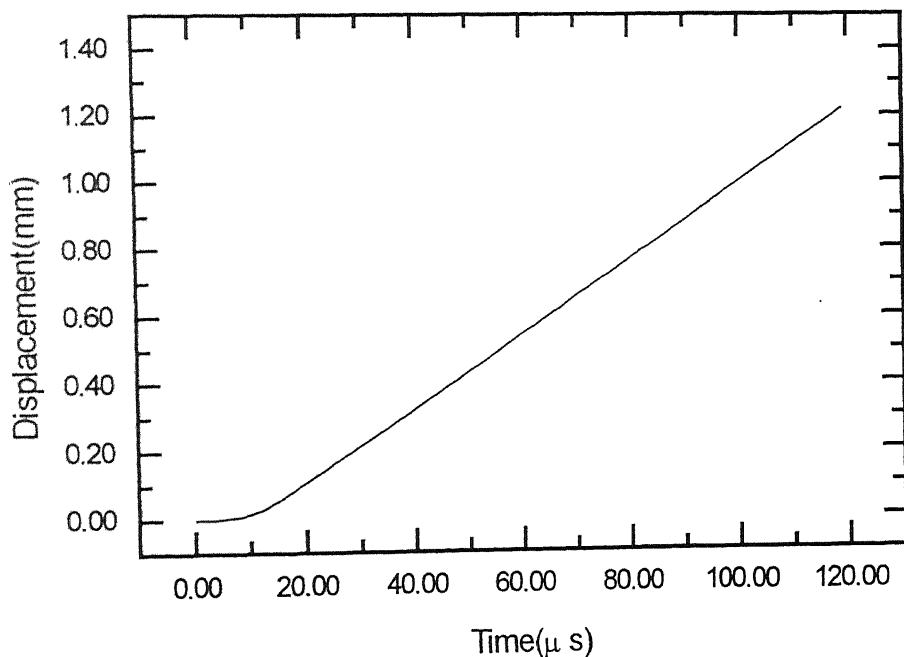


Fig. 7.4c: Displacement Record of Cantilever End for Expt.B4

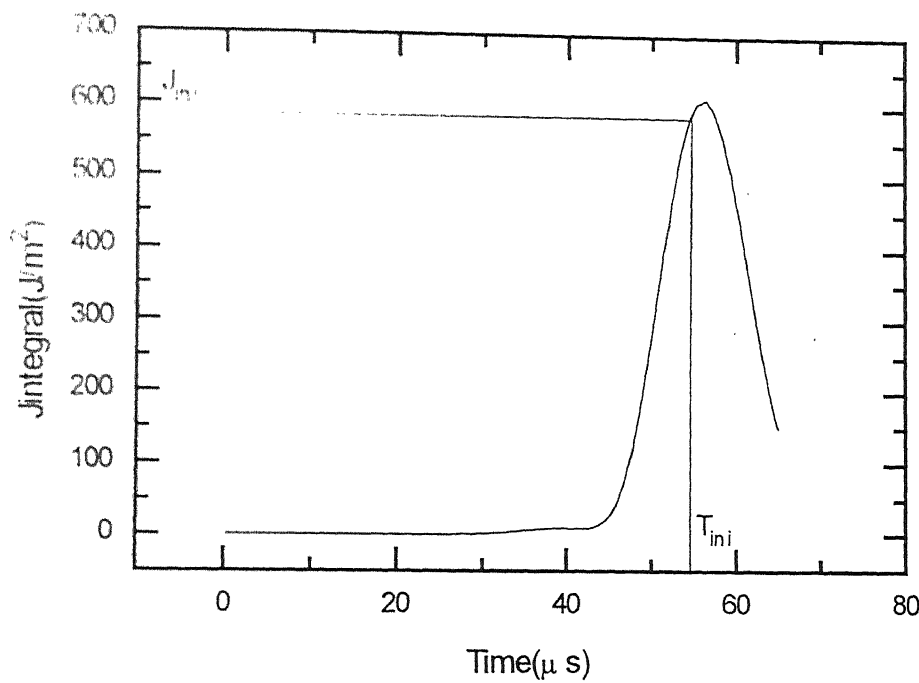


Fig. 7.4d: Jintegral Record for Stationary Crack for Expt.B4

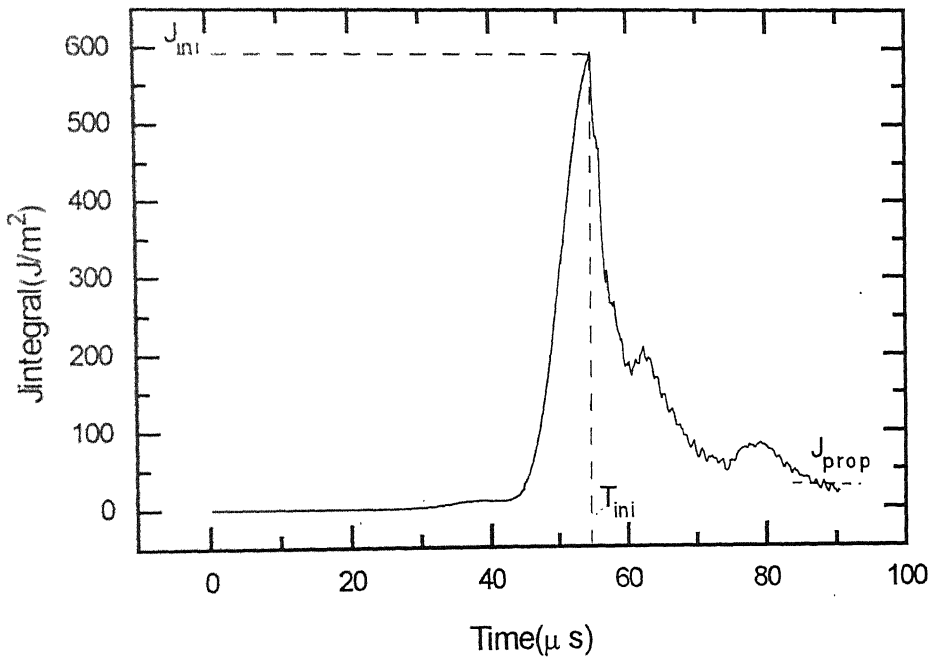


Fig. 7.4e: Jintegral Record for Propogating crack for Expt.B4

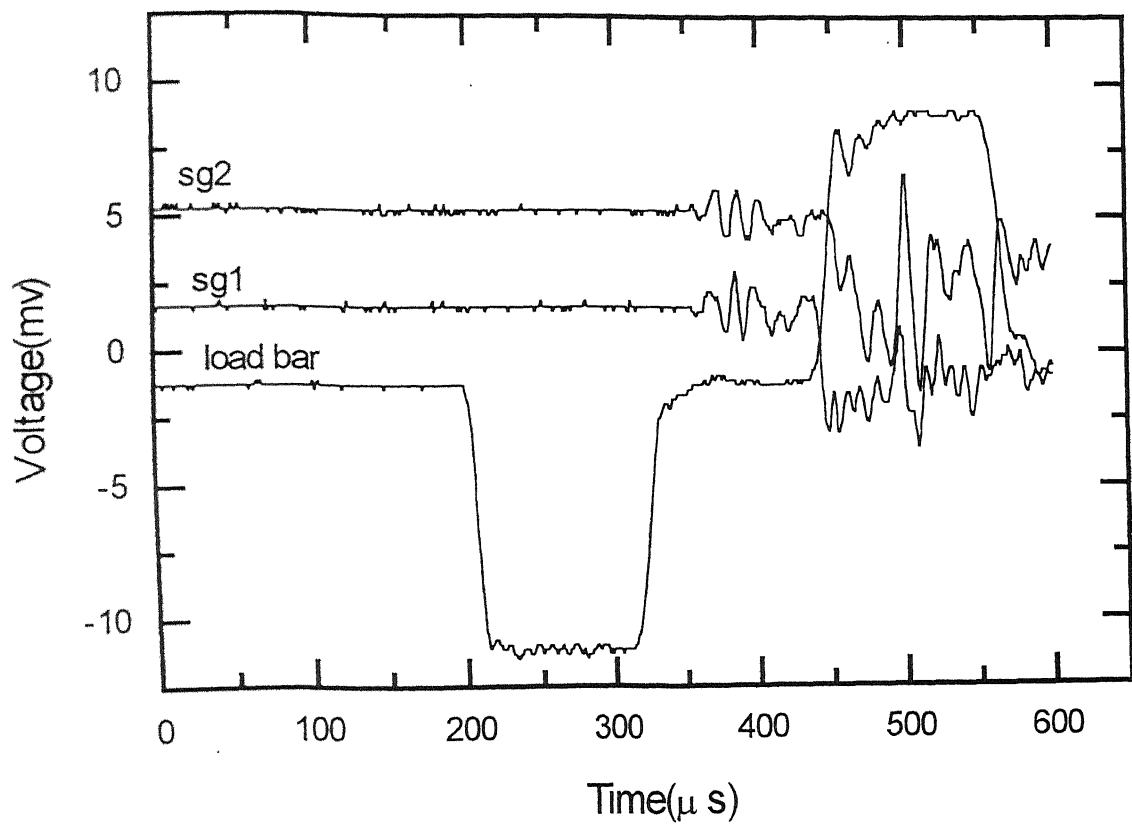


Fig. 7.5a: Oscilloscope Record for Expt. B5

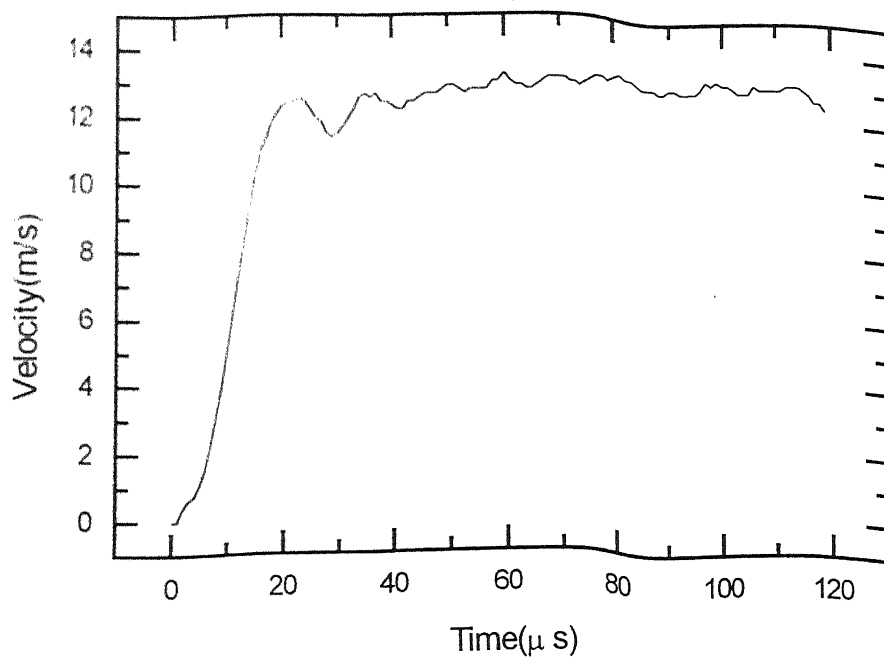


Fig. 7.5b: Velocity Record of Load bar End for Expt.B5

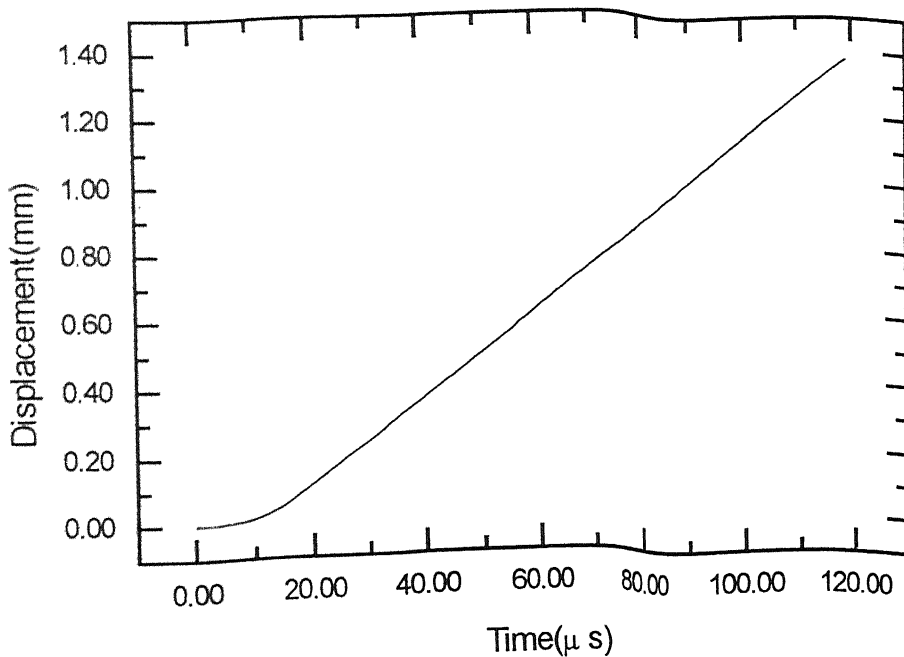


Fig. 7.5c: Displacement Record of Cantilever End for Expt.B5

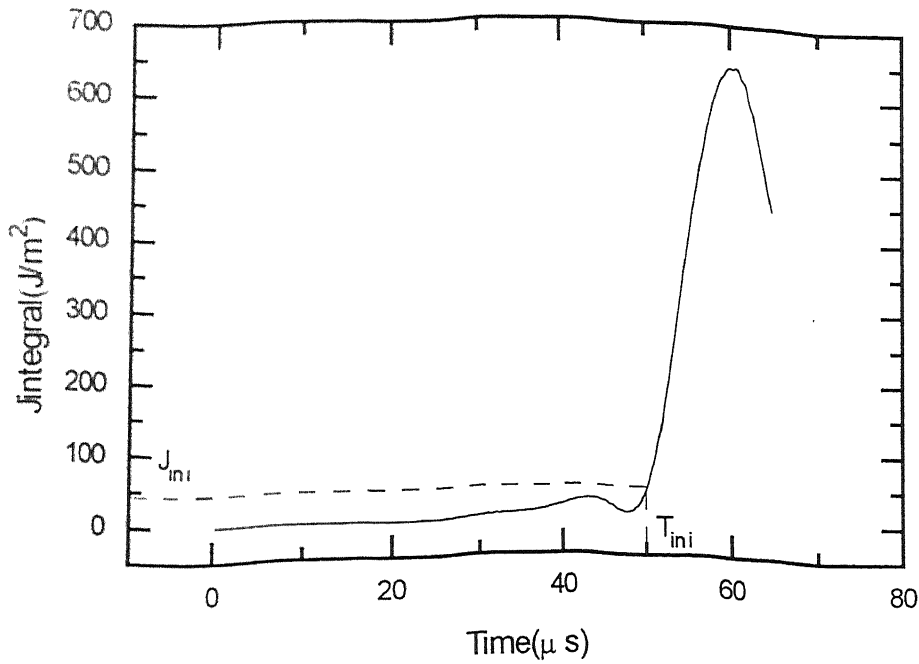


Fig. 7.5d: Jintegral Record for Stationary Crack for Expt.B5

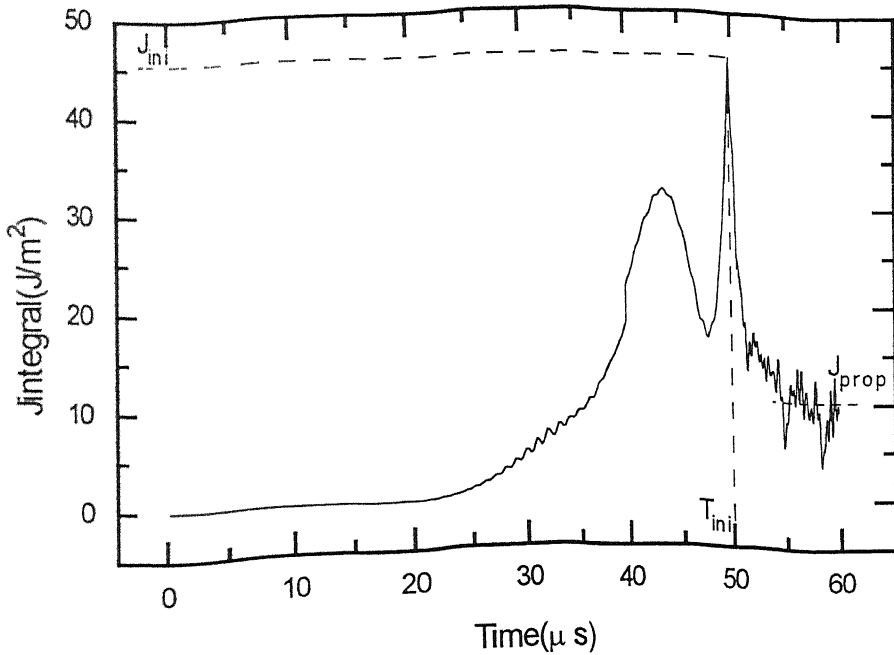


Fig. 7.5e: Jintegral Record for Propagating Crack for Expt.B5

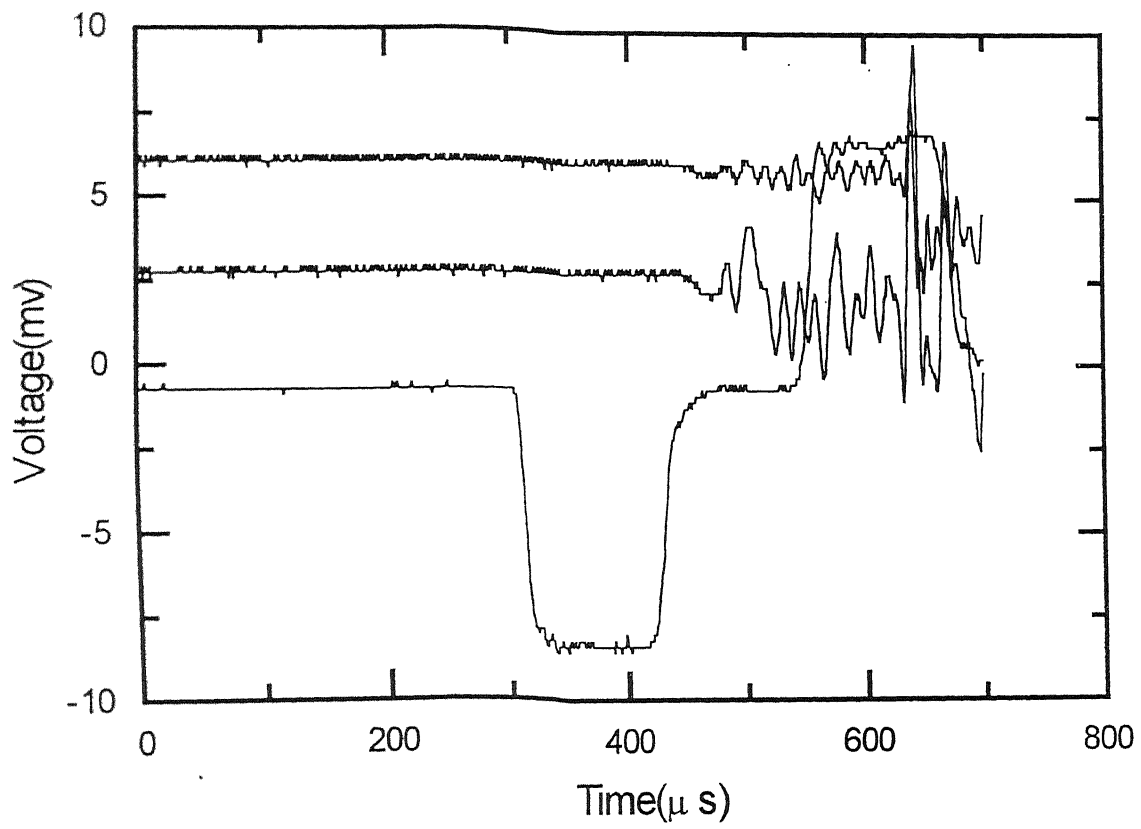


Fig. 7.6a: Oscilloscope Record for Expt. B6

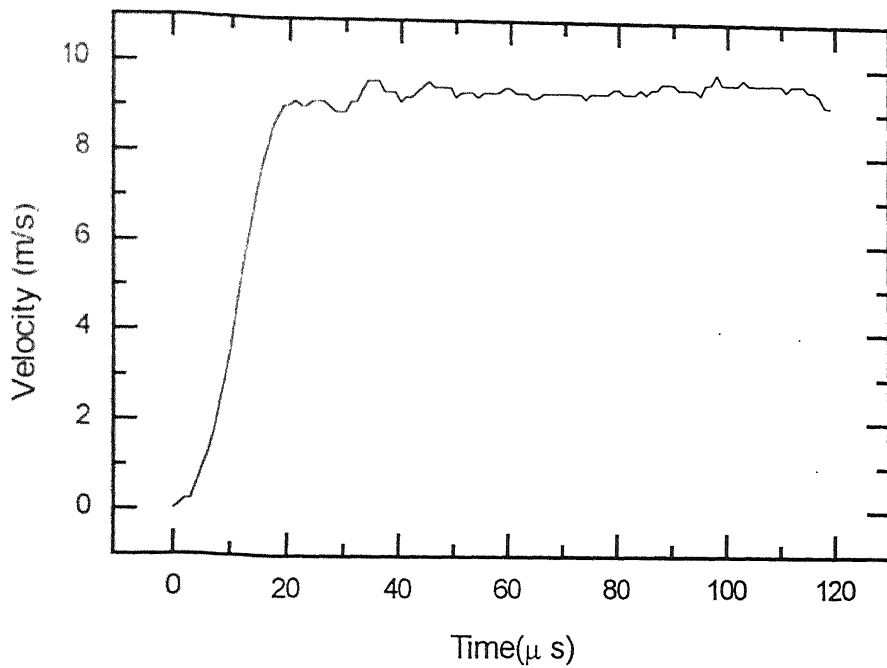


Fig. 7.6b: Velocity Record of Load bar End for Expt.B6

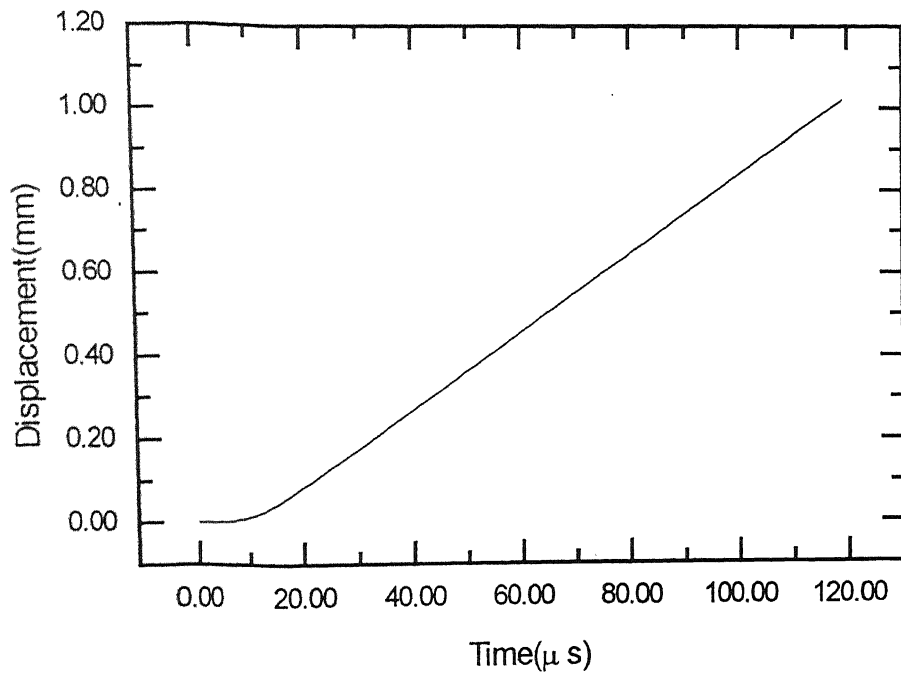


Fig. 7.6b: Displacement Record of Cantilever End for Expt.B6

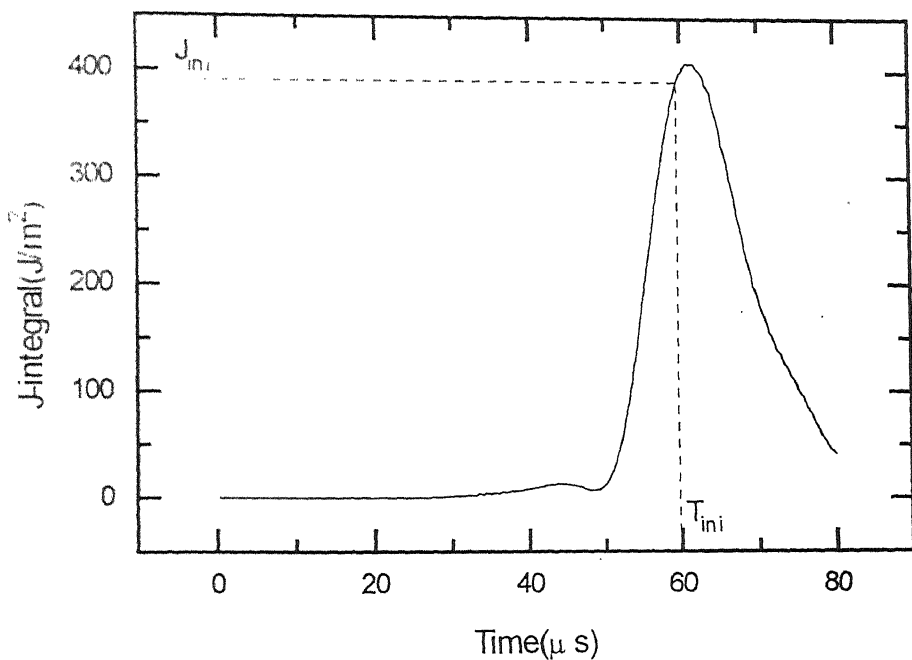


Fig. 7.6d: Jintegral Record for Stationary Crack for Expt. B6

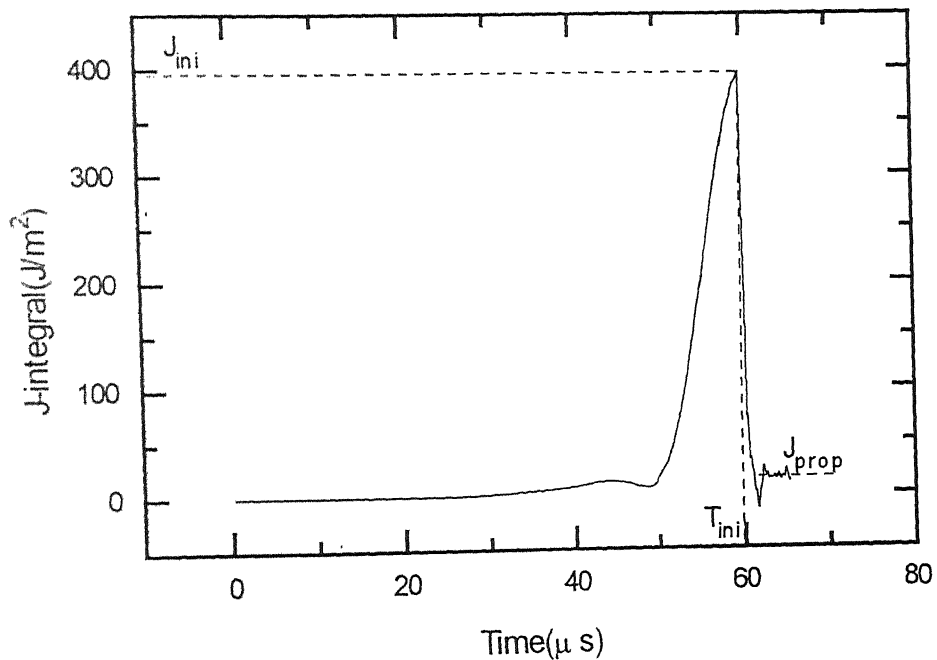


Fig. 7.6e: Jintegral Record for Propagating Crack for Expt. B6

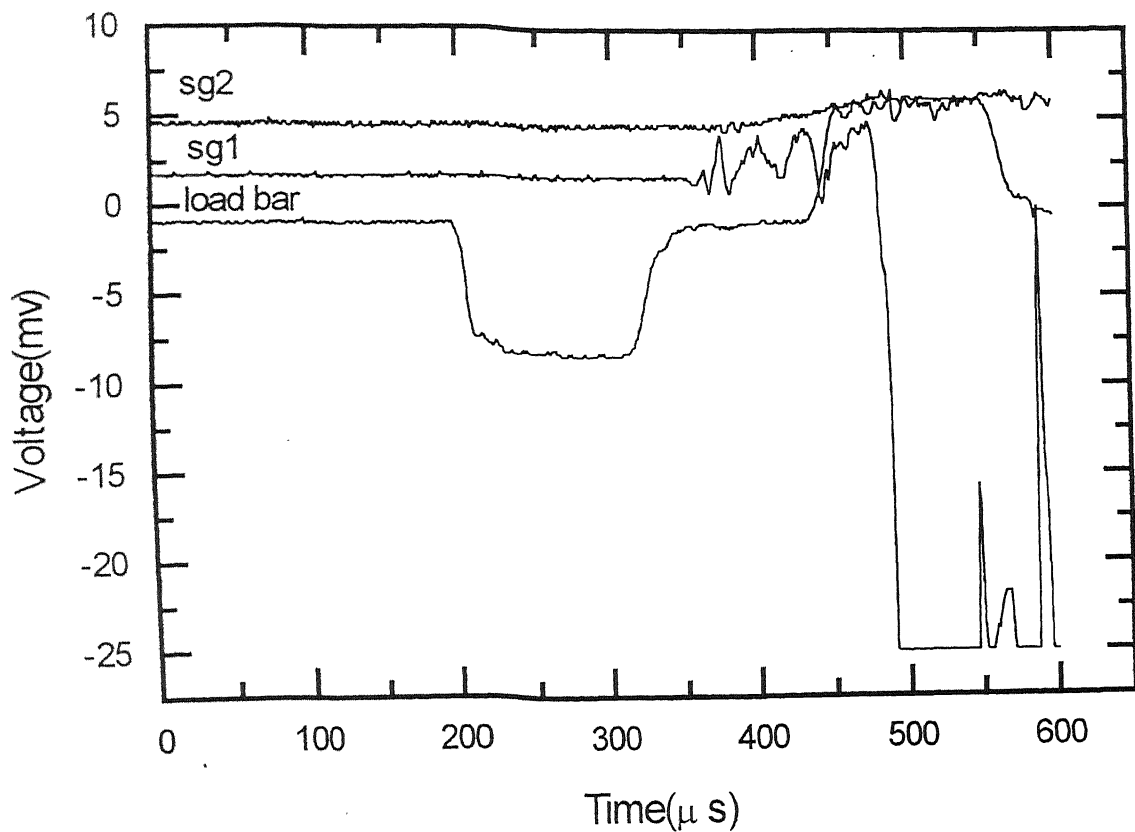


Fig. 7.7a: Oscilloscope Record for Expt. B7

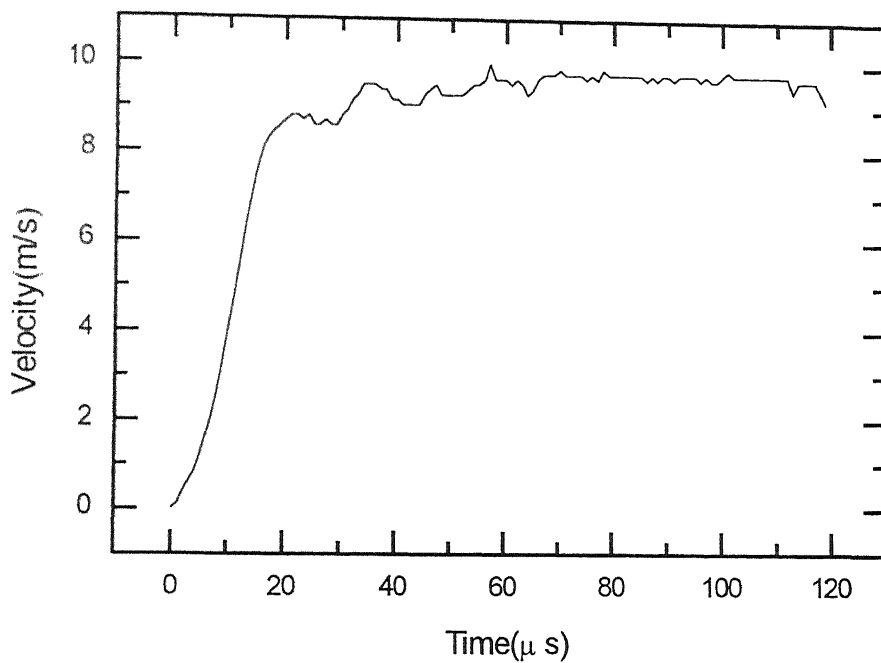


Fig. 7.7b: Velocity Record for Load bar End for Expt.B7

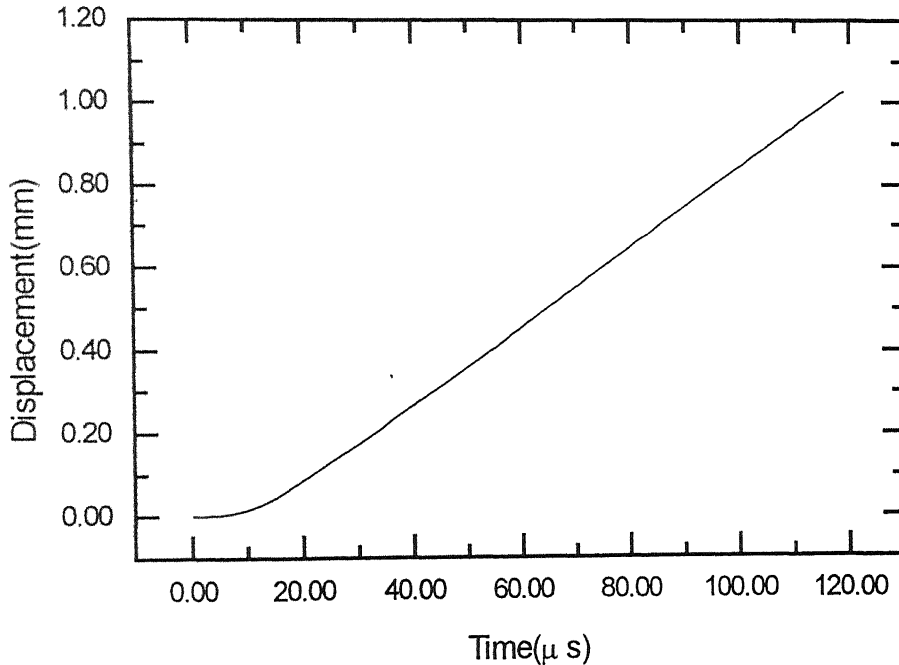


Fig. 7.7c: Displacement Record of Cantilever End for Expt.B7

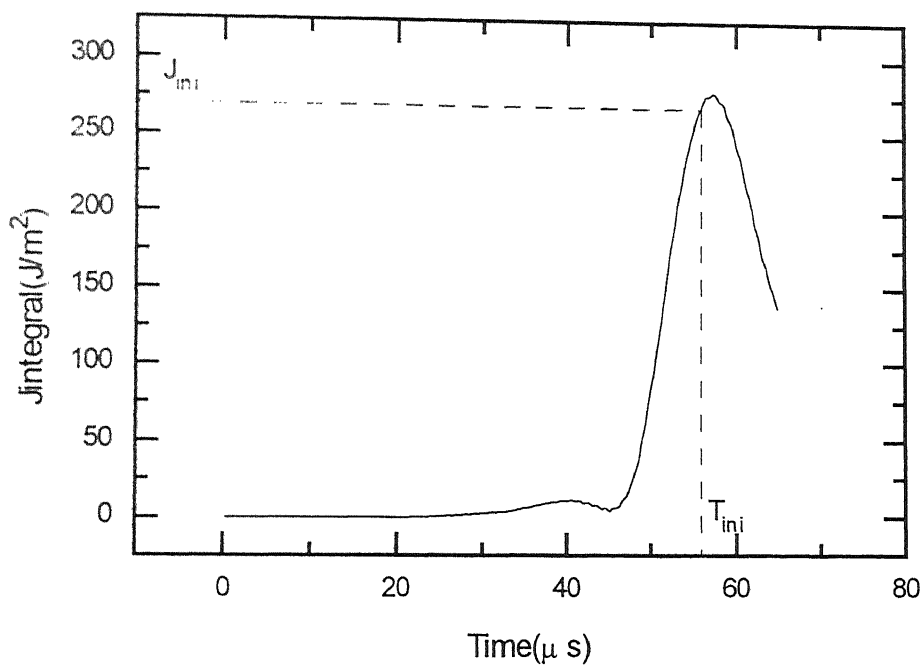


Fig. 7.7d: Jintegral Record for Stationary Crack for Expt.B7

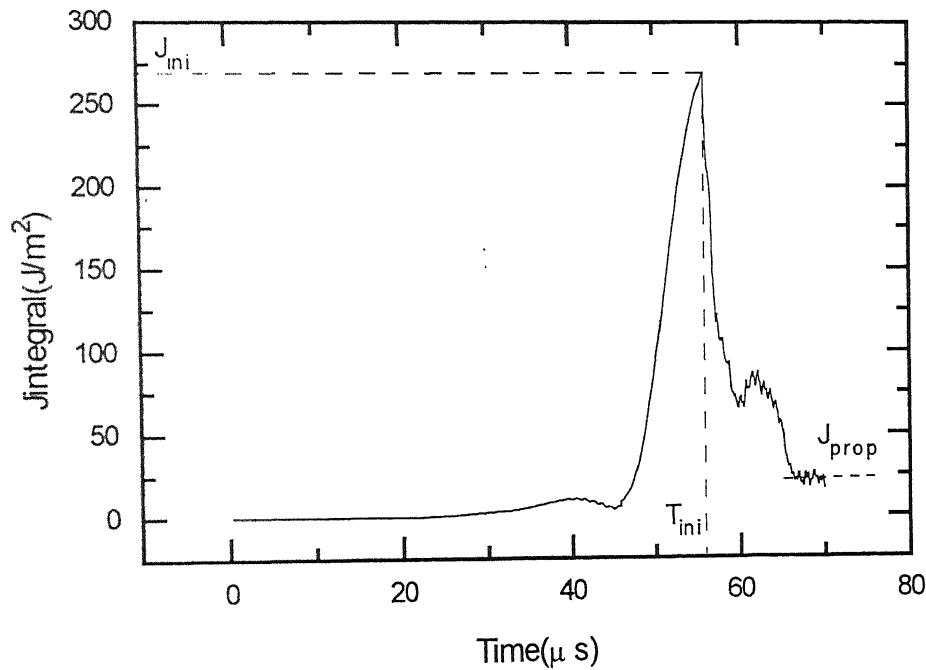


Fig. 7.7e: Jintegral Record for Propagating Crack for Expt.B7

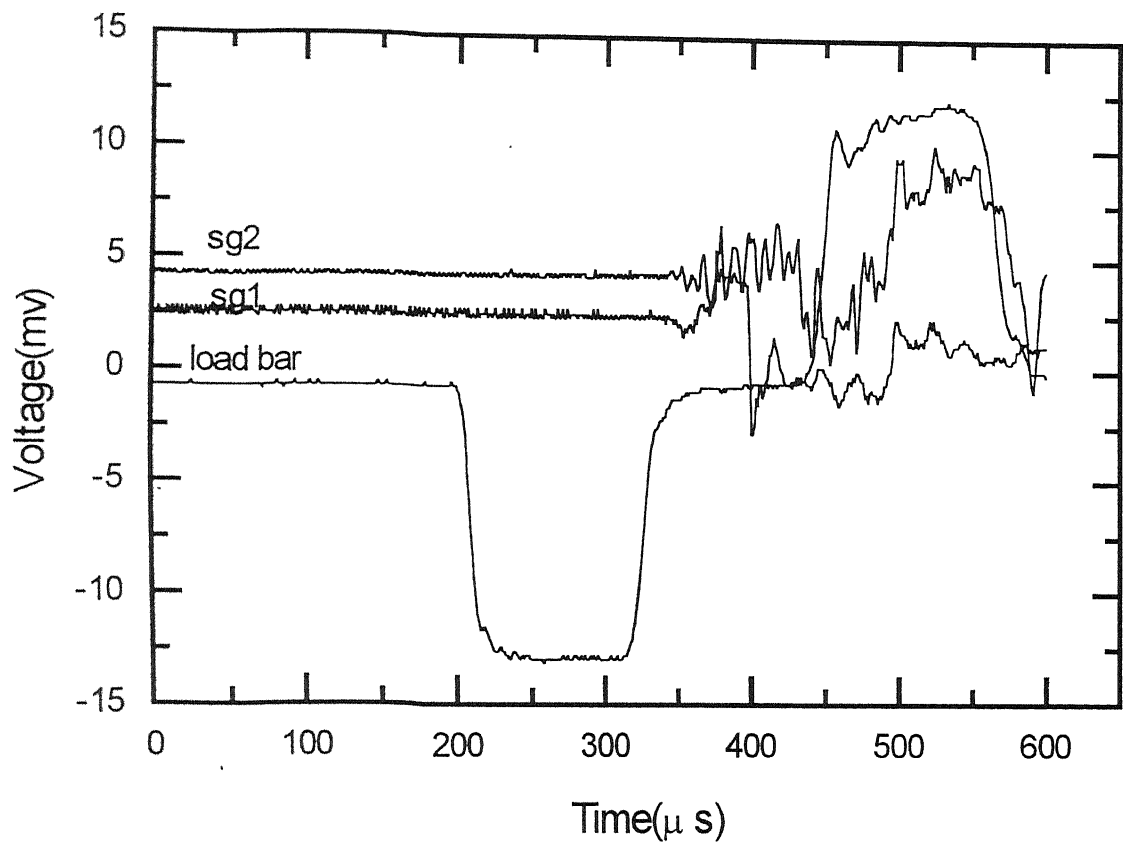


Fig. 7.8a: Oscilloscope Record for Expt.B8

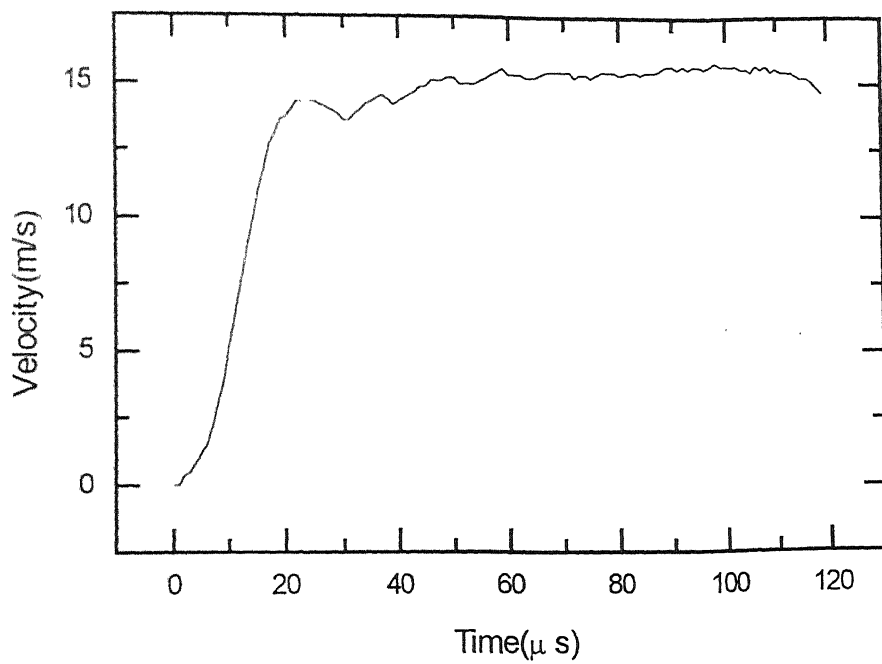


Fig. 7.8b: Velocity Record of Load bar End for Expt.B8

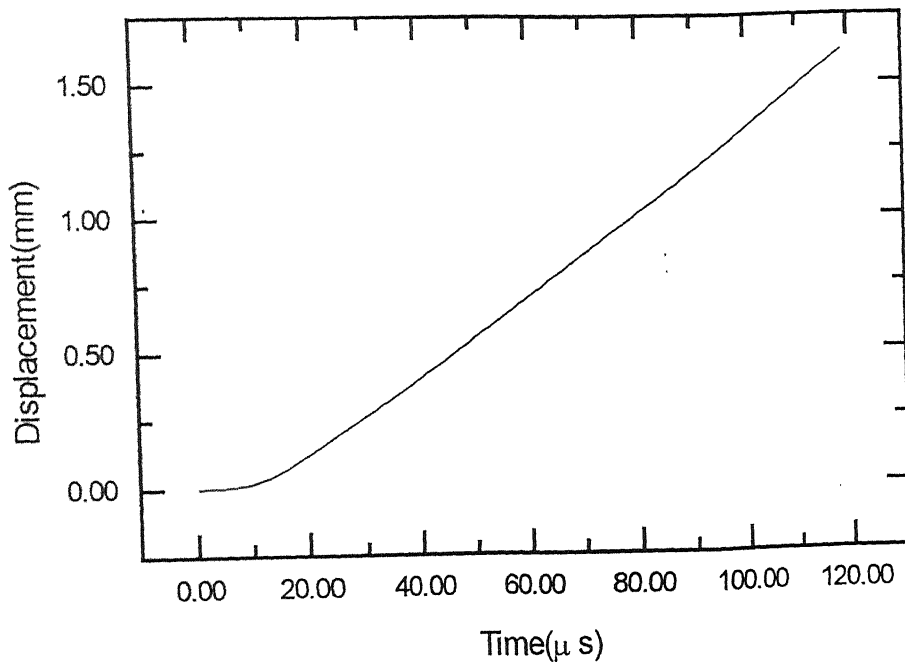


Fig. 7.8c: Displacement Record for Cantilever End for Expt.B8

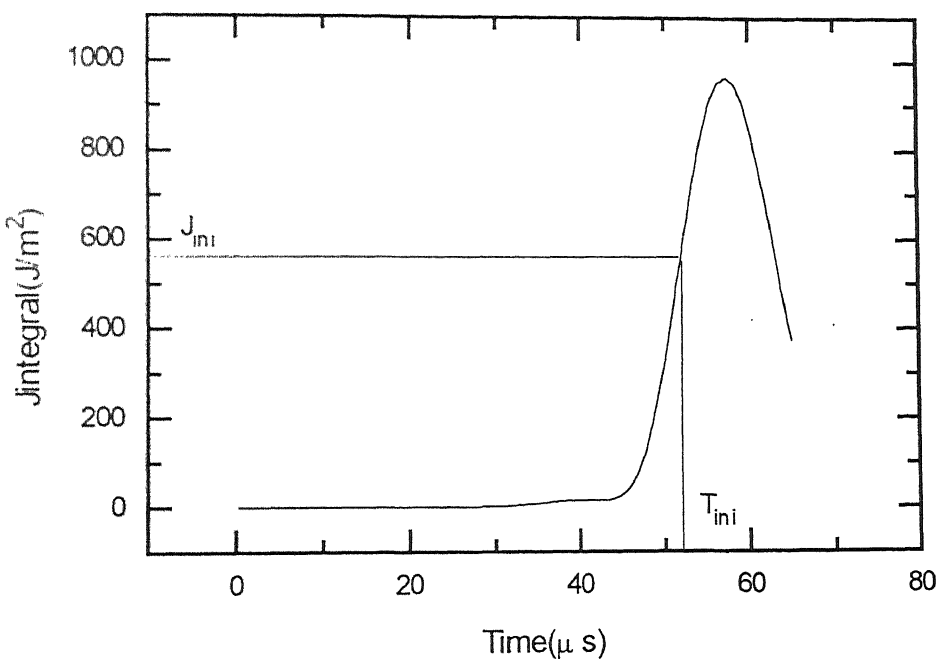


Fig. 7.8d: Jintegral Record for Stationary Crack for Expt.B8

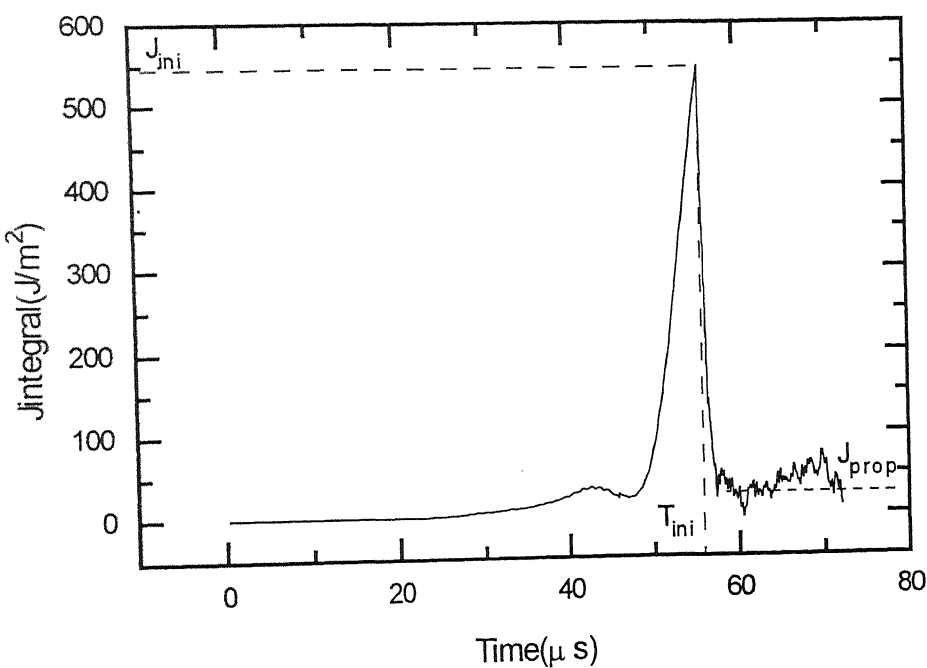


Fig. 7.8e: Jintegral Record for Propogating Crack for Expt.B8

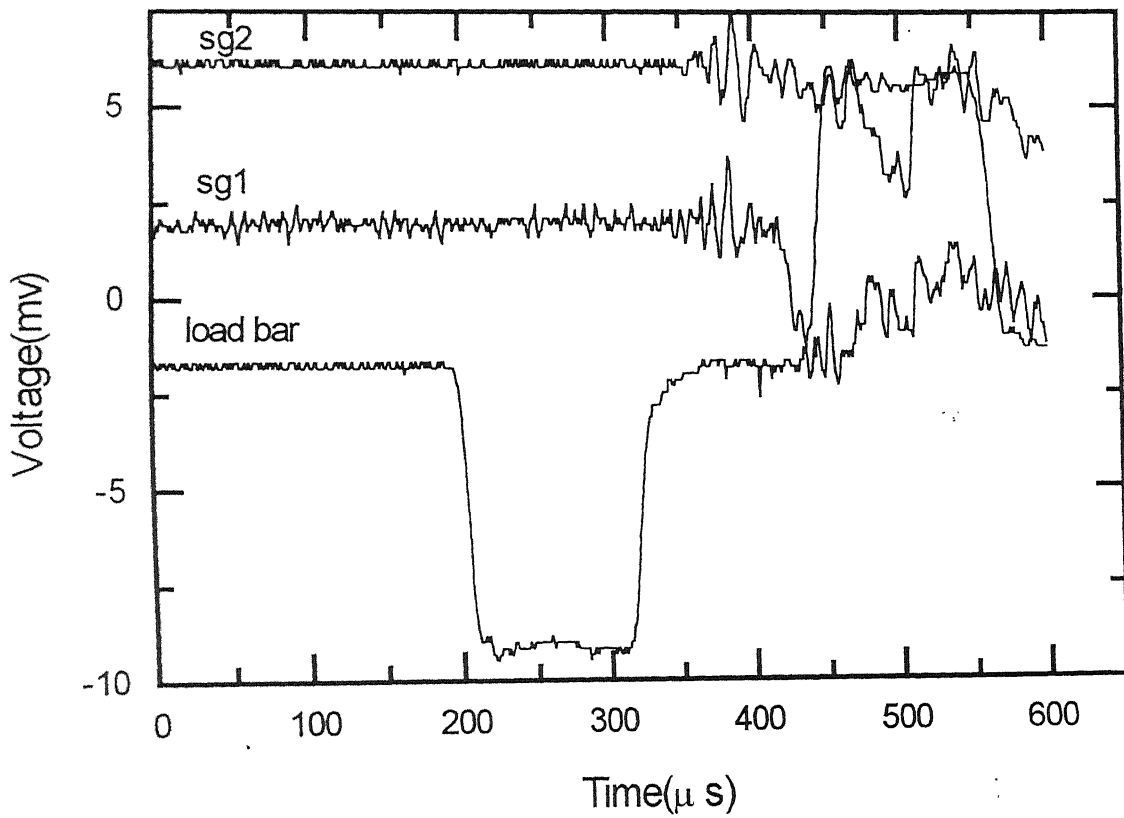


Fig. 7.9a: Oscilloscope Record for Expt.B9

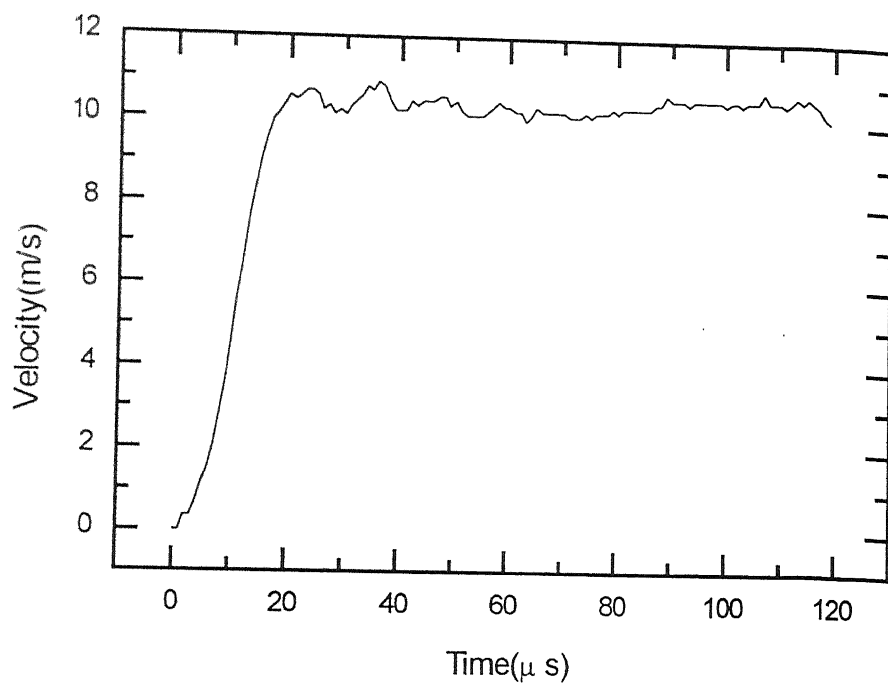


Fig. 7.9b: Velocity Record of Load bar end for Expt.B9

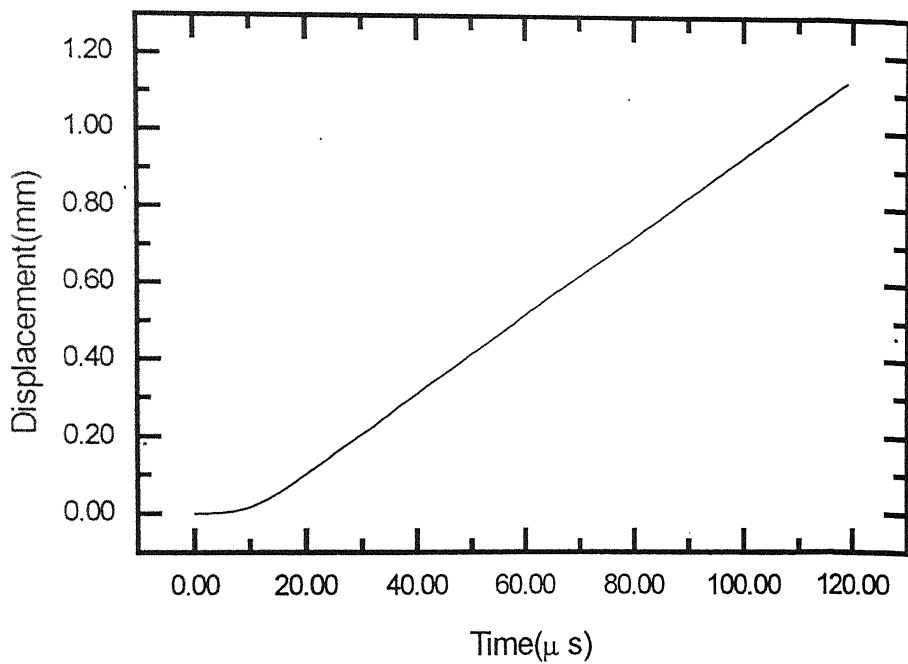


Fig. 7.9c: Displacement Record for Cantilever End for Expt.B9

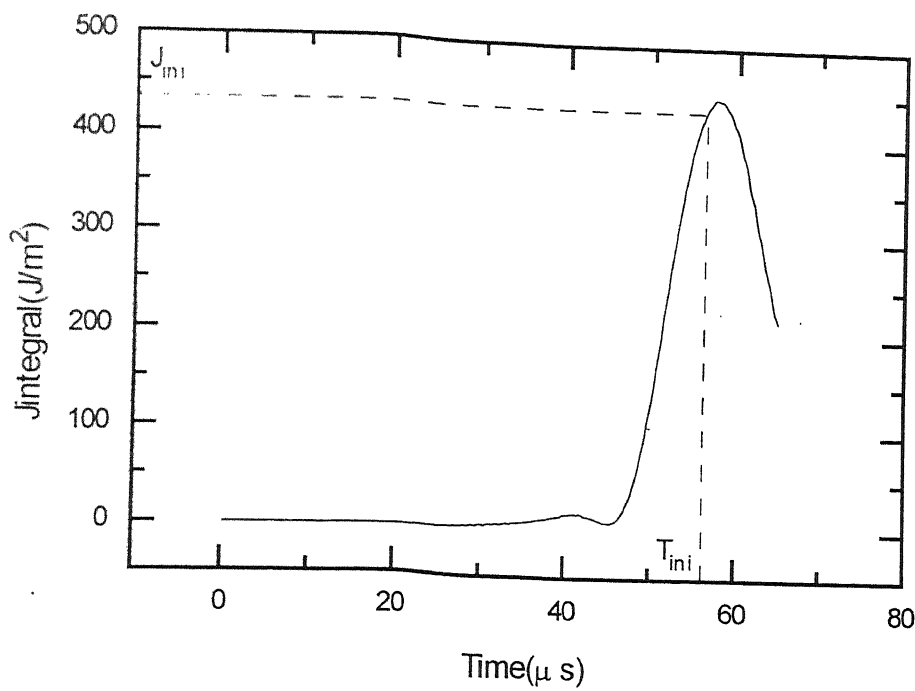


Fig. 7.9d: Jintegral Record for Stationary Crack for Expt.B9

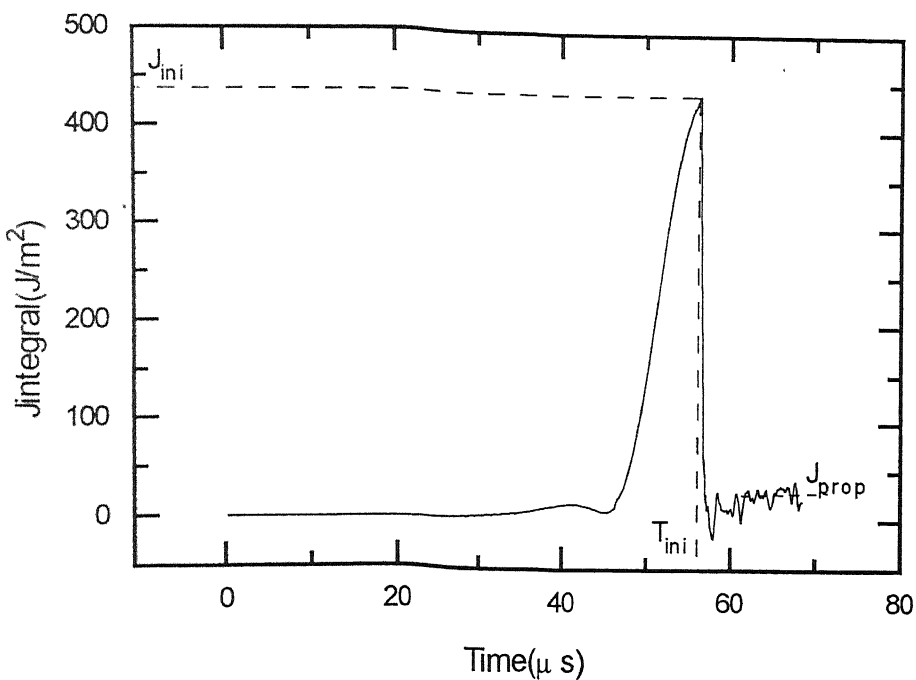


Fig. 7.9e: Jintegral Record for Propogating crack for Expt.B9

REFERENCES

Aminpour M.A. and Holsapple K.A. (1991) Finite element solutions for propagating interface crack with singularity elements, *Engineering Fracture Mechanics*, 39, 451-468.

Atluri Satya N. (1982) Path independent integrals in finite elasticity and inelasticity with body forces, inertia and arbitrary crack-face conditions, *Engineering Fracture Mechanics*, 16, 341-364.

Babu N.K. (1998) Interlaminar dynamic toughness of unidirectional GFRP laminates, M.Tech. thesis, Indian Institute of Technology, Kanpur, India.

Berger J.R. and Dally J.W. (1990a) A spatially overdetermined analysis for propagation toughness using strain gages, *Mechanics Research Communications*, 17, 93-99.

Berger J.R., Dally J.W. and Sanford R.J. (1990b) Determining the dynamic stress intensity factor with strain gages using a crack tip location algorithm, *Engineering Fracture Mechanics*, 36, 145-156.

Crouch B.A. and Williams J.G. (1987) Application of dynamic solution to high speed fracture experiments -I. Analysis of experimental geometries, *Engineering Fracture Mechanics*, 26, 541-551.

Freund L.B., (1990) *Dynamic Fracture Mechanics*, Cambridge University Press, Newyork.

John Lambros and Ares J. Rosakis (1997) An experimental study of dynamic delamination of thick fiber reinforced polymeric matrix composites, *Journal of Experimental Mechanics*.

Jones R.M., (1975) Mechanics of composite materials, McGraw-Hill Book Company, Newyork.

Kalthoff J.F., (1985) On the Measurement of Dynamic Fracture Toughness - A Review of Recent Work, *International Fracture Mechanics*, 27, 277-298.

Kishimoto K., Aoki S. and Sakata M. (1980) On the path independent integral-J, *Engineering Fracture Mechanics*, 13, 841-850.

Kobayasi A.S., Mall S., Urabe Y. and Emery A.F. (1978) A numerical dynamic fracture analysis of three wedge load DCB specimen, *Numerical methods in fracture mechanics*, eds. A.R. Luxmoore and D.R.J. Owen, Univ. College, Swesna, 673-684.

Kolednik O., (1991) On the physical meaning of J-a curves, *Engineering Fracture Mechanics*, 38 (6), 403-412.

Kumar Prashant and Narayanan. M.D (1993) Energy dissipation of projectile impacted panels of glass fabric reinforced composites, *Composite structures*, 15, 75-90.

Kumar Prashant and Rai Badri (1993) Delamination of barely visible impact damage in CFRP laminates, *Composite Structure*, 23, 313-318.

Kumar Prashant, Verma S.K., Kishore N.N. and Iyenger N.G.R. (1996) An experimental cum numerical technique to determine dynamic interlaminar fracture toughness, Report No. ARDB-SP-TR-96-787-01.

Kumar Prashant, Kishore N.N., Iyenger N.G.R. and Ramakrishna A. (1997) Initiation propagation interlaminar cracks in FRP laminates under impact loading, Report No. ARDB-SP-TR-97-787-01.

Mallikharjuna R. Ravipati (1998) Determination of interlaminar toughness of GFRP laminates at very high crack velocity, M.Tech. thesis, Indian Institute of Technology, Kanpur, India.

Malluck J.F. and King W.W. (1978) Fast fracture simulated by finite element analysis which accounts for crack tip energy dissipation, *Numerical Methods in Fracture Mechanics*, eds. A.R. Luxmoore and D.R.J. Owen, Univ. College, Swesna, 648-659.

Manogg P. (1966) Investigations of the rupture of a plexiglass plate by means of an optical method involving high speed filming of shadow originating around holes drilled in plate, *International Journal of Fracture*, 2, 604-613.

Nishioka T. and Atluri S.N. (1982a) Numerical analysis of dynamic crack propagation: Generation and prediction studies, *Engineering Fracture Mechanics*, 16, 303-332.

Nishioka T. and Atluri S.N. (1982b) FInite element simulation of fast fracture in steel DCB specimen, *Engineering Fracture Mechanics*, 16, 157-175.

Nishioka T. and Atluri S.N. (1983) Path independent integrals, energy release rate and general solution of near-tip fields in mixed mode dynamic fracture mechanics, *Engineering Fracture Mechanics*, 18, 1-22.

Owen D.J.R. and Shantaram D. (1977) Numerical study of dynamic crack growth by the

Finite element method, *International Journal of Fracture*, 13, 821-837.

Parton V.Z. and Boriskovsky V.G. (1989) *Dynamic Fracture Mechanics*, Hemisphere Publishing Corporation, 1, 203-204.

Popadopoulos George A. (1993) Fracture Mechanics : *The Experimental Method of Caustics and The Det.-criterion of Fracture*, Springer-Verlag, London.

Ramakrishna Alluri (1997) Initiation and propagation toughness of interlaminar cracks in FRP laminates under impact loading, M.Tech. thesis, Indian Institute of Technology, Kanpur, India.

Raman P. S, John Lambros, Arun Shukla and Ares Rosakis (1997), Investigation of mechanics of intersonic crack propagation along a bimaterial interface using CGS and photoelasticity, Department of Aerospace Engineering, California Institute of Technology (submitted for publication).

Ravichandran G. and Clifton R.J., 1989, Dynamic fracture under plane wave loading, *International Journal of Fracture*, 40, 157-201.

Ravi Chandar K. and Knauss W.G. (1982) Dynamic crack tip stresses under stress wave loading - A comparison of theory and experiment, *International Journal of Fracture*, 20, 202-222.

Ravi Chandar K. and Knauss W.G. (1984a) An experimental investigation into dynamic fracture : I. Crack initiation and arrest, *International Journal of Fracture*, 25, 247-262.

Ravi Chandar K. and Knauss W.G. (1984b) An experimental investigation into dynamic fracture - II. Micro-structural aspects, *International Journal of Fracture*, 26, 65-80.

Ravi Chandar K. and Knauss W.G. (1984c) An experimental investigation into dynamic fracture - III. On steady-state crack propagation and crack branching, *International Journal of Fracture*, 26, 141-154.

Ravi Chandar K. and Knauss W.G. (1984d) An experimental investigation into dynamic fracture - IV. On interaction of stress waves with propagating cracks, *International Journal of Fracture*, 26, 189-200.

Rosakis A.J., Duffy J. and Freund L.B. (1984) The determination of dynamic fracture toughness of AISI 4340 steel by the shadow spot method, *Journal of the Mechanics and Physics of Solids*, 4, 443-460.

Rydholm G., Fredriksson B. and Nilsson f. (1978) Numerical investigation of rapid crack propagation, *Numerical Methods in Fracture Mechanics*, eds. A.R Luxmoore and D.R.J. Owen, Univ. College, Swesna, 660-672.

Schardin H. (1959) *Velocity Effect in Fracture*, ed. B.L. Averbach, Cambridge MA, MIT Press 297-350.

Soren F.J., Sang F.G., Kindelan M. and Badal J.I., (1990) Finite Element Method for Elastic Wave Propagation, *Communications in Applied Numerical Methods*, 6, 359-368.

Sun C.T. and Grady J.E., (1998) Dynamic Delamination Fracture Toughness of a Graphite

Takeda N., Sierakowski R.L., Ross C.A. and Malvern L.E. (1982) Delamination crack propagation in ballistically impact glass/epoxy composite laminates, *Experimental Mechanics*, 22, 19-25.

Thesken J.C and Gudmundson Peter (1991) Application of a moving variable order singular element to dynamic fracture mechanics, *International Journal of Fracture*, 52, 47- 65.

Theocaris P.S. (1970) Local yielding around a crack tip in plexiglass, *Journal of Applied Mechanics*, 37, 409-415.

Truss R.W., and Hine P.J., Duckett R.A. (1997), Interlaminar and intralaminar fracture toughness of uniaxial continuous and discontinuous carbon fiber/epoxy composites, *Composites*, 28A, 627-636.

Verma S.K. (1995) Determination of Static and Dynamic Interlaminar Fracture Toughness - A combined Experimental and Finite Element Method, Ph.D. thesis, Indian Institute of Technology Kanpur, India.

Verma S.K. (1995) Evaluation of critical interlaminar SIF of DCB specimen made of slender cantilever, *Engineering Fracture Mechanics*, 50, 345-353.

Wang Y. and Williams J.G. (1994) A numerical study of dynamic crack growth in isotropic DCB specimens, *Composites*, 25, 323-331.

Zehnder Alant T. and Rosakis Ares J. (1990) Dynamic fracture initiation and propagation in 4340 steel under impact loading, *International Journal of Fracture*, 43, 271- 285.